Aus dem Institut für Physiologische Chemie

Geschäftsführender Direktor: Prof. Dr. Oliver Hantschel

des Fachbereichs Medizin der Philipps-Universität Marburg

The role of the actin regulators cyclase-associated proteins (CAP) in growth cone function and neuron differentiation

Inaugural-Dissertation

zur Erlangung des Doktorgrades

der gesamten Naturwissenschaften

(Dr. rer. nat.)

dem Fachbereich Medizin der Philipps-Universität Marburg

vorgelegt von

Felix Schneider

aus Stuttgart – Bad Cannstatt

Marburg, 2021

Angenommen vom Fachbereich Medizin der Philipps-Universität Marburg am: 29.10.2021

Gedruckt mit Genehmigung des Fachbereichs Medizin

Dekanin: Frau Prof. Dr. D. Hilfiker-Kleiner

Referent: Herr Prof. Dr. M. Rust

1. Korreferent: Herr Prof. Dr. R. Jacob

'You cannot teach a man anything; you can only help him discover it in himself.'

Galileo

Table of Contents

Table of figures

List of Abbreviations

ABP	Actin-binding protein
ADF	Actin depolymerizing factor
ADP	Adenosine diphosphate
Arp	Actin-related protein
ATP	Adenosine triphosphate
BDNF	Brain-derived neurotrophic factor
C domain	Central domain
CAP	Cyclase-associated protein
CARP	CAP and RP2 domain
Cof1-KO	Cofilin1 knockout
CTR	Control
DAR	Day(s) after replating
DiI	1,1'-dioctadecyl-3,3,3',3'-tetramethylindocarbocyanine perchlorate
DIV	Day(s) *in vitro*
dSTORM	Direct stochastic optical reconstruction microscopy
E	Embryonic day
F-actin	Filamentous actin
flx	Flanked by loxP site
FRAP	Fluorescence recovery after photobleaching
G-actin	Globular actin monomer
GFP	Green fluorescent protein
HFD	Helical fold domain
KD	Knockdown
KO	Knockout
NGF	Nerve growth factor
P	Postnatal day
P domain	Periphery domain
PP1	Proline-rich domain 1
RP2	Retinitis pigmentosa 2 protein
shRNA	Small hairpin ribonucleic acid
T zone	Transition zone
WASP	Wiscott Aldrich Syndrome protein
WH2	WASP homology 2 domain

1 Summary

Wiring of the brain is established by axons, which elongate from a neuron and are guided through the brain to their target neurons. Growth cones are actin-rich structures located at the tips of axons and are responsible for sensing environmental cues as well as controlling directed axonal outgrowth. Motility and function of growth cones are mediated by underlying actin dynamics, which in turn are regulated by actin-binding proteins (ABPs). Among these proteins is the family of cyclase-associated proteins (CAPs), which comprises two members (CAP1, CAP2), which are both expressed in the brain. Despite recent progress in uncovering their molecular function in actin dynamics, their physiological role during brain development remains largely unknown. Therefore, we used knockout (KO) mouse models for both CAPs to investigate their function in brain development. We found both proteins expressed in the embryonic brain as well as in cultured neurons and being localized within growth cones. CAP1-KO brains displayed impaired fiber track formation, but had no alterations in neuron migration or precursor proliferation. In addition, CAP1-KO neurons were delayed in development and exhibited shorter and thicker neurites. This was accompanied by enlarged growth cones, which had fewer filopodia, reduced motility, impaired actin dynamics and consequently disturbed responses to guidance cues. Instead, the loss of CAP2 did not cause any changes in brain morphology or neuron differentiation. Alterations in differentiation and morphology in CAP1-KO neurons as well as growth cone size could be rescued by overexpression of either CAP1 or CAP2, suggesting functional redundancy of both proteins. Further analysis exploiting CAP1 mutants revealed that the helical fold domain and therefore the interaction with the actin regulator cofilin1 is important in mediating growth cone function. Establishing a neuron replating protocol to study early neuron differentiation and growth cone function upon knockout of either CAP1, cofilin1 or both ABPs allowed a more detailed analysis on the functional interaction of CAP1 and cofilin1 in the growth cone. This approach revealed that both proteins synergistically regulate F-actin dynamics within the growth cone and that they are functionally dependent on each other. Taken together, this study showed that CAP1 and CAP2 are redundant in regulating growth cone function *in vitro*, but that CAP1 is the dominant family member in neuron differentiation and brain development. Furthermore, this study provides a new protocol for studying protein function during early aspects of neuron differentiation and showed that CAP1 and cofilin1 functionally interact in the growth cone and regulate its dynamics, thereby providing new insights into the physiological role of CAP1-cofilin1 interaction.

2 Zusammenfassung

Das Axon ist der verlängerte Neurit eines Neurons, welches durch das Gehirn migriert um mit anderen Neuronen neuronale Schaltkreise zu bilden. Verantwortlich für die Navigation sind Wachstumskegel, welche sich an der Spitze ein jedes Axons befinden. Wachstumskegel sind reich an F-Aktin, deren Dynamik von Aktin-bindenden Proteinen (ABP) reguliert wird. Zyklase-assoziierte Proteine (CAPs) gehören zu den ABP und kommen in Säugetieren in zwei Isoformen vor (CAP1, CAP2), welche beide im Gehirn exprimiert werden. Obwohl in kürzlich veröffentlichten Studien gezeigt werden konnte wie CAPs Aktindynamik regulieren, ist über deren physiologische Funktion in der Gehirnentwicklung nahezu nichts bekannt. Um dieser Frage nachzugehen wurden Knockout (KO) Mäuse für beide Proteine analysiert. CAP1-KO Mäuse zeigten stark reduzierte Nervenfaserbildung, wohingegen andere wichtige Entwicklungsprozesse wie neuronale Migration und Vorläuferzellproliferation unverändert waren. Des Weiteren war die neuronale Differenzierung verlangsamt, die Neuriten verkürzt als auch verdickt und die Wachstumskegel vergrößert mit weniger Filopodien. Die Wachstumskegel wiesen zusätzlich eine verminderte Aktindynamik auf und zeigten eine gestörte Reaktion auf chemotaktische Reize. Im Gegensatz zu CAP1-KO Mäusen wiesen CAP2-KO Mäuse keinerlei Veränderungen in der Gehirnentwicklung auf und auch die neuronale Differenzierung blieb unverändert. Veränderungen in der neuronalen Differenzierung und der Morphologie der Neurone als auch in den Wachstumskegeln im CAP1-KO konnten durch die Überexpression von CAP1, als auch von CAP2, rückgängig gemacht werden. Daraus ließ sich schließen, dass beide Proteine redundante Funktionen in differenzierenden Neuronen ausüben. Des Weiteren konnte herausgefunden werden, dass die „helical fold domain", welche die Interaktion mit dem Aktinregulator Cofilin1 vermittelt, wichtig für die Funktion von CAP1 im Wachstumskegel ist. Um die Interaktion von CAP1 und Cofilin1 im Wachstumskegel zu entschlüsseln, wurde ein Protokoll entwickelt, welches Neurone replattiert um somit frühe neuronale Differenzierung und Wachstumskegel nach dem KO von CAP1, Cofilin1 oder beiden Proteinen zu untersuchen. Damit konnte gezeigt werden, dass CAP1 und Cofilin1 synergistisch die Aktindynamik in Wachstumskegeln regulieren und dass deren Funktion vom jeweils anderen Protein abhängt. Zusammengefasst zeigt diese Studie, dass CAP1 und CAP2 redundant in ihrer Funktion bezüglich der Regulation der Dynamik von Wachstumskegeln sind, aber das CAP1 der wichtigere Regulator in der neuronalen Differenzierung ist.

Zusätzlich bietet diese Studie ein Protokoll um Proteine in früher neuronaler Differenzierung zu untersuchen. Damit konnte gezeigt werden, dass CAP1 und Cofilin1 gemeinsam Wachstumskegel regulieren, welches einen neuen Einblick in die physiologische Relevanz der CAP1-Cofilin1-Interaktion gibt.

3 Introduction

3.1 Axons are the backbone of neuron connectivity

In 1875, Camillo Golgi laid the basis for modern cellular neuroscience when he discovered a method to visualize single neurons in the brain (Shepherd et al. 2011; Zupanc 2017). His discovery paved the way for neuroscientists to uncover the mechanisms of brain function on a cellular and molecular level. The human brain is a highly complex organ consisting of billions of neurons with even more synapses (von Bartheld, Bahney, and Herculano-Houzel 2016). This allows the brain to store memories as well as process difficult and complex tasks. Axonal fibers traversing the brain and the body allow quick signal transmission and are a prerequisite for fast data processing (Debanne et al. 2011). During differentiation, neurons form several neurites but only the fastest growing neurite will become the axon (Dotti, Sullivan, and Banker 1988) and together with dendrites and the soma build up the neuronal circuit. Axon formation is a crucial step in the development of a neuron as it defines its polarity (Da Silva and Dotti 2002). On the way to maturation, the neuron undergoes several distinct stages, which are morphologically distinguishable (Figure 1).
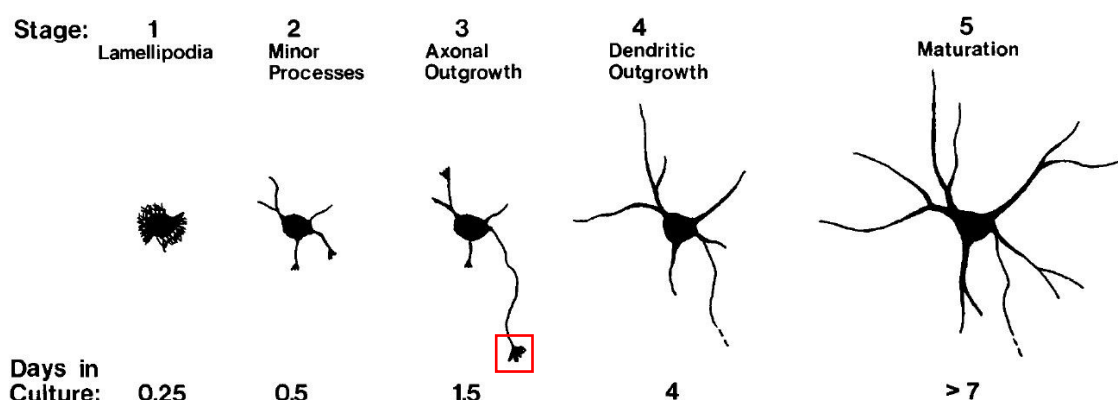

Figure 1 – Differentiation stages of cultured hippocampal neurons and the approximate time points. Newly plated neurons exhibit a round shape, from which neurites start to grow out. The axon develops after one and a half days and during this time growth cones at the tip of the axon and neurites (red box) are clearly visible. After four days, the dendritic tree starts to outgrow, followed by neuron maturation after seven days. Modified scheme from Dotti, Sullivan and Banker 1988.

The newly plated hippocampal or cortical neurons exhibit a round shape (stage 1), which is disrupted after one day *in vitro* (DIV1) as the neurons form neurites that protrude out of the soma (stage 2). At DIV2, one neurite rapidly elongates and becomes the axon (stage 3) and at DIV4, the neuronal dendritic tree develops (stage 4). In the last stage (stage 5) the neuron matures, forming dendritic spines and synapses (Dotti, Sullivan, and Banker 1988; Polleux and Snider 2010).

To properly connect neurons and build neuronal circuits, the axon has to be guided through the brain to its target cells. To guide the axon on its way, neuron and glia cells provide a variety of cues, which can be either repulsive or attractive (Dudanova and Klein 2013; Chédotal and Richards 2010; Stoeckli 2018). Besides chemical cues, the stiffness of the surrounding tissue equally contributes to the guidance of the axon (Koser et al. 2016). Failed axon guidance or outgrowth is known to result in neurological disorders and diseases, with epilepsy being one of the more prominent ones (Izzi and Charron 2011; Van Battum, Brignani, and Pasterkamp 2015).

3.2 Structure and function of the growth cone

A structure crucial for axon guidance is the growth cone, which is located at the tip of neurites and the axon. The growth cone has a 'hand-shaped' appearance and was first described by Ramon y Cajal in 1890 (Tamariz and Varela-Echavarria 2015). It can be separated into three different domains according to their shape and composition of cytoskeletal elements (Figure 2).
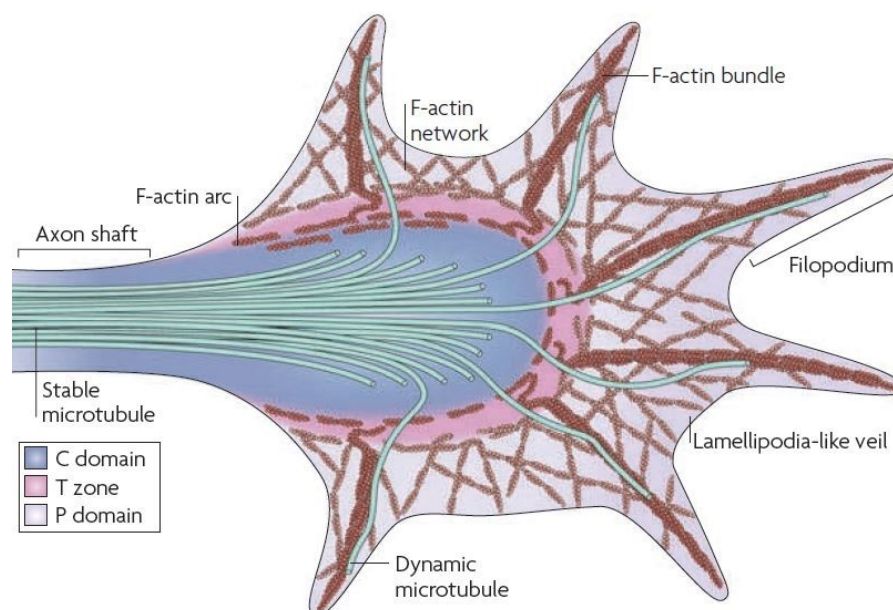

Figure 2 – Scheme of a growth cone. The central (C) domain encloses organelles and bundled microtubules, which originate from the axonal shaft. The periphery (P) domain contains an F-actin meshwork that builds up lamellipodia and F-actin bundles, which in turn define filopodia. Dynamic microtubules invade the P domain and align to F-actin bundles within the filopodia. The transition (T) zone is composed of short F-actin strands, which form an F-actin arc, and is located between the C and P domain. Scheme obtained from Lowery and van Vactor 2009.

Beginning from the distal end of a neurite or an axon lays the central (C) domain, which mainly consists of bundled microtubules extending from the shaft into the growth cone. This is also the place were protein synthesis takes places, supplying the growth cone with structural and regulatory components (Lowery and van Vactor 2009). Adjacent to the C domain, controlling the progression of microtubules and the axonal shaft, lays the

transition (T) zone. It consists mainly of short actin filaments (F-actin), which are decorated with myosins, granting the T zone a high degree of flexibility (Medeiros, Burnette, and Forscher 2006; Burnette et al. 2008; Lowery and van Vactor 2009). The periphery (P) domain consists primarily of F-actin, which forms lamellipodia and filopodia, thereby creating the characteristic 'hand-shaped' appearance. (Lowery and van Vactor 2009; Omotade, Pollitt, and Zheng 2017). In addition, few dynamic microtubules from the C domain invade the P domain and connect to the F-actin strands, which define the filopodia (Lowery and van Vactor 2009; Cammarata, Bearce, and Lowery 2016). The P domain is also the most outer region of the growth cone and therefore it is important for sensing environmental cues and reacting to them (Gomez and Letourneau 2015).

Besides sensing, the growth cone propels axonal outgrowth, which is driven by the actin cytoskeleton (Lowery and van Vactor 2009). F-actin polymerizes at the leading edge and builds up membrane tension, resulting in a force that pushes F-actin in the direction of the T zone (Craig et al. 2015, 2012). There, myosins pull the F-actin towards the T zone where it is then depolymerized by members of the actin depolymerizing factor (ADF)/cofilin family (Craig et al. 2015; Kerstein, Nichol IV, and Gomez 2015; Lin et al. 1996). This so-called retrograde F-actin flow enables the growth cone to constantly retract and protrude filopodia into the surrounding to sense cues, but does not result in any directed movement of the growth cone. The 'molecular-clutch' theory hypothesizes that these F-actin strands can be coupled to the underlying surface via integrins and other anchor molecules leading to a forward movement of the growth cone (Craig et al. 2015; Nichol IV et al. 2016). Hence, the velocity of the retrograde F-actin flow is inversely proportional to the growth cone advance (Lin and Forscher 1995). This can be indirectly exploited by guidance cues, as they either strengthen the molecular clutch or weaken it, resulting in growth cone advance either into the direction of the source or away from it (Gomez and Letourneau 2015; Nichol IV et al. 2016). In addition, guidance cues indirectly control actin-binding proteins (ABPs), which regulate the retrograde F-actin flow, as well as couple microtubules to F-actin thus determining the direction of expansion of the growth cone and subsequently of the axon (Lowery and van Vactor 2009; Craig 2018).

3.3 F-actin treadmilling and its regulating proteins

The constant polymerization and depolymerization of actin described above co-drives retrograde F-actin flow. It is a well-known concept in biology, called the F-actin treadmilling mechanism that describes a process in which under 'steady-state' conditions the rate of polymerization and depolymerization of F-actin is equal (Neuhaus et al. 1983; Baum et al. 2006). There are multiple ABPs, which control the actin cytoskeleton, but

key regulators of the actin treadmilling are members of the three protein families ADF/cofilin, profilins and cyclase-associated proteins (CAPs) (Baum et al. 2006) (Figure 3).
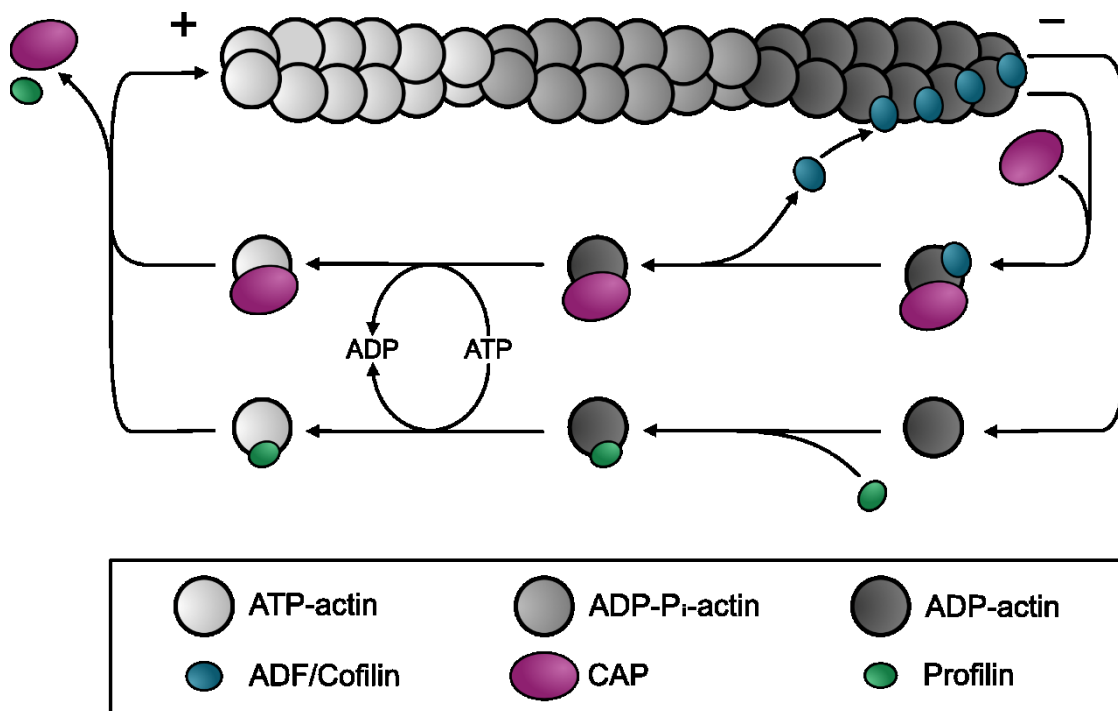

Figure 3 – F-actin treadmilling and its regulating proteins. ADF/cofilin binds at the (-)-end of F-actin to dissociate G-actin subunits. CAP enhances the depolymerization through ADF/cofilin and releases ADF/cofilin from G-actin. CAP as well as profilin exchange ADP with ATP on G-actin allowing for a new round of polymerization at the (+)-end. Scheme obtained from Isabell Metz unpublished.

The protein family ADF/cofilin consists of the three proteins namely ADF, cofilin1 and cofilin2, with all of them being expressed in the brain (Vartiainen et al. 2002; Gurniak et al. 2014). ADF/cofilin binds to F-actin and enhances its severing as well as depolymerization, thereby producing ADP-bound monomeric, globular actin (G-actin) (Bamburg, McGough, and Ono 1999; Ono 2013; Baum et al. 2006). The profilin family comprises four members of which only profilin1 and profilin2 are expressed in the brain (Witke et al. 1998; Braun et al. 2002; Obermann et al. 2005). In contrast to ADF/cofilin, profilins bind G-actin and promote the exchange from ADP to ATP thereby providing new polymerization-competent G-actin (Ono 2013; Baum et al. 2006; Goldschmidt-Clermont et al. 1992).

CAPs compose the third protein family that regulates actin treadmilling. It comprises two members, CAP1 and CAP2, whereof the first one is broadly expressed with the exception of adult skeletal muscle and the latter being restricted to certain tissues including the brain (Rust et al. 2020; Ono 2013; Bertling et al. 2004). CAPs are multi-domain proteins (Rust et al. 2020) with multiple functions in regulating actin treadmilling. The N-terminal

half of the protein contains the helical fold domain (HFD), which binds to ADF/cofilin-decorated F-actin and enhances the depolymerization rate of actin subunits (Kotila et al. 2019; Ono 2013; Rust et al. 2020). In addition, CAPs form oligomers via their N-terminal oligomerization domain (OD) to further enhance the ADF/cofilin-mediated depolymerization of F-actin (Quintero-Monzon et al. 2009; Purde et al. 2019). The second large domain is the CAP and Retinitis Pigementosa protein 2 (CARP) domain, which is located at the C-terminus. It binds to G-actin and promotes the exchange from ADP to ATP on G-actin (Kotila et al. 2018; Ono 2013; Rust et al. 2020). In between the HFD and CARP domain are two proline-rich regions, which are important for the interaction with other regulatory proteins like profilins (Makkonen et al. 2012; Bertling et al. 2007; Rust et al. 2020). Both proline-rich stretches flank the WASP homology 2 (WH2) domain, which is crucial for the nucleotide exchange on G-actin and the release of ADF/cofilin from the ADF/cofilin-actin complex (Chaudhry et al. 2010; Kotila et al. 2019; Rust et al. 2020).

3.4 ABPs are important regulators of growth cone function

Actin dynamics are crucial for growth cone function and motility with ABPs playing an essential role in regulating growth cone dynamics (Omotade, Pollitt, and Zheng 2017). Over the past years, different studies deciphered the role of a variety of ABPs in regulating the growth cone and actin dynamics within the growth cone. Among them is the actin-related protein 2/3 (Arp2/3) complex, which nucleates actin on existing F-actin and thereby promotes F-actin branching and building of an F-actin meshwork (Goley and Welch 2006). In growth cones, Arp2/3 builds up lamellipodia and initiates filopodia formation (Korobova and Svitkina 2008). Furthermore, it regulates the retrograde F-actin flow and the formation of focal adhesions (Korobova and Svitkina 2008; Yang et al. 2012). As a result, it was shown that Arp2/3 is also important in growth cone translocation and axonal guidance (Norris, Dyer, and Lundquist 2009; Strasser et al. 2004; San Miguel-Ruiz and Letourneau 2014). Another ABP family are formins that are involved in actin polymerization (Le et al. 2020). Formins were shown to fulfill several functions within growth cones, including filopodia formation (Matusek et al. 2008; Gonçalves-Pimentel et al. 2011) and coupling of microtubules to F-actin, which are both important for the chemotactic behavior of the growth cone (Földi, Szikora, and Mihály 2017; Kundu et al. 2021). Besides axonal guidance, formins are also essential in mediating traction force, by engaging in the molecular clutch (Ghate et al. 2020), which in turn couples F-actin retrograde flow to the forward movement of the growth cone (Nichol IV et al. 2016). The family of myosin motor proteins does not modify F-actin itself, but its family members are crucial for powering retrograde F-actin flow (Lin et al. 1996), growth cone motility

(Bridgman et al. 2001) and are involved in growth cone turning during chemotaxis (Wang et al. 2003). Moreover, myosins control filopodia size and stability (Iuliano et al. 2018) and promote the actin bundle turnover in the growth cone (Medeiros, Burnette, and Forscher 2006).

Among the proteins described earlier in directly controlling F-actin treadmilling, profilin was shown to regulate axonal outgrowth in *Drosophila* (Wills et al. 1999; Kim et al. 2001). Furthermore, profilins provide G-actin at the leading edge hence promoting polymerization (Lee et al. 2013) and regulate filopodia elongation in the growth cone (Gonçalves-Pimentel et al. 2011). Moreover, a recent study showed that profilin1 is important for axon regeneration by controlling retrograde F-actin flow as well as growth and invasion of microtubules into the growth cone (Pinto-Costa et al. 2020).

The family of ADF/cofilin are among the best studied ABPs in the growth cone and are considered to be key regulators of growth cone dynamics (Gungabissoon and Bamburg 2003). ADF/cofilin regulates axonal outgrowth and branching in *Drosophila* (Sudarsanam et al. 2020) as well as retrograde F-actin flow and neurite formation in mouse neurons (Flynn et al. 2012). Hence, many signaling pathways in axon guidance regulate the activity of ADF/cofilin, resulting in altered retrograde F-actin flow activity and subsequently in growth cone turning (Meberg 2000; Marsick et al. 2011; Zhang et al. 2012; Meberg and Bamburg 2000). Brain-derived neurotrophic factor (BDNF) for example controls the length, number and dynamics of filopodia via ADF/cofilin (Fass et al. 2004; Gehler et al. 2004). Besides axon guidance, cofilin1 was also shown to be crucial in promoting axonal regeneration after axonal injury (Tedeschi et al. 2019).

3.5 Aim of study

Two decades ago, CAPs were identified as ABPs (Freeman and Field 2000; Balcer et al. 2003) and recent studies unraveled their molecular function on regulating F-actin dynamics (Kotila et al. 2019, 2018). Despite the progress in uncovering the functions of CAPs in cancer (Hasan and Zhou 2019; Wu et al. 2019), fat metabolism (Jang et al. 2019), muscle differentiation (Kepser et al. 2019; Colpan, Iwanski, and Gregorio 2021; Iwanski, Gregorio, and Colpan 2021), heart physiology (Peche et al. 2012; Field et al. 2015; Stöckigt et al. 2016; Aspit et al. 2019) and oocyst division (Jin et al. 2018), the role of CAPs in the brain remains largely unknown. A first study in *Drosophila* described that the CAP homologue capulet is implicated in axonal pathfinding and effector of the slit pathway (Wills et al. 2002). Further recent studies showed that CAP2 is important for dendritic complexity, spine density and synapse physiology with implications in Alzheimer's disease (Kumar et al. 2016; Pelucchi et al. 2020). Moreover, it was shown that CAP1 is important for astrocyte proliferation and Schwann cell differentiation after

brain injury (Zhang et al. 2014; Zhu et al. 2014). However, the function of CAPs during neuron differentiation and brain development is still unknown. A global approach that investigated protein expression in different brain areas and cell types at different time points confirmed that CAPs are expressed during brain development (Sharma et al. 2015). Therefore, I aimed to uncover the function of CAPs in early brain development, by exploiting knockout (KO) mouse models for both CAPs. Furthermore, by performing life cell imaging and super-resolution microscopy on isolated hippocampal neurons, I aimed to unravel the role of CAPs in neuronal differentiation and the growth cone machinery.

4 Results

4.1 CAP1 is relevant for neuronal connectivity in the brain

Before delineating the function of CAPs in mouse nervous system, we aimed to determine the expression levels of CAP1 and CAP2 in the developing mouse brain. Western blot analysis revealed protein expression of both CAP family members during embryonic brain development and CAP1 as well as CAP2 were equally expressed in different brain regions including hippocampus at postnatal day (P) 0 (Schneider et al. 2021a Fig.1 A+B; Schneider et al. 2021c Fig. 1 A+B). To gain a deeper knowledge of the role of CAPs in the developing brain, we exploited KO mice for both CAP1 and CAP2 to investigate their function during mouse brain development.

To generate a CAP1-KO, we bred conditional KO mice by crossing mice expressing Cre recombinase under the *nestin* promotor (Tronche et al. 1999) with mice carrying loxP sites (flx) flanking exon 3 of the CAP1 gene (Schneider et al., 2021a Fig. 1 C). The resulting CAP1$^{flx/flx, Nestin-Cre}$ mice (CAP1-KO) were deficient for CAP1 in all neural cells including neurons and glia cells (Tronche et al. 1999; Liang, Hippenmeyer, and Ghashghaei 2012). Using real time PCR and Western blot assays, we confirmed that CAP1 was indeed knocked out in the brain of CAP1-KO mice at the respective developmental stage (Schneider et al. 2021a Fig. 1 D+E) without affecting CAP2 protein expression levels (Schneider et al. 2021c Fig. 5 A). However, these CAP1-KO mice died shortly after birth, which limited our analysis to embryonic stages. In contrast to CAP1 (Jang et al. 2019), systemic CAP2-KO mice are viable. Western blot analysis confirmed that in CAP2-KO mouse brains CAP2 was not detectable and showed that CAP1 protein expression levels were not affected (Schneider et al. 2021c Fig. 2 A).

To describe the role of CAPs in the developing brain, we started with performing Nissl staining to examine the brain anatomy in both KO mice. Adult and embryonic CAP2-KO brains exhibited normal brain anatomy (Schneider et al. 2021c Fig. 4 A+B), whereas CAP1-KO animals displayed larger ventricles and a differently shaped hippocampus at E18.5, which was unchanged in area, but altered in length and shape (Schneider et al. 2021a Fig. S1 A-E).

Furthermore, immunostaining against Neurofilament and DiI staining in CAP1-KO brains revealed hypomorphic or missing fiber tracks in the cerebral cortex and striatum (Schneider et al. 2021a Fig. 1 F+G), which were normally developed in CAP2-KO mice (Schneider et al. 2021c Fig. 4 C). However, no changes in neuronal migration or proliferation of neuronal progenitors in the CAP1-KO mice could be observed (Schneider, et al. 2021a Fig. S1 F+G). Taken together, CAP1 played a crucial role in establishing neuronal connectivity, whereas CAP2 was dispensable for brain development.

4.2 CAP1 is required for proper neuron differentiation

To study the role of CAPs in neuronal development and hence in neuronal circuitry formation on both a cellular and molecular level, we switched to isolated hippocampal neurons from E18.5 mouse embryos. These cultured hippocampal neurons expressed substantial amounts of CAP1 and CAP2 *in vitro* (Schneider et al. 2021a Fig. 2 A; Schneider et al. 2021c Fig. 1 C). Immunostaining against the microtubule marker doublecortin allowed us to study early neuron differentiation, by classifying single neurons into different developmental stages (Dotti, Sullivan, and Banker 1988). This approach revealed a developmental delay of CAP1-KO neurons, as more neurons were categorized into earlier differentiation stages (Schneider et al. 2021a Fig. 2 B+C). Interestingly, when treating CAP1-KO neurons with cytochalasin D, we rescued the developmental delay (Schneider et al. 2021a Fig. 2 D+E), suggesting impaired actin depolymerization in these neurons (Flynn et al. 2012). Despite the delayed development, CAP1-KO neurons possessed an axon after two days *in vitro* (DIV) and general morphology in terms of number of primary neurites and neurite endpoints was unchanged (Schneider et al. 2021a Fig. 2 F, Fig. S2 A+B). Yet, CAP1-KO neurons exhibited significantly shorter and thicker neurites compared to control (CTR) neurons (Schneider et al. 2021a Fig. 2 G+H). In contrast to CAP1-KO neurons, loss of CAP2 neither affected neuronal differentiation (Schneider et al. 2021c Fig. 2 B+C) nor neuron morphology (Schneider et al. 2021c Fig. 2 D-H).

In summary, CAP1 controlled neurite length as well as diameter and therefore early neuron differentiation, whereas CAP2 was dispensable for early neuron development.

4.3 CAPs are centrally localized in the neuronal growth cone

By determining the subcellular localization of CAPs, we aimed to elucidate where CAP is localized during neuron development. Compared to green fluorescent protein (GFP)-transfected neurons, GFP-tagged CAP1 (GFP-CAP1) was enriched in the growth cone (Schneider et al. 2021a Fig. S3 A). Immunostaining against endogenous CAP1 revealed a subcellular localization similar to GFP-CAP1. Antibody staining additionally confirmed the deletion of CAP1 in CAP1-KO neurons (Schneider et al. 2021a Fig. 3 A). Cross-sectional line scans of growth cones showed that CAP1 was located in areas with high F-actin content (Schneider et al. 2021a Fig. 3 B). Interestingly, a line scan along filopodia revealed that CAP1 was largely absent from the filopodia tip and shaft (Schneider et al. 2021a Fig. 3 C). Similar to GFP-CAP1, GFP-CAP2 as well as myc-CAP2 were enriched within the growth cone (Schneider et al. 2021c Fig. 1 D+E) and a cross-sectional line scan revealed co-localization of overexpressed GFP-CAP2 and mCherry-CAP1 (Schneider et al. 2021c Fig. 1 F+G).

To get more detailed information about the subcellular localization of CAP1, we performed direct stochastic optical reconstruction microscopy (dSTORM) on growth cones overexpressing myc-CAP1, which were additionally stained with the F-actin marker phalloidin. With this approach, we confirmed that CAP1 was mainly localized in the C domain, T zone and P domain, but was largely absent from filopodia ends and shafts (Schneider et al. 2021a Fig. 3 D+E, Fig. S3 B).

In summary, both CAP family members were enriched within the growth cone and showed an overlapping localization along with F-actin-rich structures. Moreover, CAP1 was largely undetectable in filopodia shafts and ends of neuronal growth cones.

4.4 CAP1 regulates growth cone size, morphology and motility

As ABPs are essential for regulating growth cone motility (Omotade, Pollitt, and Zheng 2017) and as we confirmed that CAPs are located within the growth cone, we performed life cell imaging to investigate whether the loss of CAPs affects growth cone motility. Similar to CTR, CAP2-KO growth cones displayed a normal explorative behavior and frequently protruded and retracted filopodia (Schneider et al. 2021a Movie S1; Schneider et al. 2021c Movie S1+2). Additionally, fixed CAP2-KO growth cones were comparable to CTR in size and morphology (Schneider et al. 2021c Fig. 3 A-C). To out rule the possibility that CAP1 compensates for the loss of CAP2 and to exclude other possible compensatory effects, we created a small hairpin RNA (shRNA) against CAP2 to acutely down regulating CAP2 in neurons. Western Blot analysis confirmed that the shRNA successfully knocked down (KD) CAP2 in cortical neurons (Schneider et al. 2021c Fig. 3 D). To investigate the effect of CAP2 KD on growth cones, we established a protocol that allowed us to knockdown CAP2 but at the same time quantify early neuronal stages, by resetting the neurons into an undifferentiated state. For this, we transfected the neurons with shRNA, replated them two days post transfection as protein levels were sufficiently knocked down after this time and analyzed them 24 to 48 hours later (Schneider et al. 2021b Fig. 1). Replated neurons behaved similarly to freshly plated neurons allowing us to directly compare neurons and their growth cones one day after replating (DAR) with neurons at DIV1 (Schneider et al. 2021b Fig. 2-5, Movie S1-S4). Applying this method using a shRNA against CAP2, we observed that similar to CAP2-KO neurons, growth cone size and morphology was unaltered compared to CTR growth cones (Schneider et al. 2021c Fig. 3 E-G). In contrast to CAP2-KO neurons, CAP1-KO growth cones largely lacked filopodia and were clearly less motile (Schneider et al. 2021a Movie S2). Furthermore, fixed growth cones were larger and exhibited a smooth morphology as quantified by determining the fraction of growth cones lacking filopodia

and measuring the shape indices circularity and solidity (Schneider et al. 2021a Fig. 3 F-I).

To exclude that the observed differences in the CAP1-KO growth cones were caused by different culture conditions, we seeded CTR and CAP1-KO neurons in the same culture dish. CAP1-KO neurons co-cultured with CTR neurons displayed similar growth cone changes as in CAP1-KO cultures (Schneider et al. 2021a Fig. 3 J), demonstrating that the growth cone phenotype was not caused from environmental cues that might have been missing in the pure KO culture.

To investigate the changes in growth cone appearance in the CAP1-KO in more detail, we resolved the ultra-structure of the growth cone with dSTORM (Schneider et al. 2021a Fig. 4 A, Fig. S4 A). Hereby we showed that the number of phalloidin localizations per square-micrometer was unchanged (Schneider et al. 2021a Fig. 4 B), but that the number of actin bundles was strongly decreased in the CAP1-KO (Schneider et al. 2021a Fig. 4 C, Fig. S4 C). Furthermore, CAP1-KO growth cones did not exhibit a clearly defined C-domain (Schneider et al. 2021a Fig. 4 A, Fig. S4 A), which would normally be devoid of F-actin signal (Lowery and van Vactor 2009). Additionally, microtubules in the CAP1-KO were less bundled and more microtubules invaded the growth cone, which also more frequently reached the leading edge (Schneider et al. 2021a Fig. S4 B-D).

As CAP1-KO growth cones exhibited more lamellipodia, we treated these cells with an inhibitor of the Arp2/3 complex, which is important for building branched F-actin and hence affects lamellipodia and filopodia formation (Korobova and Svitkina 2008). CAP1-KO growth cones treated with the Arp2/3 inhibitor showed more filopodia in comparison to the untreated CAP1-KO growth cones, which was also obvious from the changes in the parameters circularity and solidity (Schneider et al. 2021a Fig. 4 D-F).

Taken together, CAP1 controlled size and morphology of the growth cone, as well as its motility. CAP2 was not important in any of these parameters. Additionally, we observed that CAP1 regulated F-actin architecture of the growth cone and indirectly orchestrated the microtubule cytoskeleton.

4.5 Both CAPs are functionally redundant in neurons

As we observed that loss of CAP1 severely impaired neuron connectivity, neuron differentiation and growth cone morphology, we focused on CAP1-KO neurons. To confirm that the observed phenotype was caused by the loss of CAP1, we overexpressed either GFP-CAP1 or myc-CAP1 and were able to rescue the CAP1-KO phenotype *in vitro* (Schneider et al. 2021c Fig. 5 B-G). As CAP1 and CAP2 share 60 % sequence similarity (Ono 2013), we overexpressed either GFP-CAP2 or myc-CAP2 in CAP1-KO neurons to test, whether CAP2 is able to compensate for the loss of CAP1. Quantification

of neuron development as well as neurite length and width in CAP1-KO neurons overexpressing CAP2 revealed a similar rescue compared to CAP1-KO neurons overexpressing CAP1 (Schneider et al. 2021c Fig. 5 B-G). However, overexpression of CAP2 only partially reduced growth cone size in the CAP1-KO neuron unlike overexpression of CAP1 (Schneider et al. 2021c Fig. 5 B-G).

In summary, we showed that overexpression of CAP2 compensated for the loss of CAP1 in neuronal development showing functional redundancy *in vitro.*

4.6 CAP1 controls growth cone guidance by regulating its F-actin dynamics

As CAP2 was dispensable for growth cone function, we examined the role of CAP1 in F-actin dynamics, the driving force of growth cone motility (Kerstein, Nichol IV, and Gomez 2015). In order to determine F-actin dynamics, neurons were transfected with GFP-actin and fluorescence recovery after photobleaching (FRAP) was measured (Schneider et al. 2021a Fig. 5 A, Movie S3+S4). Quantification of the fraction of dynamic actin that recovered within five minutes and the fluorescence half-recovery time revealed that CAP1-KO growth cones had less dynamic actin and needed longer to recover their fluorescence signal (Schneider et al. 2021a Fig. 5 B-D). These data revealed impaired actin turnover in growth cones from CAP1-KO neurons. In addition, neurons were transfected with GFP-tagged lifeAct to monitor retrograde F-actin flow in the growth cone (Flynn et al. 2012), which was about seven-fold reduced in the CAP1-KO neurons (Schneider et al. 2021a Fig. 5 E+F, Movie S5+S6).

Dynamic actin remodeling and regulation in the growth cone is essential for reacting to guidance cues and for proper steering of the axon (Omotade, Pollitt, and Zheng 2017). As we showed disturbed actin dynamics in CAP1-KO neurons, we investigated if this affected growth cone behavior in CAP1-KO neurons. For this reason, CTR and CAP1-KO neurons were either treated with the chemo-attractant brain-derived neurotrophic factor (BDNF) or the chemo-repellants ephrin A5, slit-1 or semaphorin 4D (Ye et al. 2019). BDNF increased growth cone size in CTR neurons and all three repellant cues increased the fraction of collapsed growth cones (Schneider et al. 2021a Fig. 6 A-D). In CAP1-KO neurons, growth cone size did not change upon treatment with BDNF and only ephrin 5, unlike slit-1 and semaphorin 4D, was able to increase the fraction of collapsed growth cones, but not to the same extend as in CTR neurons (Schneider et al. 2021a Fig. 6 A-D).

In summary, CAP1-KO neurons showed impaired F-actin dynamics in the growth cone, which was accompanied with absent or impaired responsiveness to various guidance cues.

4.7 CAP1's helical fold domain is crucial for growth cone function

After characterizing the phenotype in CAP1-KO growth cones, we aimed to get more insights into CAP1-dependent mechanisms in regulating F-actin dynamics in growth cones. To achieve this, we overexpressed mutant CAP1 variants to determine the domains relevant for regulating growth cone morphology (Schneider et al. 2021a Fig.7 A) and measured growth cone size as a readout.

First, we created deletion mutants where the entire N- (Δ1-213) or C-terminus (Δ319-474) was missing to see which part of the protein might be important for regulating growth cone size. Furthermore, we mutated specific amino acid residues known to be relevant for protein interaction (Kotila et al. 2019, 2018, Schneider et al. 2021a Fig.7 A). We mutated i) the helical fold domain (CAP1-HFD), ii) the proline-rich stretch 1 (CAP1-PP1, iii) the WASP homology domain 2 (CAP1-WH2) and iv) β-sheets within the CARP domain (CAP1-CARP) (Kotila et al. 2019; Rust et al. 2020; Shekhar et al. 2019; Chaudhry et al. 2010). In addition, we also deleted the last four amino acids of the C-terminus (Δ4CT), which were shown to be important for actin dynamics (Kotila et al. 2018). For direct comparison, we overexpressed GFP-CAP1, which fully rescued growth cone size in CAP1-KO neurons, but did not had any effect in CTR neurons (Schneider et al. 2021a Fig. 7 B+C).

After confirming that all CAP1 mutants were located in growth cones (Schneider et al. 2021a Fig. S3 A), we overexpressed both Δ1-213 and Δ319-474, which both failed to rescue growth cone size in the CAP1-KO neurons (Schneider et al. 2021a Fig. 7 C). To narrow down which domain is responsible in mediating growth cone function, we overexpressed the CAP1 mutants, where either the single domains were mutated or the last four amino acids of the C-terminus were missing. Interestingly, all CAP1 mutants except for the CAP1-HFD were able to rescue growth cone size in CAP1-KO neurons (Schneider et al. 2021a Fig. 7 C).

To sum this up, we showed that the domain enabling the interaction between CAP1 and cofilin1, was crucial to rescue the CAP1-KO phenotype in the growth cone.

4.8 CAP1 and Cofilin1 synergistically regulate growth cone function

Studies in yeast showed that the HFD is important for the interaction of CAP1 with cofilin1 as it enhances F-actin depolymerization (Kotila et al. 2019; Shekhar et al. 2019). In addition, we and others showed that ADF/cofilin is important for regulating growth cone size and motility in neurons (Gungabissoon and Bamburg 2003; Schneider et al. 2021b Fig. 6). Therefore we made use of the replating protocol described above (Schneider et al. 2021b Fig. 1) aiming to investigate whether there is a functional co-dependency between CAP1 and cofilin1 in regulating growth cone dynamics. For this, we cultured

neurons of mice with either floxed cofilin1 gene (Bellenchi et al. 2007), floxed CAP1 gene or a combination of both. Before plating, we transfected the cells with either mCherry-tagged Cre recombinase to knockout the respective proteins or mCherry-tagged catalytically inactive Cre recombinase (Kullmann et al. 2020a) as CTR. At DIV2, we obtained a full KO of CAP1 (Schneider et al. 2021a Fig. S5), replated the cells and performed analysis on the subsequent day.

First, we investigated F-actin dynamics by co-transfecting the neurons with GFP-actin and measuring the recovery rate of the fluorescence signal after photobleaching (Schneider et al. 2021a Fig. 8 A, Movie S7-S10). The replated CAP1$^{flx/flx}$ neurons expressing mCherry-tagged Cre recombinase (CAP1-KO) showed a comparable reduction in fluorescence recovery as the non-replated CAP1-KO neurons described above. Similar to the replated CAP1-KO, the replated cofilin1 floxed neurons expressing Cre (Cof1-KO) displayed a comparable impairment in fluorescence recovery as the CAP1-KO. In both conditions, the fraction of dynamic actin was reduced and the fluorescence recovery time was increased compared to CTR (Schneider et al. 2021a Fig. 8 B-D). Compared to the single KOs, the replated CAP1/cofilin1 floxed neurons expressing Cre (dKO) exhibited a stronger impairment in fluorescence recovery and a decreased fraction of dynamic actin (Schneider et al. 2021a Fig. 8 B+D). The same was true for the recovery time, which was slower than in the single KOs (Schneider et al. 2021a Fig. 8 C). When we overexpressed GFP-lifeAct and measured the retrograde F-actin flow, we again observed a severe decrease in velocity in all three KOs, similar to the CAP1-KO neurons described above (Schneider et al. 2021a Fig. 8 E+F, Movie S11-S14).

We also compared growth cone size between all four conditions and observed a comparable increase in both single KOs and in dKO neurons (Schneider et al. 2021a Fig. 9). Overexpression of GFP-CAP1 in Cof1-KO neurons (Schneider et al. 2021a Fig. 9 B) or GFP-cofilin1 in CAP1-KO neurons (Schneider et al. 2021a Fig. 7 C) were both not able to rescue growth cone size. Instead, overexpressing GFP-CAP1 in CAP1-KO neurons and GFP-cofilin1 in Cof1-KO neurons successfully rescued growth cone size in the respective single KO neurons (Schneider et al. 2021a Fig. 7 C, Fig. 9 B). Overexpression of a cofilin1 mutant that cannot bind to actin (Cof1-S3D) in Cof1-KO neurons, even slightly increased growth cone size (Schneider et al. 2021a Fig. 9 B). The fact that neither CAP1 nor cofilin1 could rescue growth cone size in the respective other single KO, let us hypothesize that both ABPs functionally interact in the growth cone. To confirm this interaction, we measured growth cone size in dKO neurons after overexpressing either GFP-CAP1, GFP-cofilin1 or both ABPs. Interestingly, overexpression of either GFP-CAP1 or GFP-cofilin1 could not rescue growth cone size

in dKO neurons. Only overexpression of both ABPs decreased growth cone size in dKO neurons to CTR levels (Schneider et al. 2021a Fig. 9 B). To investigate whether their interaction is only restricted in regulating the actin cytoskeleton, we overexpressed Δ1-213/CAP1-HFD together with wildtype cofilin1 and wildtype CAP1 with Cof1-S3D in dKO neurons. In both cases, we were not able to observe a rescue in growth cone size in dKO neurons (Schneider et al. 2021a Fig. 9 C).

In summary, only both wildtype proteins together were able to rescue the dKO and neither protein could compensate for the loss of the other.

4.9 Description of own contribution

For the publication 'Mutual functional dependence of cyclase-associated protein 1 (CAP1) and cofilin1 in neuronal actin dynamics and growth cone function' (*Prog Neurobiol.* 2021), I performed biochemical analysis, analysis of CAP1 localization *in vitro*, growth cone analysis (on fixed cells, live cell imaging, FRAP, retrograde F-actin flow measurements) in CAP1-KO neurons, retrograde flow measurements in replated neurons, analysis of neuron differentiation, pharmacological inhibition, growth cone guidance, DiI staining, rescue experiments in CAP1-KO neurons and selected rescue conditions of replated neurons (CAP1, cofilin1 and cofilin1-S3D in Cof1-KO, CAP1+cofilin1-S3D in dKO). I. Metz carried out histology and immunohistology on CAP1-KO brains. dSTORM data were generated and analyzed in cooperation with J. Winkelmeier and U. Endesfelder. Growth cone analysis, including rescue experiments (excluding the above mentioned) and FRAP of replated neurons was performed by the MD student T.A. Duong under my supervision. M. Rust and I wrote the article.

For the publication 'Neuron replating - a powerful and versatile approach to study early aspects of neuron differentiation' (*eNeuro* 2021), I performed analysis of neuron differentiation, growth cone guidance, retrograde F-actin flow measurements of plated and replated neurons, growth cone analysis and FRAP of plated neurons as well as analysis of growth cones of ADF/cofilin1 dKO neurons. Growth cone analysis and FRAP of replated neurons was carried out by the MD student T.A. Duong under my supervision. M. Rust and I wrote the article.

For the publication 'Functional redundancy of cyclase-associated proteins CAP1 and CAP2 in differentiating neurons' (*Cells* 2021), I performed Western blot analysis, analysis of neuron differentiation, analysis of fixed growth cone, life cell imaging, *in vitro* localization and rescue experiments. I. Metz carried out histology and immunohistology on CAP1-KO brains. S. Khudayberdiev designed and validated shRNAs. M. Rust and I designed the scheme and wrote the article.

5 Discussion

In this dissertation I aimed to uncover the role of CAPs in murine brain development, which I found to be enriched in growth cones and expressed during neuron differentiation. Analysis of KO brains and neurons for both CAP1 and CAP2 showed that CAP1 was important for neuronal circuitry formation *in vivo* and neuronal differentiation *in vitro*. Furthermore, this study identified CAP1 as a novel regulator of growth cone dynamics and consequently of axonal guidance. In addition, rescue experiments revealed a functional redundancy of CAP1 and CAP2 in neuron differentiation and a functional dependency of CAP1 and cofilin1 in regulating growth cone dynamics.

Since the discovery of CAPs 30 years ago (Field et al. 1990), recent studies unraveled the mechanism on actin regulation through CAPs by exploiting yeast cells or recombinant proteins (Kotila et al. 2019, 2018; Shekhar et al. 2019). In line with these studies, I found CAP1 to be essential in regulating actin dynamics in the growth cone. Despite the progress in depicting the physiological role of CAPs in different biological systems (Kepser et al. 2019; Kumar et al. 2016; Field et al. 2015; Peche et al. 2012), the physiological function in the brain remains largely unknown, which is partially caused by the lack of appropriate CAP1 mouse models (Jang et al. 2019). By generating conditional KO mice for CAP1 and exploiting systemic KO mice for CAP2, I showed that CAP1 was essential for neuronal circuitry formation *in vivo* and neuronal differentiation *in vitro*, whereas CAP2 was largely dispensable for both processes. This suggests that CAP2 is dispensable for early brain development and early neuron differentiation and might be important in later developmental stages, as it was shown that CAP2 is important for dendritic complexity and synapse physiology (Kumar et al. 2016; Pelucchi et al. 2020). Despite the fact that both CAPs are expressed during embryonic development, possible differences in their total protein amount could account for the lack of a CAP2-KO phenotype during embryonic brain development. Therefore, it remains to be shown whether CAP1 and CAP2 are expressed at equal or different amounts during brain development. Interestingly, other important brain developmental processes like neuronal progenitor proliferation or neuronal migration were unaffected in CAP1-KO brains, contrary to what is reported for other actin-regulating proteins such as cofilin1 or profilin1 (Bellenchi et al. 2007; Kullmann et al. 2020b; Wang et al. 2016). This suggests that CAP1 evolutionary developed a distinct function in axonal guidance and neuronal circuitry formation, which fits to a study in *Drosophila* that assigned a role for the CAP1 homologue capulet in axonal midline crossing (Wills et al. 2002).

Despite numerous studies uncovering the proteins implicated in controlling the growth cone machinery (Lowery and van Vactor 2009; Omotade, Pollitt, and Zheng 2017), our

knowledge is still incomplete. In line with a study that identified neuronal growth cone-associated proteins in the rat forebrain (Nozumia et al. 2009), I found endogenous CAP1 as well as overexpressed CAP2 to be enriched in the growth cone. In fact, my study adds CAP1 to the list of actin regulators in the growth cone machinery, as life imaging and pharmacological approaches revealed that CAP1 is relevant for regulating actin dynamics in the growth cone and that it acts downstream of guidance cues like ephrin A4, slit-1, semaphorin 4D or BDNF. Furthermore, while CAP1 regulated growth cone F-actin architecture, CAP2 was again dispensable for the growth cone machinery, postulating that CAP1 is the major player in early neuron differentiation and growth cone regulation. Enlarged growth cones, delayed neuronal differentiation and disturbed actin dynamics in CAP1-KO neurons support that hypothesis and are in line with studies showing the same effects when knocking out or down regulating ADF/cofilin, another important regulator of the F-actin treadmilling, in neurons (Garvalov et al. 2007; Tedeschi et al. 2019; Flynn et al. 2012). Furthermore, CAP1 KD in HeLa cells has been shown to result in increased lamellipodia size (Zhang et al. 2013) and CAP1 KD in PC12 cells resulted in decreased axonal and neurite length (Nozumia et al. 2009; Lu et al. 2011), similar to the enlarged growth cones and shorter neurites upon KO of CAP1 in neurons as shown in this study. Contrary to our findings, CAP1 KD in PC12 cells reduced growth cone size (Lu et al. 2011), which might be explained by the fact that PC12 cells and hippocampal neurons represent different biological systems (Westerink and Ewing 2008). Additionally, Lu and colleagues supplied their culture medium with nerve growth factor (NGF), which is absent in our medium. In our previous experiments we showed that CTR neurons treated with BDNF, a chemoattractant similar to NGF (Ye et al. 2019), increased growth cone size, similar to what is shown in a study from Meier and colleagues (Meier, Anastasiadou, and Knöll 2011). CAP1-KO neurons however were unresponsive to treatment with BDNF and did not change growth cone size. It is thus likely that in the study from Lu and colleagues CTR growth cones were larger because of a diverging responsiveness to NGF, compared to CAP1 KD neurons.

As CAP1 and CAP2 share 60 % sequence similarity (Ono 2013) and as both are expressed in neurons, it is thus likely that both proteins might be functional redundant, despite the fact that CAP2-KO neurons displayed no defects in neuron differentiation or growth cone function. Still, our rescue experiments support this hypothesis as they showed that overexpression of CAP2 at least partially compensated for the loss of CAP1. Moreover, it was shown in dendritic spines that CAP2 interacts with cofilin1 to regulate actin dynamics (Pelucchi et al. 2020), similar to yeast studies showing actin regulation through CAP together with cofilin (Kotila et al. 2019; Shekhar et al. 2019; Rust et al. 2020). This suggests that CAP2 is partially redundant, but might be regulated differently

compared to CAP1. Furthermore, as only overexpression of GFP-CAP2 rescued growth cone size in CAP1-KO neurons, it is again likely that differences in total amounts of CAP1 and CAP2 account for the differences in CAP1-KO and CAP2-KO neurons. However, further analysis on neurons with a double KO for both CAP1 and CAP2 are required to investigate the functional redundancy of CAP1 and CAP2 in regulating early neuron differentiation. Moreover, additional screens for proteins regulating both CAPs need to be carried out to shed light on their function during neuron differentiation.

Given that the loss of ADF/cofilin and CAP1 in neurons show comparable defects in growth cone size and motility as well as actin dynamics, it is likely that CAP1 is involved in regulating depolymerization of F-actin in neurons. Furthermore, as overexpression of cofilin1 or CAP1-HFD were not able to rescue the CAP1 growth cone phenotype, I hypothesized that the interaction of CAP1 with cofilin1 is relevant for controlling F-actin dynamics in the growth cone. Indeed, a genetic approach revealed that KOs of either CAP1, cofilin1 or both ABPs resulted in similar increase in growth cone size, similar disturbed actin dynamics and only overexpression of both CAP1 and cofilin1 in the dKO reduced growth cone size to CTR levels. Moreover, overexpression of cofilin1 together with Δ1-213 or CAP1-HFD or CAP1 together with cofilin1-S3A were unable to rescue the dKO. This shows that not only CAP1 and cofilin1 synergistically regulate actin dynamics in the growth cone, but that they are also dependent on each other. Cofilin1 is considered to be a key regulator in actin dynamics within growth cones (Gungabissoon and Bamburg 2003; Omotade, Pollitt, and Zheng 2017; Schneider et al. 2021b) and several studies demonstrated the importance of cofilin1 in neuronal actin dynamics (Bellenchi et al. 2007; Wolf et al. 2015; Rust and Maritzen 2015; Flynn et al. 2012). Similar to CAP1, cofilin1 is implicated in growth cone motility (Dent, Gupton, and Gertler 2011; Zhang et al. 2019; Gomez and Letourneau 2015) and acts as a downstream target of many pathways relevant for axonal guidance (Hsieh 2006; Piper et al. 2006; Grintsevich et al. 2016). Therefore, a cooperation of CAP1 and cofilin1 in regulating the growth cone is in line with the above mentioned studies and with studies in yeast that proposed a model for the interaction of CAP and cofilin in depolymerizing F-actin (Kotila et al. 2019; Shekhar et al. 2019). More important, a recent study implicated cofilin1 to be crucial for axon regeneration in the central nervous system, by regulating actin dynamics in the growth cone (Tedeschi et al. 2019). As my study showed a functional co-dependency of CAP1 and cofilin1, it would be interesting to investigate whether CAP1 similarly plays a role in axon regeneration in the central nervous system. Moreover, it would be exciting to address the question, whether CAP1 is needed for cofilin1-mediated axon regeneration. Several publications used replating of neurons as paradigm for axon regeneration (Lee et al. 2020; Saijilafu et al. 2013; Frey et al. 2015). As I established a

protocol to replate hippocampal neurons, where I validated that replated neurons differentiate normally, this would be a good approach to study whether CAP1 is relevant in axonal regeneration of neurons of the central nervous system. If this experiment hints towards a role of CAP1 in axon regeneration, it would then be exciting to further validate this hypothesis *in vivo*.

Besides the interaction with cofilin, studies in yeast also showed that the CARP domain of CAP can promote the nucleotide exchange on G-actin (Kotila et al. 2018). However in our study, CAP1-CARP was able to rescue growth cone size in CAP1-KO neurons, suggesting that nucleotide exchange on G-actin might be covered by other ABPs like profilin1 (Omotade, Pollitt, and Zheng 2017; Vitriol and Zheng 2012). Interestingly, pharmacological inhibition of the Arp2/3 complex partially restored the hand-shaped appearance of the growth cone in CAP1-KO neurons, suggesting an increase in Arp2/3 complex activity in the CAP1-KO. In fact, this inverse behavior of actin depolymerizing factors and the Arp2/3 complex is already hypothesized in dendritic spines and would thus serve as a likely explanation for our observations in the growth cone (Spence and Soderling 2015). However, it was shown that the abundance of profilin1 at the leading edge determines the activity of the Arp2/3 complex and the shape of migrating cells (Skruber et al. 2020). If G-actin nucleotide exchange upon loss of CAP1 is mainly mediated by profilin1, this could increase the abundance of profilin1 at the leading edge of the growth cone and therefore influences its shape in an Arp2/3 complex-related manner. Further experiments manipulating profilin1 activity in a CAP1-KO background would be interesting as it would cover two questions: First, if profilin1 supplies the growth cone with polymerization-competent G-actin in the absence of CAP1. Second, as profilin1 and CAP1 were shown to interact with each other (Ono 2013; Rust et al. 2020), if they are also functionally dependent.

Besides cofilin1 and profilin1, CAP1 can also interact with various different proteins via its N-terminal half or its proline-rich stretches (Rust et al. 2020). For example, it was shown that CAP1 inhibits INF2 activity and hence actin polymerization (A et al. 2019) and together with twinfilin1 depolymerizes F-actin (Hilton et al. 2018). This could be an additional reason why the growth cones in the CAP1-KO were enlarged as actin polymerization through INF2 was not inhibited and similar to cofilin1, F-actin depolymerization through twinfilin1 was not possible or slower. Therefore, it would be interesting to look for additional potential interaction partners of CAP1 in neurons and manipulate their activity in a CAP1-KO background.

Microtubule disorganization in the CAP1-KO growth cones could be also explained by a potential interaction between CAP1 and tubulin. However, it is more likely that this represents a secondary effect caused by a less dynamic T zone and missing F-actin

strands, which are both needed for constraining microtubules in the growth cone neck (Burnette et al. 2008; Geraldo and Gordon-Weeks 2009) and for regulating microtubules invasion and their length in the growth cone (Sánchez-Huertas et al. 2020; Cammarata, Bearce, and Lowery 2016; Coles and Bradke 2015; Biswas and Kalil 2017).

Further investigations are needed addressing the question how CAP1 is regulated during axonal outgrowth and guidance. Until now, two protein kinases are known to phosphorylate CAP1, namely CDK5 (Haitao Zhang et al. 2019) and GSK3 (Wu et al. 2019; Xie et al. 2018; Zhou, Zhang, and Field 2014), whereof the latter one is already described in regulating neuronal polarity, axonal outgrowth and guidance (Meli, Weisová, and Propst 2015; Hur et al. 2011; Jiang et al. 2005). Only one study so far described a regulatory mechanism of the CAP homologue capulet downstream of robo/slit signaling in *Drosophila* via the tyrosine kinase ABL1 that directly interacts with capulet (Wills et al. 2002). Studies in mice or murine neurons *in vitro* should investigate whether CAP1 also acts downstream of robo/slit or other known guidance cues (Ye et al. 2019).

To sum up, I found CAP1 to be an important actin regulator of the growth cone and gave new insights on actin regulation via CAP1-cofilin1 interaction. Furthermore, I propose a model in which CAP1 acts as a hub for interacting with signaling pathways and to mediate actin dynamics in the growth cone. Hence, this dissertation gives a new perspective on growth cone function, axon guidance and could provide new concepts in curing neurological disorders or axonal damage.

References

A, Mu, Tak Shun Fung, Arminja N. Kettenbach, Rajarshi Chakrabarti, and Henry N. Higgs. 2019. "A Complex Containing Lysine-Acetylated Actin Inhibits the Formin INF2." *Nature Cell Biology* 21 (5): 592–602. https://doi.org/10.1038/s41556-019-0307-4.

Aspit, Liam, Aviva Levitas, Sharon Etzion, Hanna Krymko, Leonel Slanovic, Raz Zarivach, Yoram Etzion, and Ruti Parvari. 2019. "CAP2 Mutation Leads to Impaired Actin Dynamics and Associates with Supraventricular Tachycardia and Dilated Cardiomyopathy." *Journal of Medical Genetics* 56 (4): 228–35. https://doi.org/10.1136/JMEDGENET-2018-105498.

Balcer, Heath I., Anya L. Goodman, Avital A. Rodal, Ellen Smith, Jamie Kugler, John E. Heuser, and Bruce L. Goode. 2003. "Coordinated Regulation of Actin Filament Turnover by a High-Molecular- Weight Srv2/CAP Complex, Cofilin, Profilin, and Aip1." *Current Biology* 13 (24): 2159–69. https://doi.org/10.1016/j.cub.2003.11.051.

Bamburg, J R, A McGough, and S Ono. 1999. "Putting a New Twist on Actin: ADF/Cofilins Modulate Actin Dynamics." *Trends in Cell Biology* 9 (9): 364–70. https://doi.org/10.1016/S0962-8924(99)01619-0.

Bartheld, Christopher S. von, Jami Bahney, and Suzana Herculano-Houzel. 2016. "The Search for True Numbers of Neurons and Glial Cells in the Human Brain: A Review of 150 Years of Cell Counting." *Journal of Comparative Neurology*. Wiley-Liss Inc. https://doi.org/10.1002/cne.24040.

Battum, Eljo Y Van, Sara Brignani, and R Jeroen Pasterkamp. 2015. "Axon Guidance Proteins in Neurological Disorders." *The Lancet Neurology* 14 (5): 532–46. https://doi.org/10.1016/S1474-4422(14)70257-1.

Baum, Jake, Anthony T Papenfuss, Buzz Baum, Terence P Speed, and Alan F Cowman. 2006. "Regulation of Apicomplexan Actin-Based Motility." *Nature Reviews. Microbiology* 4 (8): 621–28. https://doi.org/10.1038/nrmicro1465.

Bellenchi, Gian Carlo, Christine B Gurniak, Emerald Perlas, Silvia Middei, Martine Ammassari-teule, and Walter Witke. 2007. "N-Cofilin Is Associated with Neuronal Migration Disorders and Cell Cycle Control in the Cerebral Cortex." *Genes & Developement*, 2347–57. https://doi.org/10.1101/gad.434307.genetic.

Bertling, Enni, Omar Quintero-Monzon, Pieta K. Mattila, Bruce L. Goode, and Pekka Lappalainen. 2007. "Mechanism and Biological Role of Profilin-Srv2/CAP Interaction." *Journal of Cell Science* 120 (7): 1225–34. https://doi.org/10.1242/JCS.000158.

Bertling, Henni, Pirta Hotulainen, Pieta K. Mattila, Tanja Matilainen, Marjo Salminen, and Pekka Lappalainen. 2004. "Cyclase-Associated Protein 1 (CAP1) Promotes Cofilin- Induced Actin Dynamics in Mammalian Nonmuscle Cells." *Molecular Biology of the Cell* 15 (May). https://doi.org/10.1091/mbc.E04.

Biswas, Sayantanee, and Katherine Kalil. 2017. "The Microtubule-Associated Protein Tau Mediates the Organization of Microtubules and Their Dynamic Exploration of Actin-Rich Lamellipodia and Filopodia of Cortical Growth Cones." *The Journal of Neuroscience* 38 (2): 291–307. https://doi.org/10.1523/jneurosci.2281-17.2017.

Braun, Attila, Attila Aszódi, Heide Hellebrand, Alejandro Berna, Reinhard Fässler, and Oliver Brandau. 2002. "Genomic Organization of Profilin-III and Evidence for a Transcript Expressed Exclusively in Testis." *Gene* 283 (1–2): 219–25. https://doi.org/10.1016/S0378-1119(01)00855-1.

Bridgman, Paul C., Sonya Dave, Clara F. Asnes, Antonella N. Tullio, and Robert S. Adelstein. 2001. "Myosin IIB Is Required for Growth Cone Motility." *Journal of Neuroscience* 21 (16): 6159–69. https://doi.org/10.1523/jneurosci.21-16-06159.2001.

Burnette, Dylan T., Lin Ji, Andrew W. Schaefer, Nelson A. Medeiros, Gaudenz Danuser, and Paul Forscher. 2008. "Myosin II Activity Facilitates Microtubule Bundling in the Neuronal Growth Cone Neck." *Developmental Cell* 15 (1): 163–69. https://doi.org/10.1016/j.devcel.2008.05.016.

Cammarata, Garrett M., Elizabeth A. Bearce, and Laura Anne Lowery. 2016. "Cytoskeletal Social Networking in the Growth Cone: How +TIPs Mediate Microtubule-Actin Cross-Linking to Drive Axon Outgrowth and Guidance." *Cytoskeleton* 73 (9): 461–76. https://doi.org/10.1002/cm.21272.

Chaudhry, Faisal, Kristin Little, Lou Talarico, Omar Quintero-Monzon, and Bruce L. Goode. 2010. "A Central Role for the WH2 Domain of Srv2/CAP in Recharging Actin Monomers to Drive Actin Turnover in Vitro and in Vivo." *Cytoskeleton (Hoboken, N.J.)* 67 (2): 120. https://doi.org/10.1002/CM.20429.

Chédotal, Alain, and Linda J. Richards. 2010. "Wiring the Brain: The Biology of Neuronal Guidance." *Cold Spring Harbor Perspectives in Biology* 2 (6): 1–17. https://doi.org/10.1101/cshperspect.a001917.

Coles, Charlotte H, and Frank Bradke. 2015. "Coordinating Neuronal Actin – Microtubule Dynamics." *Current Biology* 25: 677–91. https://doi.org/10.1016/j.cub.2015.06.020.

Colpan, Mert, Jessika Iwanski, and Carol C. Gregorio. 2021. "CAP2 Is a Regulator of Actin Pointed End Dynamics and Myofibrillogenesis in Cardiac Muscle." *Communications Biology 2021 4:1* 4 (1): 1–15. https://doi.org/10.1038/s42003-021-01893-w.

Craig, Erin M. 2018. "Model for Coordination of Microtubule and Actin Dynamics in Growth Cone Turning." *Frontiers in Cellular Neuroscience* 12 (October): 1–7. https://doi.org/10.3389/fncel.2018.00394.

Craig, Erin M., David Van Goor, Paul Forscher, and Alex Mogilner. 2012. "Membrane Tension, Myosin Force, and Actin Turnover Maintain Actin Treadmill in the Nerve Growth Cone." *Biophysical Journal* 102 (7): 1503–13. https://doi.org/10.1016/j.bpj.2012.03.003.

Craig, Erin M., Jonathan Stricker, Margaret Gardel, and Alex Mogilner. 2015. "Model for Adhesion Clutch Explains Biphasic Relationship between Actin Flow and Traction at the Cell Leading Edge." *Physical Biology* 12 (3): 1–15. https://doi.org/10.1088/1478-3975/12/3/035002.

Debanne, Dominique, Emilie Campanac, Andrzej Bialowas, Edmond Carlier, and GISÈLE Alcaraz. 2011. "Axon Physiology." *Physiological Reviews* 91 (2): 555–602. https://doi.org/10.1152/physrev.00048.2009.

Dent, Erik W, Stephanie L Gupton, and Frank B Gertler. 2011. "The Growth Cone Cytoskeleton in Axon Outgrowth and Guidance." *Cold Spring Harb Perspect Biol*. https://doi.org/10.1101/cshperspect.a001800.

Dotti, CG, CA Sullivan, and GA Banker. 1988. "The Establishment of Polarity by Hippocampal Neurons in Culture." *The Journal of Neuroscience* 8 (4): 1454–68. https://doi.org/10.1523/jneurosci.08-04-01454.1988.

Dudanova, Irina, and Rüdiger Klein. 2013. "Integration of Guidance Cues: Parallel Signaling and Crosstalk." *Trends in Neurosciences* 36 (5): 295–304. https://doi.org/10.1016/j.tins.2013.01.007.

Fass, Joseph, Scott Gehler, Patrick Sarmiere, Paul Letourneau, and James R. Bamburg. 2004. "Regulating Filopodial Dynamics through Actin-Depolymerizing Factor/Cofilin." *Anatomical Science International*. Blackwell Publishing. https://doi.org/10.1111/j.1447-073x.2004.00087.x.

Field, J., A. Vojtek, R. Ballester, G. Bolger, J. Colicelli, K. Ferguson, J. Gerst, et al. 1990. "Cloning and Characterization of CAP, the S. Cerevisiae Gene Encoding the 70 Kd Adenylyl Cyclase-Associated Protein." *Cell* 61 (2): 319–27. https://doi.org/10.1016/0092-8674(90)90812-S.

Field, Jeffrey, Diana Z. Ye, Manasi Shinde, Fang Liu, Kurt J. Schillinger, Minmin Lu, Tao Wang, et al. 2015. "CAP2 in Cardiac Conduction, Sudden Cardiac Death and Eye Development." *Scientific Reports* 5: 1–16. https://doi.org/10.1038/srep17256.

Flynn, Kevin C., Farida Hellal, Dorothee Neukirchen, Sonja Jacob, Sabina Tahirovic, Sebastian Dupraz, Sina Stern, et al. 2012. "ADF/Cofilin-Mediated Actin Retrograde Flow Directs Neurite Formation in the Developing Brain." *Neuron* 76 (6): 1091–1107. https://doi.org/10.1016/j.neuron.2012.09.038.

Földi, István, Szilárd Szikora, and József Mihály. 2017. "Formin' Bridges between Microtubules and Actin Filaments in Axonal Growth Cones." *Neural Regeneration Research*. Wolters Kluwer Medknow Publications. https://doi.org/10.4103/1673-5374.221148.

Freeman, Nancy L., and Jeffrey Field. 2000. "Mammalian Homolog of the Yeast Cyclase Associated Protein, CAP/Srv2p, Regulates Actin Filament Assembly." *Cell Motility and the Cytoskeleton* 45 (2): 106–20. https://doi.org/10.1002/(SICI)1097-0169(200002)45:2<106::AID-CM3>3.0.CO;2-3.

Frey, E., V. Valakh, S. Karney-Grobe, Y. Shi, J. Milbrandt, and A. DiAntonio. 2015. "An in Vitro Assay to Study Induction of the Regenerative State in Sensory Neurons." *Experimental Neurology* 263 (January): 350–63. https://doi.org/10.1016/j.expneurol.2014.10.012.

Garvalov, Boyan K., Kevin C. Flynn, Dorothee Neukirchen, Liane Meyn, Nicole Teusch, Xunwei Wu, Cord Brakebusch, James R. Bamburg, and Frank Bradke. 2007. "Cdc42 Regulates Cofilin during the Establishment of Neuronal Polarity." *Journal of Neuroscience* 27 (48): 13117–29. https://doi.org/10.1523/JNEUROSCI.3322-07.2007.

Gehler, Scott, Alisa E. Shaw, Patrick D. Sarmiere, James R. Bamburg, and Paul C. Letourneau. 2004. "Brain-Derived Neurotrophic Factor Regulation of Retinal Growth Cone Filopodial Dynamics Is Mediated through Actin Depolymerizing Factor/Cofilin." *Journal of Neuroscience* 24 (47): 10741–49. https://doi.org/10.1523/JNEUROSCI.2836-04.2004.

Geraldo, Sara, and Phillip R. Gordon-Weeks. 2009. "Cytoskeletal Dynamics in Growth-Cone Steering." *Journal of Cell Science* 122 (20): 3595–3604. https://doi.org/10.1242/jcs.042309.

Ghate, Ketakee, Sampada P. Mutalik, Lakshmi Kavitha Sthanam, Shamik Sen, and Aurnab Ghose. 2020. "Fmn2 Regulates Growth Cone Motility by Mediating a Molecular Clutch to Generate Traction Forces." *Neuroscience* 448 (November): 160–71. https://doi.org/10.1016/j.neuroscience.2020.09.046.

Goldschmidt-Clermont, P J, M I Furman, D Wachsstock, D Safer, V T Nachmias, and Thomas D Pollard. 1992. "The Control of Actin Nucleotide Exchange by Thymosin Beta 4 and Profilin. A Potential Regulatory Mechanism for Actin Polymerization in Cells." *Mol Biol Cell* 3 (9): 1015–24. https://doi.org/10.1091/mbc.3.9.1015.

Goley, Erin D., and Matthew D. Welch. 2006. "The ARP2/3 Complex: An Actin Nucleator Comes of Age." *Nature Reviews Molecular Cell Biology*. Nature Publishing Group. https://doi.org/10.1038/nrm2026.

Gomez, Timothy M., and Paul C. Letourneau. 2015. "Actin Dynamics in Growth Cone Motility and Navigation." *Journal of Neurochemistry* 129 (2): 221–34. https://doi.org/10.1161/ATVBAHA.114.303112.ApoA-I.

Gonçalves-Pimentel, Catarina, Rita Gombos, József Mihály, Natalia Sánchez-Soriano, and Andreas Prokop. 2011. "Dissecting Regulatory Networks of Filopodia Formation in a Drosophila Growth Cone Model." *PLoS ONE* 6 (3): 18340. https://doi.org/10.1371/journal.pone.0018340.

Grintsevich, Elena E., Hunkar Gizem Yesilyurt, Shannon K. Rich, Ruei-Jiun Hung, Jonathan R. Terman, and Emil Reisler. 2016. "F-Actin Dismantling through a Redox-Driven Synergy between Mical and Cofilin." *Nature Cell Biology 2016 18:8* 18 (8): 876–85. https://doi.org/10.1038/ncb3390.

Gungabissoon, Ravine A., and James R. Bamburg. 2003. "Regulation of Growth Cone Actin Dynamics by ADF/Cofilin." In *Journal of Histochemistry and Cytochemistry*, 51:411–20. Histochemical Society Inc. https://doi.org/10.1177/002215540305100402.

Gurniak, Christine B., Frédéric Chevessier, Melanie Jokwitz, Friederike Jönsson, Emerald Perlas, Hendrik Richter, Gabi Matern, et al. 2014. "Severe Protein Aggregate Myopathy in a Knockout Mouse Model Points to an Essential Role of Cofilin2 in Sarcomeric Actin Exchange and Muscle Maintenance." *European Journal of Cell Biology* 93 (5–6): 252–66. https://doi.org/10.1016/J.EJCB.2014.01.007.

Hasan, Rokib, and Guo Lei Zhou. 2019. "The Cytoskeletal Protein Cyclase-Associated Protein 1 (CAP1) in Breast Cancer: Context-Dependent Roles in Both the Invasiveness and Proliferation of Cancer Cells and Underlying Cell Signals." *International Journal of Molecular Sciences*. MDPI AG. https://doi.org/10.3390/ijms20112653.

Hilton, Denise M., Rey M. Aguilar, Adam B. Johnston, and Bruce L. Goode. 2018. "Species-Specific Functions of Twinfilin in Actin Filament Depolymerization." *Journal of Molecular Biology* 430 (18): 3323–36. https://doi.org/10.1016/j.jmb.2018.06.025.

Hsieh, S. H.-K. 2006. "Myelin-Associated Inhibitors Regulate Cofilin Phosphorylation and Neuronal Inhibition through LIM Kinase and Slingshot Phosphatase." *Journal of Neuroscience* 26 (3): 1006–15. https://doi.org/10.1523/jneurosci.2806-05.2006.

Hur, Eun Mi, Saijilafu, Byoung Dae Lee, Seong Jin Kim, Wen Lin Xu, and Feng Quan Zhou. 2011. "GSK3 Controls Axon Growth via CLASP-Mediated Regulation of Growth Cone Microtubules." *Genes and Development* 25 (18): 1968–81. https://doi.org/10.1101/gad.17015911.

Iuliano, Olga, Azumi Yoshimura, Marie Thérèse Prospéri, René Martin, Hans Joachim Knölker, and Evelyne Coudrier. 2018. "Myosin 1b Promotes Axon Formation by Regulating Actin Wave Propagation and Growth Cone Dynamics." *Journal of Cell Biology* 217 (6): 2033–46. https://doi.org/10.1083/jcb.201703205.

Iwanski, Jessika, Carol C. Gregorio, and Mert Colpan. 2021. "Redefining Actin Dynamics of the Pointed-End Complex in Striated Muscle." *Trends in Cell Biology*. Elsevier. https://doi.org/10.1016/j.tcb.2021.06.006.

Izzi, L., and F. Charron. 2011. "Midline Axon Guidance and Human Genetic Disorders." *Clinical Genetics* 80 (3): 226–34. https://doi.org/10.1111/j.1399-0004.2011.01735.x.

Jang, Hyun-Duk, Sang Eun Lee, Jimin Yang, Hyun-Chae Lee, Dasom Shin, Hwan Lee, Jaewon Lee, et al. 2019. "Cyclase-Associated Protein 1 Is a Binding Partner of Proprotein Convertase Subtilisin/Kexin Type-9 and Is Required for the Degradation of Low-Density Lipoprotein Receptors by Proprotein Convertase Subtilisin/Kexin Type-9." *European Heart Journal*, 1–15. https://doi.org/10.1093/eurheartj/ehz566.

Jiang, Hui, Wei Guo, Xinhua Liang, and Yi Rao. 2005. "Both the Establishment and the Maintenance of Neuronal Polarity Require Active Mechanisms: Critical Roles of GSK-3β and Its Upstream Regulators." *Cell* 120 (1): 123–35. https://doi.org/10.1016/j.cell.2004.12.033.

Jin, Zhe-Long, Yu-Jin Jo, Suk Namgoong, and Nam-Hyung Kim. 2018. "CAP1-Mediated Actin Cycling via ADF/Cofilin Proteins Is Essential for Asymmetric Division in Mouse Oocytes." *Journal of Cell Science* 131 (23): jcs222356. https://doi.org/10.1242/jcs.222356.

Kepser, Lara Jane, Fidan Damar, Teresa De Cicco, Christine Chaponnier, Tomasz J. Prószynski, Axel Pagenstecher, and Marco B. Rust. 2019. "CAP2 Deficiency Delays Myofibril Actin Cytoskeleton Differentiation and Disturbs Skeletal Muscle Architecture and Function." *Proceedings of the National Academy of Sciences of the United States of America* 116 (17): 8397–8402. https://doi.org/10.1073/pnas.1813351116.

Kerstein, Patrick C., Robert H. Nichol IV, and Timothy M. Gomez. 2015. "Mechanochemical Regulation of Growth Cone Motility." *Frontiers in Cellular Neuroscience* 9 (July): 1–16. https://doi.org/10.3389/fncel.2015.00244.

Kim, You Seung, Senta Furman, Helen Sink, and Mark F.A. Vanberkum. 2001. "Calmodulin and Profilin Coregulate Axon Outgrowth in Drosophila." *Journal of Neurobiology* 47 (1): 26–38. https://doi.org/10.1002/neu.1013.

Korobova, Farida, and Tatyana Svitkina. 2008. "Arp2/3 Complex Is Important for Filopodia Formation, Growth Cone Motility, and Neuritogenesis in Neuronal Cells." *Molecular Biology of the Cell* 19 (April): 1561–74. https://doi.org/10.1091/mbc.e07-09-0964.

Koser, David E., Amelia J. Thompson, Sarah K. Foster, Asha Dwivedy, Eva K. Pillai, Graham K. Sheridan, Hanno Svoboda, et al. 2016. "Mechanosensing Is Critical for Axon Growth in the Developing Brain." *Nature Neuroscience* 19 (12): 1592–98. https://doi.org/10.1038/nn.4394.

Kotila, Tommi, Konstantin Kogan, Giray Enkavi, Siyang Guo, Ilpo Vattulainen, Bruce L. Goode, and Pekka Lappalainen. 2018. "Structural Basis of Actin Monomer Re-Charging by Cyclase-Associated Protein." *Nature Communications* 9 (1): 1–12. https://doi.org/10.1038/s41467-018-04231-7.

Kotila, Tommi, Hugo Wioland, Giray Enkavi, Konstantin Kogan, Ilpo Vattulainen, Antoine Jégou, Guillaume Romet-Lemonne, and Pekka Lappalainen. 2019. "Mechanism of Synergistic Actin Filament Pointed End Depolymerization by Cyclase-Associated Protein and Cofilin." *Nature Communications*, 1–14. https://doi.org/10.1038/s41467-019-13213-2.

Kullmann, Jan A., Niraj Trivedi, Danielle Howell, Christophe Laumonnerie, Vien Nguyen, Shalini S. Banerjee, Daniel R. Stabley, Abbas Shirinifard, David H. Rowitch, and David J. Solecki. 2020. "Oxygen Tension and the VHL-Hif1α Pathway Determine Onset of Neuronal Polarization and Cerebellar Germinal Zone Exit." *Neuron* 106 (4): P607-623.E5. https://doi.org/10.1016/j.neuron.2020.02.025.

Kullmann, Jan A, Sophie Meyer, Fabrizia Pipicelli, Christina Kyrousi, Felix Schneider, Nora Bartels, Silvia Cappello, and Marco B Rust. 2020. "Profilin1-Dependent F-Actin Assembly Controls Division of Apical Radial Glia and Neocortex Development." *Cerebral Cortex* 30 (6): 3467–82. https://doi.org/10.1093/cercor/bhz321.

Kumar, Atul, Lars Paeger, Kosmas Kosmas, Peter Kloppenburg, Angelika A. Noegel, and Vivek S. Peche. 2016. "Neuronal Actin Dynamics, Spine Density and Neuronal Dendritic Complexity Are Regulated by CAP2." *Frontiers in Cellular Neuroscience* 10 (July): 1–17. https://doi.org/10.3389/fncel.2016.00180.

Kundu, Tanushree, Priyanka Dutta, Dhriti Nagar, Sankar Maiti, and Aurnab Ghose. 2021. "Coupling of Dynamic Microtubules to F-Actin by Fmn2 Regulates Chemotaxis of Neuronal Growth Cones." *Journal of Cell Science*, June. https://doi.org/10.1242/jcs.252916.

Le, Shimin, Miao Yu, Alexander Bershadsky, and Jie Yan. 2020. "Mechanical Regulation of Formin-Dependent Actin Polymerization." *Seminars in Cell and Developmental Biology*. Elsevier Ltd. https://doi.org/10.1016/j.semcdb.2019.11.016.

Lee, Chi Wai, Eric A. Vitriol, Sangwoo Shim, Ariel L. Wise, Radhi P. Velayutham, and James Q. Zheng. 2013. "Dynamic Localization of G-Actin during Membrane Protrusion in Neuronal Motility." *Current Biology* 23 (12): 1046–56. https://doi.org/10.1016/j.cub.2013.04.057.

Lee, Jinyoung, Jung Eun Shin, Bohm Lee, Hyemin Kim, Yewon Jeon, Seung Hyun Ahn, Sung Wook Chi, and Yongcheol Cho. 2020. "The Stem Cell Marker Prom1 Promotes Axon Regeneration by Down-Regulating Cholesterol Synthesis via Smad Signaling." *Proceedings of the National Academy of Sciences of the United States of America* 117 (27): 15955–66. https://doi.org/10.1073/pnas.1920829117.

Liang, Huixuan, Simon Hippenmeyer, and H. Troy Ghashghaei. 2012. "A Nestin-Cre Transgenic Mouse Is Insufficient for Recombination in Early Embryonic Neural Progenitors." *Biology Open* 1 (12): 1200–1203. https://doi.org/10.1242/bio.20122287.

Lin, Chi Hung, E. M. Espreafico, M.S. Mooseker, and P. Forscher. 1996. "Myosin Drives Retrograde F-Actin Growth Cones." *Neuron* 16: 769–782. https://doi.org/10.1016/s0896-6273(00)80097-5.

Lin, Chi Hung, and Paul Forscher. 1995. "Growth Cone Advance Is Inversely Proportional to Retrograde F-Actin Flow." *Neuron* 14 (4): 763–71. https://doi.org/10.1016/0896-6273(95)90220-1.

Lowery, Laura Anne, and David van Vactor. 2009. "The Trip of the Tip: Understanding the Growth Cone Machinery." *Nature Reviews Molecular Cell Biology* 10 (5): 332–43. https://doi.org/10.1038/nrm2679.

Lu, Jia, Motohiro Nozumi, Kosei Takeuchi, Haruki Abe, and Michihiro Igarashi. 2011. "Expression and Function of Neuronal Growth-Associated Proteins (NGAPs) in PC12 Cells." *Neuroscience Research* 70 (1): 85–90. https://doi.org/10.1016/j.neures.2011.01.006.

Makkonen, Maarit, Enni Bertling, Natalia A. Chebotareva, Jake Baum, and Pekka Lappalainen. 2012. "Mammalian and Malaria Parasite Cyclase-Associated Proteins Catalyze Nucleotide Exchange on G-Actin through a Conserved Mechanism." *Journal of Biological Chemistry* 288 (2): 984–94. https://doi.org/10.1074/jbc.m112.435719.

Marsick, Bonnie M., Kevon C. Flynn, Miguel Santiago-Medina, James R. Bamburg, and Paul C Letourneau. 2011. "Activation of ADF/Cofilin Mediates Attractive Growth Cone Turning toward Nerve Growth Factor and Netrin-1." *Developmental Neurobiology* 70 (8): 565–88. https://doi.org/10.1002/dneu.20800.Activation.

Matusek, Tamás, Rita Gombos, Anita Szécsényi, Natalia Sánchez-Soriano, Ágnes Czibula, Csilla Pataki, Anita Gedai, Andreas Prokop, István Raskó, and József Mihály. 2008. "Formin Proteins of the DAAM Subfamily Play a Role during Axon Growth." *Journal of Neuroscience* 28 (49): 13310–19. https://doi.org/10.1523/JNEUROSCI.2727-08.2008.

Meberg, P. J. 2000. "Signal-Regulated ADF/Cofilin Activity and Growth Cone Motility." *Molecular Neurobiology* 21 (1–2): 97–107. https://doi.org/10.1385/mn:21:1-2:097.

Meberg, Peter J., and James R. Bamburg. 2000. "Increase in Neurite Outgrowth Mediated by Overexpression of Actin Depolymerizing Factor." *Journal of Neuroscience* 20 (7): 2459–69. https://doi.org/10.1523/jneurosci.20-07-02459.2000.

Medeiros, Nelson A., Dylan T. Burnette, and Paul Forscher. 2006. "Myosin II Functions in Actin-Bundle Turnover in Neuronal Growth Cones." *Nature Cell Biology* 8 (3): 215–26. https://doi.org/10.1038/ncb1367.

Meier, Christin, Sofia Anastasiadou, and Bernd Knöll. 2011. "Ephrin-A5 Suppresses Neurotrophin Evoked Neuronal Motility, ERK Activation and Gene Expression." *PLoS ONE* 6 (10). https://doi.org/10.1371/journal.pone.0026089.

Meli, Rajeshwari, Petronela Weisová, and Friedrich Propst. 2015. "Repulsive Axon Guidance by Draxin Is Mediated by Protein Kinase B (Akt), Glycogen Synthase Kinase-3β (GSK-3β) and Microtubule-Associated Protein 1B." *PLoS ONE* 10 (3): 1–16. https://doi.org/10.1371/journal.pone.0119524.

Neuhaus, Jean Marc, Michael Wanger, Thomas Keiser, and Albrecht Wegner. 1983. "Treadmilling of Actin." *Journal of Muscle Research and Cell Motility*. Kluwer Academic Publishers. https://doi.org/10.1007/BF00712112.

Nichol IV, Robert H., Kate M. Hagen, Derek C. Lumbard, Erik W. Dent, and Timothy M. Gómez. 2016. "Guidance of Axons by Local Coupling of Retrograde Flow to Point Contact Adhesions." *Journal of Neuroscience* 36 (7): 2267–82. https://doi.org/10.1523/JNEUROSCI.2645-15.2016.

Norris, Adam D., Jamie O. Dyer, and Erik A. Lundquist. 2009. "The Arp2/3 Complex, UNC-115/AbLIM, and UNC-34/Enabled Regulate Axon Guidance and Growth Cone Filopodia Formation in Caenorhabditis Elegans." *Neural Development* 4 (1): 38. https://doi.org/10.1186/1749-8104-4-38.

Nozumia, Motohiro, Tetsuya Toganoa, Kazuko Takahashi-Nikia, Jia Lu, Atsuko Hondaa, Masato Taokad, Takashi Shinkawad, et al. 2009. "Identification of Functional Marker Proteins in the Mammalian Growth Cone." *Proceedings of the National Academy of Sciences* 106 (40): 17211–16. https://doi.org/10.1073/pnas.0904092106.

Obermann, Heike, Inka Raabe, Marga Balvers, Bärbel Brunswig, Wolfgang Schulze, and Christiane Kirchhoff. 2005. "Novel Testis-Expressed Profilin IV Associated with Acrosome Biogenesis and Spermatid Elongation." *Molecular Human Reproduction* 11 (1): 53–64. https://doi.org/10.1093/molehr/gah132.

Omotade, Omotola F., Stephanie L. Pollitt, and James Q. Zheng. 2017. "Actin-Based Growth Cone Motility and Guidance." *Molecular and Cellular Neuroscience* 84: 4–10. https://doi.org/10.1016/j.mcn.2017.03.001.

Ono, Shoichiro. 2013. "The Role of Cyclase-Associated Protein in Regulating Actin Filament Dynamics - More than a Monomer-Sequestration Factor." *Journal of Cell Science* 126 (Pt 15): 3249–58. https://doi.org/10.1242/jcs.128231.

Peche, Vivek S., Tad A. Holak, Bhagyashri D. Burgute, Kosmas Kosmas, Sushant P. Kale, F. Thomas Wunderlich, Fatiha Elhamine, et al. 2012. "Ablation of Cyclase-Associated Protein 2 (CAP2) Leads to Cardiomyopathy." *Cellular and Molecular Life Sciences 2012 70:3* 70 (3): 527–43. https://doi.org/10.1007/S00018-012-1142-Y.

Pelucchi, Silvia, Lina Vandermeulen, Lara Pizzamiglio, Bahar Aksan, Jing Yan, Anja Konietzny, Elisa Bonomi, et al. 2020. "Cyclase-Associated Protein 2 Dimerization Regulates Cofilin in Synaptic Plasticity and Alzheimer's Disease." *Brain Communications* 2 (2): 1–25. https://doi.org/10.1093/braincomms/fcaa086.

Pinto-Costa, Rita, Sara C. Sousa, Sérgio C. Leite, Joana Nogueira-Rodrigues, Tiago Ferreira da Silva, Diana Machado, Joana Marques, et al. 2020. "Profilin 1 Delivery Tunes Cytoskeletal Dynamics toward CNS Axon Regeneration." *Journal of Clinical Investigation* 130 (4): 2024–40. https://doi.org/10.1172/JCI125771.

Piper, Michael, Richard Anderson, Asha Dwivedy, Christine Weinl, Francis Van Horck, Kin Mei Leung, Emily Cogill, and Christine Holt. 2006. "Signaling Mechanisms Underlying Slit2-Induced Collapse of Xenopus Retinal Growth Cones." *Neuron* 49 (2): 215–28. https://doi.org/10.1016/J.NEURON.2005.12.008.

Polleux, F., and William Snider. 2010. "Initiating and Growing an Axon." *Cold Spring Harbor Perspectives in Biology* 2 (4). https://doi.org/10.1101/cshperspect.a001925.

Purde, Vedud, Florian Busch, Elena Kudryashova, Vicki H. Wysocki, and Dmitri S. Kudryashov. 2019. "Oligomerization Affects the Ability of Human Cyclase-Associated Proteins 1 and 2 to Promote Actin Severing by Cofilins." *International Journal of Molecular Sciences* 20 (22): 1–22. https://doi.org/10.3390/ijms20225647.

Quintero-Monzon, Omar, Erin M. Jonasson, Enni Bertling, Lou Talarico, Faisal Chaudhry, Maarit Sihvo, Pekka Lappalainen, and Bruce L. Goode. 2009. "Reconstitution and Dissection of the 600-KDa Srv2/CAP Complex: ROLES FOR OLIGOMERIZATION AND COFILIN-ACTIN BINDING IN DRIVING ACTIN TURNOVER*." *The Journal of Biological Chemistry* 284 (16): 10923. https://doi.org/10.1074/JBC.M808760200.

Rust, Marco B., Sharof Khudayberdiev, Silvia Pelucchi, and Elena Marcello. 2020. "CAPt'n of Actin Dynamics: Recent Advances in the Molecular, Developmental and Physiological Functions of Cyclase-Associated Protein (CAP)." *Frontiers in Cell and Developmental Biology* 8 (September): 1–17. https://doi.org/10.3389/fcell.2020.586631.

Rust, Marco B., and Tanja Maritzen. 2015. "Relevance of Presynaptic Actin Dynamics for Synapse Function and Mouse Behavior." *Experimental Cell Research*. https://doi.org/10.1016/j.yexcr.2014.12.020.

Saijilafu, Eun Mi Hur, Chang Mei Liu, Zhongxian Jiao, Wen Lin Xu, and Feng Quan Zhou. 2013. "PI3K-GSK3 Signalling Regulates Mammalian Axon Regeneration by Inducing the Expression of Smad1." *Nature Communications* 4 (1): 1–14. https://doi.org/10.1038/ncomms3690.

San Miguel-Ruiz, José E., and P. C. Letourneau. 2014. "The Role of Arp2/3 in Growth Cone Actin Dynamics and Guidance Is Substrate Dependent." *Journal of Neuroscience* 34 (17): 5895–5908. https://doi.org/10.1523/JNEUROSCI.0672-14.2014.

Sánchez-Huertas, Carlos, Marion Bonhomme, Amandine Falco, Christine Fagotto-Kaufmann, Jeffrey Van Haren, Freddy Jeanneteau, Niels Galjart, Anne Debant, and Jérôme Boudeau. 2020. "The +TIP Navigator-1 Is an Actin-Microtubule Crosslinker That Regulates Axonal Growth Cone Motility." *Journal of Cell Biology* 219 (9). https://doi.org/10.1083/JCB.201905199.

Schneider, Felix, Thuy An Duong, Isabell Metz, Jannik Winkelmeier, Christian A. Hübner, Ulrike Endesfelder, and Marco B. Rust. 2021. "Mutual Functional Dependence of Cyclase-Associated Protein 1 (CAP1) and Cofilin1 in Neuronal Actin Dynamics and Growth Cone Function." *Progress in Neurobiology* 202 (July): 102050. https://doi.org/10.1016/j.pneurobio.2021.102050.

Schneider, Felix, Thuy An Duong, and Marco B. Rust. 2021. "Neuron Replating, a Powerful and Versatile Approach to Study Early Aspects of Neuron Differentiation." *ENeuro* 8 (3): 1–11. https://doi.org/10.1523/ENEURO.0536-20.2021.

Schneider, Felix, Isabell Metz, Sharof Khudayberdiev, and Marco B. Rust. 2021. "Functional Redundancy of Cyclase-Associated Proteins CAP1 and CAP2 in Differentiating Neurons." *Cells* 10 (6): 1525. https://doi.org/10.3390/cells10061525.

Sharma, Kirti, Sebastian Schmitt, Caroline G. Bergner, Stefka Tyanova, Nirmal Kannaiyan, Natalia Manrique-Hoyos, Karina Kongi, et al. 2015. "Cell Type- and Brain Region-Resolved Mouse Brain Proteome." *Nature Neuroscience* 18 (12): 1819–31. https://doi.org/10.1038/nn.4160.

Shekhar, Shashank, J Chung, J Kondev, J Gelles, and Bruce Goode. 2019. "Synergy between Cyclase-Associated Protein and Cofilin Accelerates Actin Filament Depolymerization by Two Orders of Magnitude." *Nature Communications*, no. 2019: 1–11. https://doi.org/10.1038/s41467-019-13268-1.

Shepherd, Gordon M., Charles A. Greer, Paolo Mazzarello, and Marco Sassoè-Pognetto. 2011. "The First Images of Nerve Cells: Golgi on the Olfactory Bulb 1875." *Brain Research Reviews*. Elsevier. https://doi.org/10.1016/j.brainresrev.2010.09.009.

Silva, Jorge Santos Da, and Carlos G. Dotti. 2002. "Breaking the Neuronal Sphere: Regulation of the Actin Cytoskeleton in Neuritogenesis." *Nature Reviews Neuroscience* 3 (9): 694–704. https://doi.org/10.1038/nrn918.

Skruber, Kristen, Peyton V. Warp, Rachael Shklyarov, James D. Thomas, Maurice S. Swanson, Jessica L. Henty-Ridilla, Tracy Ann Read, and Eric A. Vitriol. 2020. "Arp2/3 and Mena/VASP Require Profilin 1 for Actin Network Assembly at the Leading Edge." *Current Biology* 30 (14): 2651-2664.e5. https://doi.org/10.1016/J.CUB.2020.04.085.

Spence, Erin F., and Scott H. Soderling. 2015. "Actin out: Regulation of the Synaptic Cytoskeleton." *Journal of Biological Chemistry*. American Society for Biochemistry and Molecular Biology Inc. https://doi.org/10.1074/jbc.R115.655118.

Stöckigt, Florian, Vivek Shahaji Peche, Markus Linhart, Georg Nickenig, Angelika Anna Noegel, and Jan Wilko Schrickel. 2016. "Deficiency of Cyclase-Associated Protein 2 Promotes Arrhythmias Associated with Connexin43 Maldistribution and Fibrosis." *Archives of Medical Science : AMS* 12 (1): 188. https://doi.org/10.5114/AOMS.2015.54146.

Stoeckli, Esther T. 2018. "Understanding Axon Guidance: Are We Nearly There Yet?" *Development (Cambridge)* 145 (10). https://doi.org/10.1242/dev.151415.

Strasser, Geraldine A., Nazimah Abdul Rahim, Kristyn E. Vanderwaal, Frank B. Gertler, and Lorene M. Lanier. 2004. "Arp2/3 Is a Negative Regulator of Growth Cone Translocation." *Neuron* 43 (1): 81–94. https://doi.org/10.1016/j.neuron.2004.05.015.

Sudarsanam, Sriram, Shiri Yaniv, Hagar Meltzer, and Oren Schuldiner. 2020. "Cofilin Regulates Axon Growth and Branching of Drosophila γ Neurons." *Journal of Cell Science* 133 (8). https://doi.org/10.1242/jcs.232595.

Tamariz, Elisa, and Alfredo Varela-Echavarria. 2015. "The Discovery of the Growth Cone and Its Influence on the Study of Axon Guidance." *Frontiers in Neuroanatomy* 9 (May): 1–9. https://doi.org/10.3389/fnana.2015.00051.

Tedeschi, Andrea, Sebastian Dupraz, Michele Curcio, Claudia J. Laskowski, Barbara Schaffran, Kevin C. Flynn, Telma E. Santos, et al. 2019. "ADF/Cofilin-Mediated Actin Turnover Promotes Axon Regeneration in the Adult CNS." *Neuron* 103 (6): 1073-1085.e6. https://doi.org/10.1016/j.neuron.2019.07.007.

Tronche, François, Christoph Kellendonk, Oliver Kretz, Peter Gass, Katrin Anlag, Paul C. Orban, Rudolf Bock, Rüdiger Klein, and G Schutz. 1999. "Disruption of the Glucocorticoid Receptor Gene in the Nervous System Results in Reduced Anxiety." *Nature Genetics* 23 (1): 99–103. https://doi.org/10.1038/12703.

Vartiainen, Maria K., Tuija Mustonen, Pieta K. Mattila, Pauli J. Ojala, Irma Thesleff, Juha Partanen, and Pekka Lappalainen. 2002. "The Three Mouse Actin-Depolymerizing Factor/Cofilins Evolved to Fulfill Cell-Type-Specific Requirements for Actin Dynamics." *Molecular Biology of the Cell* 13 (1): 183–94. https://doi.org/10.1091/mbc.01-07-0331.

Vitriol, Eric A., and James Q. Zheng. 2012. "Growth Cone Travel in Space and Time: The Cellular Ensemble of Cytoskeleton, Adhesion, and Membrane." *Neuron* 73 (6): 1068–81. https://doi.org/10.1016/j.neuron.2012.03.005.

Wang, Feng Song, Can Wen Liu, Thomas J. Diefenbach, and Daniel G. Jay. 2003. "Modeling the Role of Myosin 1c in Neuronal Growth Cone Turning." *Biophysical Journal* 85 (5): 3319–28. https://doi.org/10.1016/S0006-3495(03)74751-1.

Wang, Pei Shan, Fu Sheng Chou, Sreekumar Ramachandran, Sheng Xia, Huei Ying Chen, Fengli Guo, Praveen Suraneni, Brady J. Maher, and Rong Li. 2016. "Crucial Roles of the Arp2/3 Complex during Mammalian Corticogenesis." *Development (Cambridge)* 143 (15): 2741–52. https://doi.org/10.1242/dev.130542.

Westerink, R. H.S., and A. G. Ewing. 2008. "The PC12 Cell as Model for Neurosecretion." In *Acta Physiologica*, 192:273–85. John Wiley & Sons, Ltd. https://doi.org/10.1111/j.1748-1716.2007.01805.x.

Wills, Zachary, Mark Emerson, Jannette Rusch, Jay Bikoff, Buzz Baum, Norbert Perrimon, and David Van Vactor. 2002. "A Drosophila Homolog of Cyclase-Associated Proteins Collaborates with the Abl Tyrosine Kinase to Control Midline Axon Pathfinding." *Neuron* 36 (4): 611–22. http://www.ncbi.nlm.nih.gov/pubmed/12441051.

Wills, Zachary, Linsey Marr, Kai Zinn, Corey S. Goodman, and David Van Vactor. 1999. "Profilin and the Abl Tyrosine Kinase Are Required for Motor Axon Outgrowth in the Drosophila Embryo." *Neuron* 22 (2): 291–99. https://doi.org/10.1016/S0896-6273(00)81090-9.

Witke, Walter, Alexander V Podtelejnikov, Alessia Di Nardo, James D Sutherland, Christine B Gurniak, Carlos Dotti, and Matthias Mann. 1998. "In Mouse Brain Profilin I and Profilin II Associate with Regulators of the Endocytic Pathway and Actin Assembly." *EMBO Journal* 17 (4): 967–76. https://doi.org/10.1093/emboj/17.4.967.

Wolf, Michael, Anika Maria Zimmermann, Andreas Görlich, Christine B. Gurniak, Marco Sassoè-Pognetto, Eckhard Friauf, Walter Witke, and Marco B. Rust. 2015. "ADF/Cofilin Controls Synaptic Actin Dynamics and Regulates Synaptic Vesicle Mobilization and Exocytosis." *Cerebral Cortex* 25 (9): 2863–75. https://doi.org/10.1093/cercor/bhu081.

Wu, Huhehasi, Rokib Hasan, Haitao Zhang, Joshua Gray, Dominic Williams, Morgan Miller, Faith Allen, Virlan Lee, Thomas Kelly, and Guo Lei Zhou. 2019. "Phosphorylation Regulates CAP1 (Cyclase-Associated Protein 1) Functions in the Motility and Invasion of Pancreatic Cancer Cells." *Scientific Reports* 9 (1): 1–13. https://doi.org/10.1038/s41598-019-41346-3.

Xie, Shuanshuan, Yang Liu, Xuan Li, Min Tan, Changhui Wang, Jeffrey Field, and Guolei Zhou. 2018. "Phosphorylation of the Cytoskeletal Protein CAP1 Regulates Non-Small Cell Lung Cancer Survival and Proliferation by GSK3β." *Journal of Cancer* 9 (16): 2825–33. https://doi.org/10.7150/jca.25993.

Yang, Qing, Xiao Feng Zhang, Thomas D. Pollard, and Paul Forscher. 2012. "Arp2/3 Complex-Dependent Actin Networks Constrain Myosin II Function in Driving Retrograde Actin Flow." *Journal of Cell Biology* 197 (7): 939–56. https://doi.org/10.1083/jcb.201111052.

Ye, Xiyue, Yan Qiu, Yuqing Gao, Dong Wan, and Huifeng Zhu. 2019. "A Subtle Network Mediating Axon Guidance: Intrinsic Dynamic Structure of Growth Cone, Attractive and Repulsive Molecular Cues, and the Intermediate Role of Signaling Pathways." *Neural Plasticity* 2019: 1–26. https://doi.org/10.1155/2019/1719829.

Zhang, Haitao, Pooja Ghai, Huhehasi Wu, Changhui Wang, Jeffrey Field, and Guo-Lei Zhou. 2013. "Mammalian Adenylyl Cyclase-Associated Protein 1 (CAP1) Regulates Cofilin Function , the Actin Cytoskeleton , and Cell Adhesion." *Journal of Biological Chemistry*. https://doi.org/10.1074/jbc.M113.484535.

Zhang, Haitao, Auburn Ramsey, Yitong Xiao, Uddhab Karki, Jennifer Y. Xie, Jianfeng Xu, Thomas Kelly, Shoichiro Ono, and Guo-Lei Zhou. 2019. "Dynamic Phosphorylation and Dephosphorylation of Cyclase-Associated Protein 1 by Antagonistic Signaling through Cyclin-Dependent Kinase 5 and CAMP Are Critical for the Protein Functions in Actin Filament Disassembly and Cell Adhesion." *Molecular and Cellular Biology* 40 (4): 1–24. https://doi.org/10.1128/mcb.00282-19.

Zhang, Haiyan, Yonghua Liu, Yao Li, Ying Zhou, Dongjian Chen, Jianhong Shen, Yaohua Yan, et al. 2014. "The Expression of CAP1 After Traumatic Brain Injury and Its Role in Astrocyte Proliferation." *Journal of Molecular Neuroscience* 54 (4): 653–63. https://doi.org/10.1007/s12031-014-0363-y.

Zhang, Xiao Feng, Visar Ajeti, Nicole Tsai, Arash Fereydooni, William Burns, Michael Murrell, Enrique M. De La Cruz, and Paul Forscher. 2019. "Regulation of Axon Growth by Myosin II–Dependent Mechanocatalysis of Cofilin Activity." *Journal of Cell Biology* 218 (7): 2329–49. https://doi.org/10.1083/jcb.201810054.

Zhang, Xiao Feng, Callen Hyland, David Van Goor, and Paul Forscher. 2012. "Calcineurin-Dependent Cofilin Activation and Increased Retrograde Actin Flow Drive 5-HT-Dependent Neurite Outgrowth in Aplysia Bag Cell Neurons." *Molecular Biology of the Cell* 23 (24): 4833–48. https://doi.org/10.1091/mbc.E12-10-0715.

Zhou, Guo Lei, Haitao Zhang, and Jeffrey Field. 2014. "Mammalian CAP (Cyclase-Associated Protein) in the World of Cell Migration: Roles in Actin Filament Dynamics and Beyond." *Cell Adhesion and Migration* 8 (1): 55–59. https://doi.org/10.4161/cam.27479.

Zhu, Xinhui, Li Yao, Aisong Guo, Aihong Li, Huiqing Sun, Ning Wang, Hanzhang Liu, Zhiqin Duan, and Jianhua Cao. 2014. "CAP1 Was Associated with Actin and Involved in Schwann Cell Differentiation and Motility after Sciatic Nerve Injury." *Journal of Molecular Histology* 45 (3): 337–48. https://doi.org/10.1007/s10735-013-9554-z.

Zupanc, Günther K.H. 2017. "Mapping Brain Structure and Function: Cellular Resolution, Global Perspective." *Journal of Comparative Physiology A: Neuroethology, Sensory, Neural, and Behavioral Physiology*. Springer Verlag. https://doi.org/10.1007/s00359-017-1163-y.

Reprints of original research articles

Mutual functional dependence of cyclase-associated protein 1 (CAP1) and cofilin1 in neuronal actin dynamics and growth cone function, *Prog Neurobiol.*, 2021
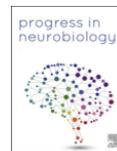
Original Research Article

Mutual functional dependence of cyclase-associated protein 1 (CAP1) and cofilin1 in neuronal actin dynamics and growth cone function

Felix Schneider [a,b,c], Thuy-An Duong [a], Isabell Metz [a,b], Jannik Winkelmeier [d,e], Christian A. Hübner [f], Ulrike Endesfelder [d,e], Marco B. Rust [a,b,c,*]

[a] *Molecular Neurobiology Group, Institute of Physiological Chemistry, University of Marburg, 35032, Marburg, Germany*
[b] *Center for Mind, Brain and Behavior (CMBB), University of Marburg and Justus-Liebig-University Giessen, 35032, Marburg, Germany*
[c] *DFG Research Training Group, Membrane Plasticity in Tissue Development and Remodeling, GRK 2213, Philipps-University of Marburg, 35032, Marburg, Germany*
[d] *Department of Systems and Synthetic Microbiology, Max Planck Institute for Terrestrial Microbiology and LOEWE Center for Synthetic Microbiology (SYNMIKRO), 35043, Marburg, Germany*
[e] *Department of Physics, Mellon College of Science, Carnegie-Mellon University, Pittsburgh, PA, USA*
[f] *Institute of Human Genetics, University Hospital Jena, 07743, Jena, Germany*

A R T I C L E   I N F O

A B S T R A C T

Neuron connectivity depends on growth cones that navigate axons through the developing brain. Growth cones protrude and retract actin-rich structures to sense guidance cues. These cues control local actin dynamics and steer growth cones towards attractants and away from repellents, thereby directing axon outgrowth. Hence, actin binding proteins (ABPs) moved into the focus as critical regulators of neuron connectivity. We found cyclase-associated protein 1 (CAP1), an ABP with unknown brain function, abundant in growth cones. Super-resolution microscopy and live cell imaging combined with pharmacological approaches on hippocampal neurons from gene-targeted mice revealed a crucial role for CAP1 in actin dynamics that is critical for growth cone morphology and function. Growth cone defects in CAP1 knockout (KO) neurons compromised neuron differentiation and was associated with impaired neuron connectivity in CAP1-KO brains. Mechanistically, by rescue experiments in double KO neurons lacking CAP1 and the key actin regulator cofilin1, we demonstrated that CAP1 was essential for cofilin1 function in growth cone actin dynamics and morphology and *vice versa*. Together, we identified CAP1 as a novel actin regulator in growth cones that was relevant for neuron connectivity, and we demonstrated functional interdependence of CAP1 and cofilin1 in neuronal actin dynamics and growth cone function.

1. Introduction

The formation of complex brain circuits depends on directed extension of axonal projections from neurons to their specific targets. During development, axons are guided by a 'hand-shaped' structure at their distal tip termed growth cone (Ramón y Cajal, 1909). The peripheral domain of growth cones, the leading edge, is highly enriched in actin filaments (F-actin) and contains receptors that translate guidance cues into intracellular signaling activities that act upstream of actin-binding proteins (ABPs) to control F-actin assembly and disassembly. Local actin dynamics steer the growth cone towards attractive and away from repellent cues and, hence, navigate axon through the developing brain (Gomez and Letourneau, 2014). To fulfill its sensory function and to explore its environment, the leading edge is highly motile and persistently protrudes and retracts actin-rich structures such as finger-like filopodia or sheet-like lamellipodia (Dent et al., 2011). Hence, actin dynamics play a central role in growth cone function, and ABPs moved into the focus as critical regulators of neuron connectivity and brain development (Vitriol and Zheng, 2012; Gomez and Letourneau, 2014; Omotade et al., 2017).

Actin dynamics are controlled by ABPs with different biochemical functions including actin nucleation and polymerization, F-actin depolymerization and severing, nucleotide exchange on globular actin monomers (G-actin), and capping of barbed or pointed ends (Pollard, 2017). Although numerous ABPs including the actin depolymerizing protein cofilin1 or the actin nucleation factor actin-related protein 2/3

(Arp2/3) complex have been implicated in growth cone motility, our knowledge about actin regulatory mechanisms in growth cones is still fragmented (Dent et al., 2011; Vitriol and Zheng, 2012; Gomez and Letourneau, 2014; Omotade et al., 2017). By exploiting recombinant proteins and yeast mutant strains, recent studies implicated cyclase-associated protein (CAP) in both F-actin disassembly and nucleotide exchange on G-actin (Johnston et al., 2015; Kotila et al., 2018, 2019; Shekhar et al., 2019; Rust et al., 2020). Mammals possess two CAP family members, CAP1 and CAP2, with different expression patterns. CAP2 is abundant in striated muscles and brain (Bertling et al., 2004), and recent mouse studies implicated CAP2 in heart physiology, skeletal muscle development and synaptic function (Peche et al., 2012; Field et al., 2015; Kepser et al., 2019; Pelucchi et al., 2020). Instead, CAP1 expression is less restricted, and its physiological functions remained unknown, also because appropriate animal models were lacking (Jang et al., 2019).

We found CAP1 expression during neuron differentiation and abundance in growth cones and therefore hypothesized a crucial role in growth cone function and brain development. To test our hypothesis, we generated a conditional mouse model and inactivated CAP1 during brain development. Analyses of hippocampal neurons from CAP1-KO mice and brain histology revealed a role for CAP1 in neuron differentiation and neuron connectivity. Further, we identified CAP1 as a novel regulator of actin dynamics that controls growth cone motility and morphology in response to guidance cues. Rescue experiments in neurons lacking either CAP1 or CAP1 together with cofilin1 revealed that CAP1 and cofilin1 synergistically control neuronal actin dynamics and growth cone morphology.

2. Results

2.1. CAP1 is relevant for neuron connectivity in the mouse brain

Immunoblots revealed presence of CAP1 in mouse cerebral cortex lysates throughout embryonic development, between embryonic day (E) 12.5 and postnatal day (P) 0 (Fig. 1A). At P0, CAP1 expression levels in hippocampal lysates were similar to those in cerebral cortex lysates (Fig. 1B). We therefore hypothesized a function for CAP1 during brain development. Systemic CAP1 mutant mice died during embryonic development and, hence, were not useful to test our hypothesis (Jang et al., 2019). We therefore generated mice carrying a targeted CAP1 allele with exon 3 being flanked by loxP sites (CAP1$^{flx/flx}$; Fig. 1C). Brain-specific CAP1 inactivation was achieved by crossing CAP1$^{flx/flx}$ mice with Nestin-Cre transgenic mice (Tronche et al., 1999). Compared to CAP1$^{flx/flx}$ littermates (CTR), CAP1 mRNA levels were strongly reduced in total brain lysates from E18.5 CAP1$^{flx/flx,Nestin-Cre}$ mice (Fig. 1D; CTR: 1.00 ± 0.15, CAP1-KO: 0.17 ± 0.06, n = 3, P < 0.05), and CAP1 protein levels dropped below detection limit (Fig. 1E). Hence, CAP1$^{flx/flx,Nestin-Cre}$ mice (termed CAP1-KO mice) were a valuable tool to study the brain function of CAP1.

When crossing CAP1$^{flx/flx}$ with CAP1$^{+/flx,Nestin-Cre}$ mice, we found the expected 25 % CAP1-KO mice among all offspring (n>300) at E18.5. However, CAP1-KO mice died shortly after birth, thereby restricting our histological analysis to embryonic stages. Antibody staining against the mitotic marker phospho-Histone 3 or the neural stem cell markers Pax6 and Tbr2 revealed no differences between CTR and CAP1-KO mice (data not shown). In line with this, Nissl staining as well as antibody staining against the neuron layer markers Tbr1 and Ctip2 revealed no obvious defects in cerebral cortex anatomy at E18.5 (Fig. S1). However, CAP1-KO mice displayed a somewhat altered morphology of the hippocampus, which we determined in Nissl-stained cross sections (Fig. S1A-B). This analysis revealed an unchanged hippocampal area in CAP1-KO mice, while the length along the cornu ammonis was reduced by 20 %, resulting in a slightly lower aspect ratio (Fig. S1C-E; area (in mm^2): CTR: 0.65 ± 0.05; CAP1-KO 0.60 ± 0.03, n = 9 images from 3 mice, P = 0.46; length (in mm): CTR: 2.28 ± 0.14; CAP1-KO 1.84 ± 0.09, P < 0.05;

aspect ratio: CTR: 2.16 ± 0.15; CAP1-KO 1.77 ± 0.06, P < 0.05). More strikingly, antibody staining against the axon marker neurofilament revealed less fiber tracks in CAP1-KO brains, e.g. in the cortical intermediate zone or in the striatum (Fig. 1F). Hypomorphic fiber tracks in E18.5 CAP1-KO brains were confirmed by DiI-labelling (Fig. 1G). Together, CAP1-KO mice displayed slight changes in hippocampal morphology as well as compromised neuron connectivity. Hence, our data demonstrated the relevance of CAP1 for brain development.

2.2. CAP1 inactivation impaired neuron differentiation

Compromised neuron connectivity in CAP1 mutant brains could be caused by impaired neuron differentiation. To test a role for CAP1 in neuron differentiation, we chose hippocampal neurons isolated from E18.5 mice as a cellular system, which expressed substantial CAP1 levels when kept *in vitro* (Fig. 2A). We stained neurons with an antibody against the neurite marker doublecortin (Dcx, Fig. 2B), which allowed us to categorize neurons according to their differentiation stage (Dotti et al., 1988). Further, we stained neurons with fluorescent phalloidin that labels F-actin (Melak et al., 2017). After five hours *in vitro* (HIV5), we found the majority of CTR and CAP1-KO neurons in stage 1, i.e. they formed lamellipodia, but not yet neurites (Fig. 2C; (in %) CTR: 69.23 ± 3.90; CAP1-KO 84.63 ± 2.76, n>300/3). All other neurons possessed minor processes, but not yet an axon, and were assigned to stage 2 (CTR: 30.77 ± 3.90, CAP1-KO: 15.37 ± 2.76). Compared to CTR, the fraction of stage 2 neurons was halved in CAP1-KO cultures, and the stage distribution was different between both groups (P < 0.001). Stage distribution differences were even more pronounced at later time points. After one day *in vitro* (DIV1), a minority of CTR neurons remained in stage 1, while the vast majority has been in stage 2 and some neurons already possessed an axon and reached stage 3 ((in %) stage 1: 10.21 ± 1.79, stage 2: 81.64 ± 3.17, stage 3: 8.15 ± 2.27; n>300/3). Conversely, approximately half of all CAP1-KO neurons remained in stage 1 and virtually no stage 3 CAP1-KO neurons were present ((in %) stage 1: 51.31 ± 2.73, stage 2: 48.38 ± 2.57, stage 3: 0.31 ± 0.31; n>300/3; P < 0.001). At DIV2, the fraction of stage 3 CTR neurons increased to roughly one third, and almost all other neurons were in stage 2 ((in %) stage 1: 4.33 ± 1.67, stage 2: 59.76 ± 3.85, stage 3: 35.91 ± 3.47; n>230/3). Instead, only a few CAP1-KO neurons reached stage 3, while one third remained in stage 1 ((in %) stage 1: 31.85 ± 4.16, stage 2: 64.80 ± 4.32, stage 3: 3.35 ± 1.21; n>230/3, P < 0.001). Antibody staining against the axon marker tau-1 in DIV2 cultures confirmed presence of axons in stage 3 CTR and CAP1-KO neurons, thereby proving correct categorization (Fig. S2A). Notably, treatment with 1 μM cytochalasin D (CYTOD), a mycotoxin that prevents polymerization of G-actin (Flynn et al., 2012), normalized stage distribution of CAP1-KO neurons at DIV2 (Fig. 2D-E; (in%) CTR-DMSO: stage 1: 7.08 ± 1.23, stage 2: 70.16 ± 1.84, stage 3: 22.77 ± 1.80; CAP1-KO-DMSO: stage 1: 28.92 ± 2.26, stage 2: 62.55 ± 1.80, stage 3: 8.53 ± 2.33, P < 0.001, n>200/3; CAP1-KO-CYTOD: stage 1: 4.17 ± 1.63, stage 2: 74.72 ± 3.89, stage 3: 21.11 ± 3.53, n>220/3). Upon CYTOD treatment, stage distribution of CAP1-KO neurons was different from DMSO-treated CAP1-KO neurons (P < 0.001), but not from DMSO-treated CTR neurons (P = 0.69). Together, our data revealed a role for CAP1 in neuron differentiation and suggested that it controls neuron differentiation via an actin-dependent mechanism.

2.3. CAP1 inactivation altered neurite length and width

Next, we determined neuron morphology by counting the numbers of primary neurites and neurite endpoints. Both parameters were unchanged in stage 2 or stage 3 CAP1-KO neurons (Figs. 2F, S2B; DIV1: stage 2: neurites: CTR: 5.31 ± 0.28, CAP1-KO: 5.17 ± 0.41, P = 0.33; endpoints: CTR: 5.90 ± 0.36, CAP1-KO: 5.79 ± 0.49, n = 30/3; DIV2: stage 2: neurites: CTR: 5.44 ± 0.27, CAP1-KO: 5.09 ± 0.45, P = 0.37; endpoints: CTR: 7.50 ± 0.58, CAP1-KO: 6.14 ± 0.69, P = 0.08, n =
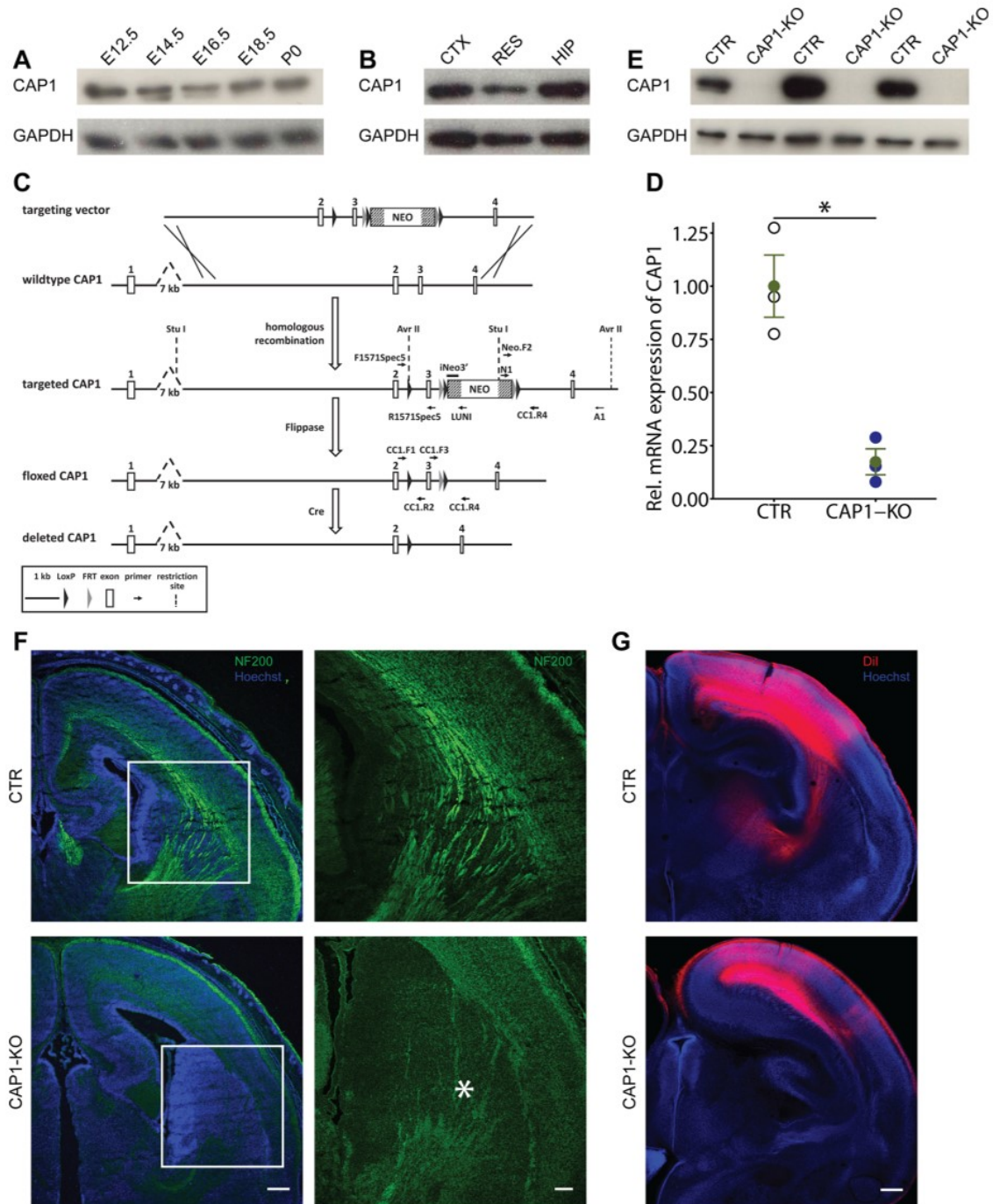
Fig. 1. Compromised neuron connectivity in CAP1 mutant mouse brain. (A) Immunoblots showing presence of CAP1 in cerebral cortex lysates during embryonic development, from embryonic day (E) 12.5 to postnatal day (P) 0. GAPDH was used as loading control. (B) Immunoblots showing equal CAP1 expression levels in cerebral cortex (CTX) and hippocampus (HIP) lysates at P0. Additionally, lysates of residual brain regions (RES) were probed. GAPDH was used as loading control. (C) Scheme showing targeting strategy for CAP1. The targeted CAP1 allele contained two loxP sites flanking exon 3 and a neomycin resistance cassette flanked by Frt sites. Upon successful homologous recombination in ES cells and blastocyst injection, the neomycin resistance cassette was removed by crossing gene targeted mice with a flippase deleter mouse. CAP1 deletion during brain development was achieved by crossing CAP1$^{flx/flx}$ mice and CAP1$^{+/flx,Nestin-Cre}$ mice. (D) Quantitative PCR (qPCR) showing reduced CAP1 mRNA levels in total brain lysates from E18.5 CAP1-KO mice. (E) Immunoblots (three biological replicates) showing absence of CAP1 from E18.5 CAP1-KO brains. GAPDH was used as a loading control. (F) Antibody staining of transversal brain sections from E18.5 CTR and CAP1-KO mice against the axonal marker NF200 (green). Boxes indicate areas shown at higher magnification. Asterisk indicates missing axon fibers in CAP1-KO brain. Further, sections were stained with the DNA dye Hoechst (blue). (G) Transversal sections of DiI-labelled E18.5 brains from CTR and CAP1-KO mice. Sections were stained with Hoechst (blue). Scale bars (in μm): 250 (F, G). *: P < 0.05.
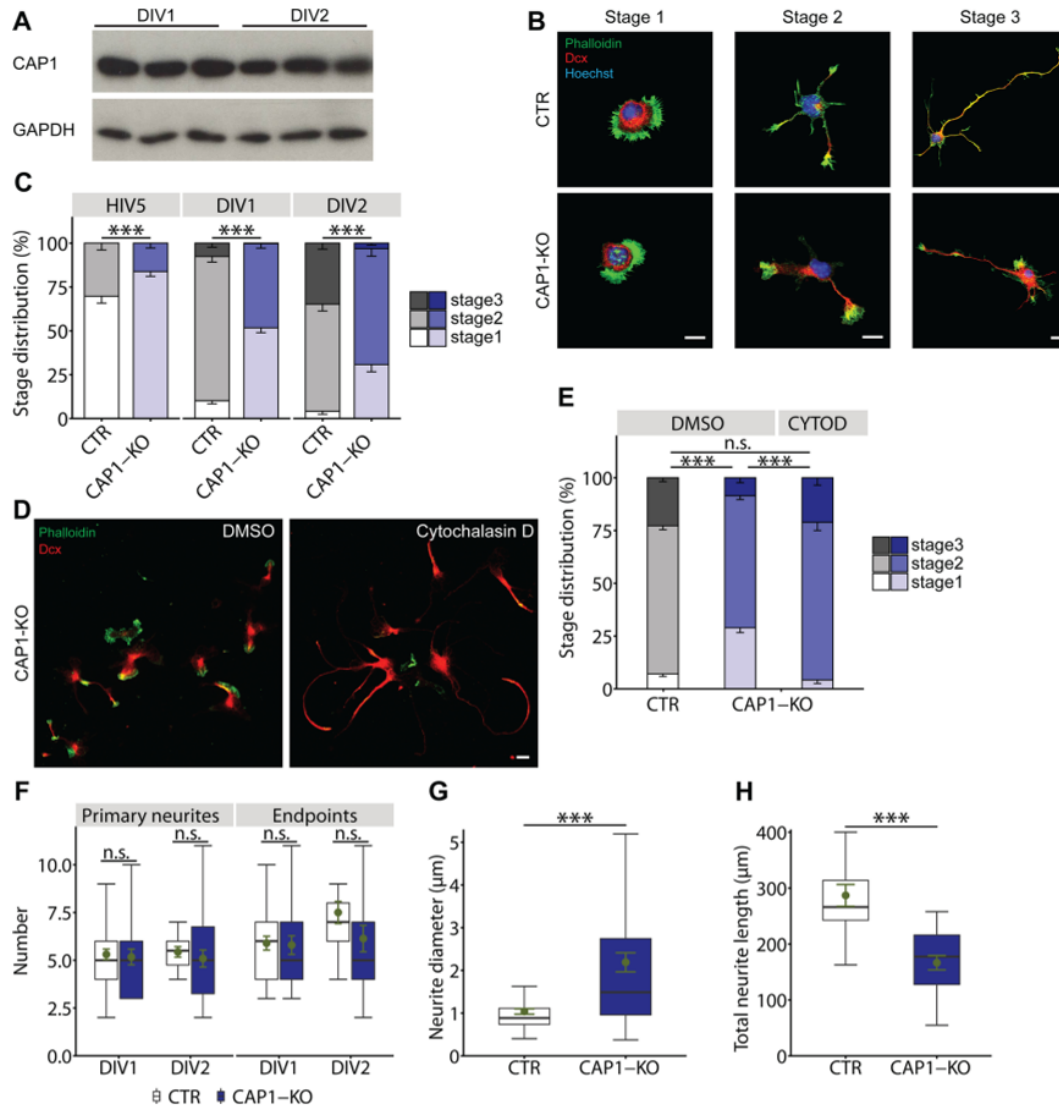
Fig. 2. Impaired differentiation and altered neurite morphology in CAP1-KO neurons. (A) Immunoblots (three biological replicates) showing presence of CAP1 in lysates from cultured hippocampal neurons at DIV1 and DIV2. GAPDH was used as loading control. **(B)** Representative hippocampal neurons from CTR and CAP1-KO mice at differentiation stages 1-3 (Dotti et al., 1988). Neurons were stained with an antibody against the neuronal marker doublecortin (Dcx, red), phalloidin (green) that labels F-actin and Hoechst (blue). **(C)** Stage distribution for CTR and CAP1-KO neurons at HIV5, DIV1 and DIV2. **(D)** Representative hippocampal CAP1-KO neurons treated either with DMSO or cytochalasin D (CYTOD). Neurons were stained with an antibody against Dcx (red) and phalloidin (green). **(E)** Stage distribution of DMSO-treated CTR and CAP1-KO neurons and CYTOD-treated CAP1-KO neurons. **(F)** Number of primary neurites and neurite endpoints in stage 2 CTR and CAP1-KO neurons. **(G)** Neurite width in stage 2 neurons. **(H)** Neurite length in stage 2 neurons. Scale bar (in µm): 10 (B), 25 (D); n.s.: P ≥ 0.05, ***: P < 0.001.

20/3; stage 3: neurites: CTR: 5.21 ± 0.26, CAP1-KO: 5.30 ± 0.62, P = 0.90; endpoints: CTR: 7.71 ± 0.85, CAP1-KO: 6.90 ± 0.99, P = 0.64, n = 10/6). Further, by exploiting Dcx-labelled neurons (Fig. 2B), we determined neurite length and width. While neurite width was doubled in CAP1-KO neurons (Fig. 2G; (in µm) CTR: 1.04 ± 0.06, CAP1-KO: 2.19 ± 0.22, P < 0.001), total neurite length was reduced by 40 % (Fig. 2H; (in µm) CTR: 286.99 ± 19.59, CAP1-KO: 166.58 ± 12.79, P < 0.001). Together, neurite numbers and branching were unchanged in CAP1-KO neurons, but their neurites were thicker and shorter.

2.4. CAP1 inactivation impaired growth cone morphology and motility

To decipher the CAP1-dependent mechanism during neuron differentiation, we determined its subcellular localization. Antibody staining

revealed CAP1 abundance in growth cones (Fig. 3A), which we identified by phalloidin labelling of F-actin. CAP1 immunoreactivity was absent from CAP1-KO growth cones, thereby proving specificity of the antibody. Localization in growth cones was confirmed by overexpression of green fluorescence protein (GFP)-tagged CAP1, which unlike GFP in control neurons was enriched in growth cones (Fig. S3A). A more thorough analysis of CAP1 immunoreactivity in growth cones revealed an intensity profile that overlapped with phalloidin in crosssectional line scans (Fig. 3B). Longitudinal line scans along filopodia revealed presence of CAP1 at the filopodia base and largely absence from the filopodia shaft and tip (Fig. 3C). To better determine CAP1 localization in growth cones, we overexpressed myc-tagged CAP1 and performed direct stochastic optical reconstruction microscopy (dSTORM) on neurons stained with antibodies against CAP1 and myc.
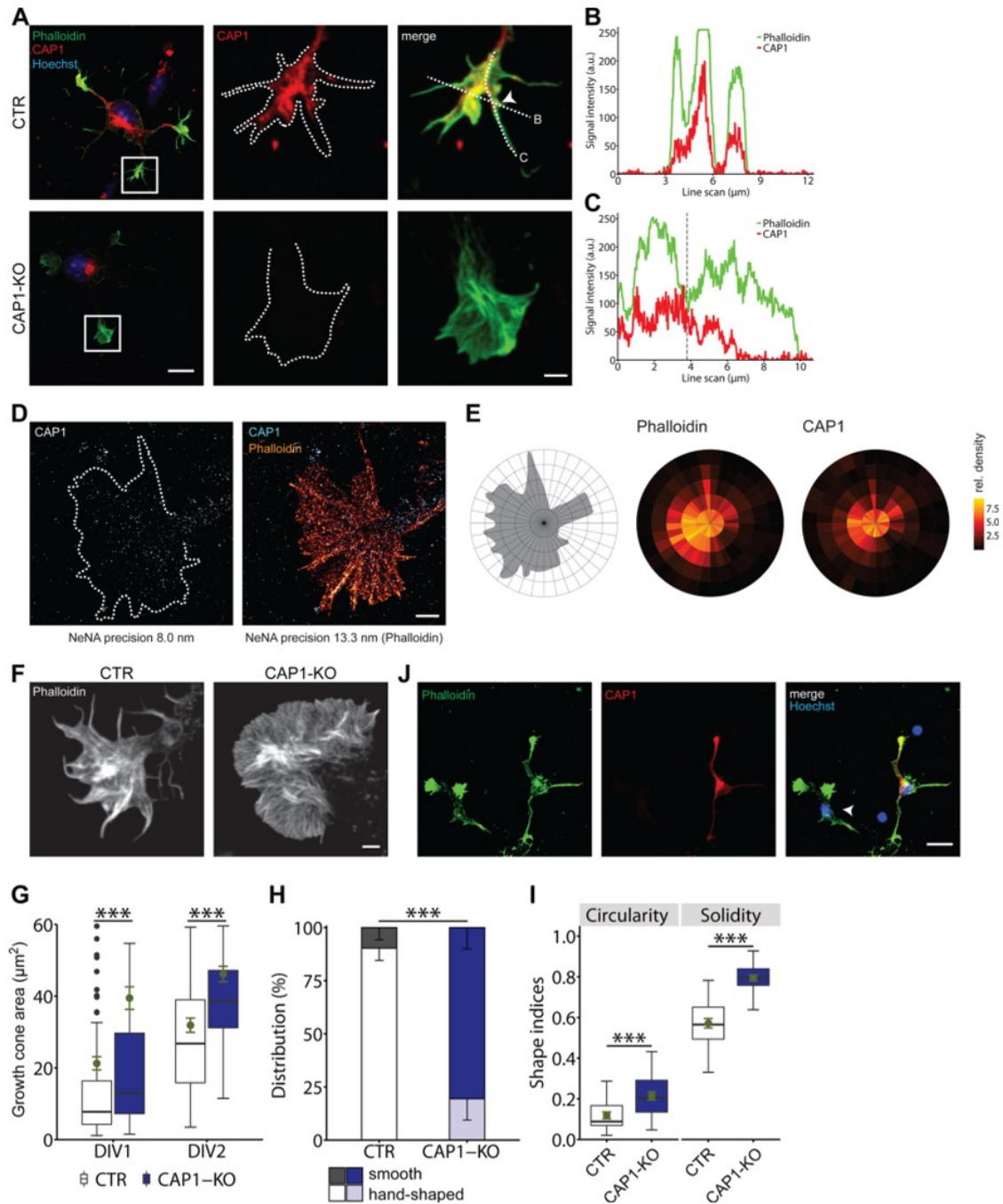
Fig. 3. Increased size and altered morphology of growth cones from CAP1-KO neurons. (A) Antibody staining against CAP1 (red) in CTR and CAP1-KO neurons. Neurons were additionally stained with phalloidin (green) and Hoechst (blue). Boxes indicate areas shown at higher magnification. Dashed lines in CAP1 micrographs outline growth cones. Dashed lines in micrograph 'merge' indicate lines analyzed for CAP1 and phalloidin intensity profiles in Fig. 3B and 3C. Arrowhead indicates beginning of the filopodium analyzed in Fig. 3C. (B) CAP1 and phalloidin fluorescence intensity profiles along cross-sectional dashed line indicated by B in Fig. 3A. (C) CAP1 and phalloidin fluorescence intensity profiles along longitudinal dashed line indicated by C in Fig. 3A. Dashed line in graph indicates beginning of filopodium (indicated by arrowhead in (Fig. 3A). (D) Representative dSTORM micrographs of a growth cone from a neuron overexpressing myc-tagged CAP1 stained with phalloidin (orange) and antibodies against CAP1 and myc (light blue). (E) Scheme showing a mask that was used to determine distribution of CAP1 and phalloidin signals in growth cones. Graphs show distribution of phalloidin (middle) and CAP1 (right) in growth cones. (F) Representative micrographs of phalloidin-stained growth cones from stage 2 neurons. (G) Growth cone size in CTR and CAP1-KO neurons at DIV1 and DIV2. (H) Growth cone fraction from CTR and CAP1-KO neurons with 'hand-shaped' or smooth morphology. (I) Shape indices circularity and solidity for CTR and CAP1-KO growth cones. (J) Mixed cultures of CTR and CAP1-KO neurons stained with an antibody against CAP1 (red), phalloidin (green) and Hoechst (blue). Arrowhead marks a CAP1-KO neuron. Scale bars (in μm): 2 (A high magnification, D, F), 10 (A low magnification), 25 (J). ***: P < 0.001.

Neurons were additionally stained with the F-actin marker phalloidin. This analysis confirmed different distribution of CAP1 and phalloidin in growth cones (Figs. 3D; S3B). To quantify signal distribution in growth cones, we used a mask that subdivides growth cones into five circles subdivided into 10° sections (scheme in Fig. 3E). As expected, phalloidin signal was high in the inner two circles mainly representing the growth cones' central domain, transition zone and peripheral domain (n = 14) (Lowery and Van Vactor, 2009). Moreover, phalloidin signal spread out into outer circles and this signal represents filopodia. Instead, CAP1 signal was mainly restricted to the inner two circles and largely absent from the others. Together, CAP1 was enriched in growth cones, but largely absent from filopodia shafts and tips.

To test whether CAP1 was relevant for growth cone function, we determined growth cone size in phalloidin-stained stage 2 neurons (Fig. 3F). Compared to CTR, size was increased by 85 % and 45 % in CAP1-KO growth cones at DIV1 and DIV2, respectively (Fig. 3G; (in μm^2) DIV1: CTR: 21.26 ± 1.83, CAP1-KO: 39.46 ± 3.13, n = 180/6, P < 0.001; DIV2: CTR: 31.90 ± 1.98, CAP1-KO: 46.19 ± 2.16, n = 90/3, P < 0.001). Further, we noted an altered growth cone morphology in CAP1-KO neurons. Opposite to CTR, only a minority of 20 % displayed the

typical 'hand-shaped' morphology, while most CAP1-KO growth cones appeared rather smooth (Fig. 3H; (in %) hand-shaped: CTR: 90.30 ± 5.78, CAP1-KO: 19.44 ± 10.02; smooth: CTR: 9.70 ± 5.78, CAP1-KO: 80.55 ± 10.02, P < 0.001, n>25/3). A smooth growth cone morphology in CAP1-KO neurons was also evident from increases in the shape indices circularity (+75 %) and solidity (+40 %; Fig. 3I; circularity: CTR: 0.12 ± 0.02, CAP1-KO: 0.21 ± 0.01, P < 0.001; solidity: CTR: 0.57 ± 0.02, CAP1-KO: 0.79 ± 0.01, P < 0.001; n = 26/3). Similar changes in growth cone size and morphology were present in CAP1-KO neurons co-cultured with CTR neurons (Fig. 3J). Together, CAP1 controls growth cone size and morphology, suggesting a role in growth cone function. Indeed, growth cones from CAP1-KO neurons were clearly less motile when compared to CTR neurons (Movies S1, S2). Since F-actin constitutes the major structural backbone relevant for growth cone morphology and motility (Gomez and Letourneau, 2014; Omotade et al., 2017), we hypothesized a CAP1 function in regulating the growth cone actin cytoskeleton.
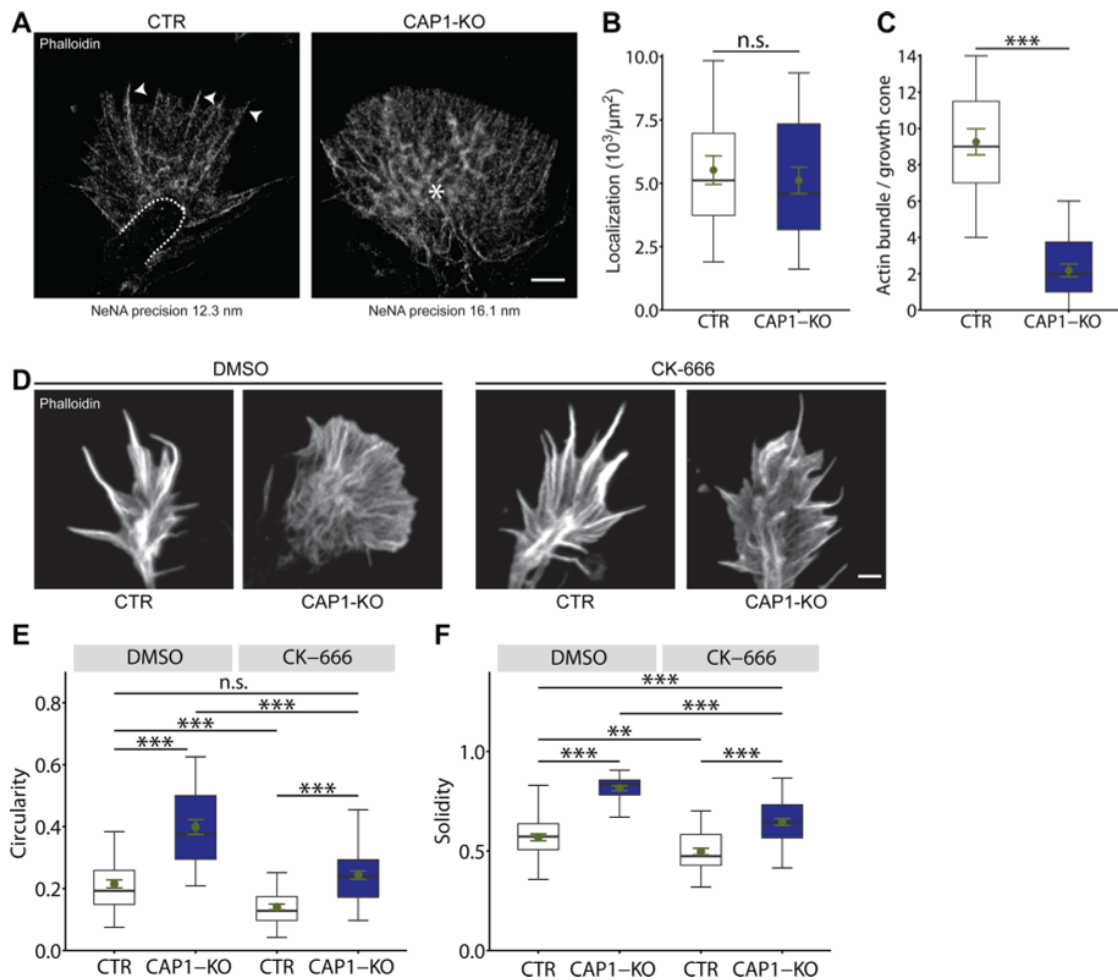
Fig. 4. CAP1 controls F-actin organization in growth cones. (A) Representative micrographs of phalloidin-stained growth cones from CTR and CAP1-KO neurons acquired by dSTORM. Dashed line marks border between C domain and T zone. Arrowheads exemplarily point to filopodia. Asterisk indicates lack of C domain in CAP1-KO growth cone. (B) F-actin density (phalloidin localizations normalized to growth cone size) in CTR and CAP1-KO growth cones. (C) Number of actin bundles per growth cone in CTR and CAP1-KO neurons. (D) Phalloidin-stained growth cones from CTR and CAP1-KO neurons treated with either DMSO or the Arp2/3 complex inhibitor CK-666. Graphs showing shape indices (E) circularity and (F) solidity for growth cones from DMSO- and CK-666-treated CTR and CAP1-KO neurons. Scale bars (in μm): 2 (A, D); n.s.: P ≥ 0.05, **: P < 0.01, ***: P < 0.001.

2.5. CAP1 controls F-actin organization and dynamics in growth cones

To test this hypothesis, we first exploited phalloidin-labelled CTR and CAP1-KO growth cones and examined F-actin organization by dSTORM (Figs. 4A, S4A). This approach revealed an overall normal F-actin density in CAP1-KO growth cones (Fig. 4B; (in localizations (10^3/μm^2)) CTR: 5.52 ± 0.56; CAP1-KO: 5.12 ± 0.52, n = 18/5, P = 0.53). Moreover, F-actin seems to be normally structured and branched in CAP1-KO growth cones. However, CAP1-KO growth cones displayed two obvious alterations. First, most of them lacked a clearly defined central domain, which normally contains only few F-actin structures (Lowery and Van Vactor, 2009; Dupraz et al., 2019). Second, the number of actin bundles was reduced by 75 % (Fig. 4C; CTR: 9.26 ± 0.72; CAP1-KO: 2.18 ± .35, n = 18/5, P < 0.001). A reduced number of actin

bundles in CAP1-KO growth cones was confirmed in an independent dSTROM analysis in which we stained CTR and CAP1-KO neurons with phalloidin and an antibody against α-tubulin (Fig. S4B-C; CTR: 7.17 ± 0.55; CAP1-KO: 1.46 ± .39, n = 35/5, P < 0.001). Unlike actin bundles, the number of microtubule was moderately increased in CAP1-KO growth cones (CTR: 6.89 ± 0.45; CAP1-KO: 10.37 ± .65, n = 35/5, P < 0.001). Interestingly, we frequently found microtubule reaching the leading edge in CAP1-KO growth cones, while this occurred in CTR growth cones only rarely (CTR: 0.77 ± 0.22; CAP1-KO: 2.60 ± .37, n = 35/5, P < 0.001). Together, altered morphology in CAP1-KO growth cones was associated with a reduction of actin bundles and a lack of filopodia accompanied by an enlarged peripheral domain. However, the peripheral domain displayed a normal F-actin density and structure. Since Arp2/3 complex is critical for branched F-actin in the growth cone
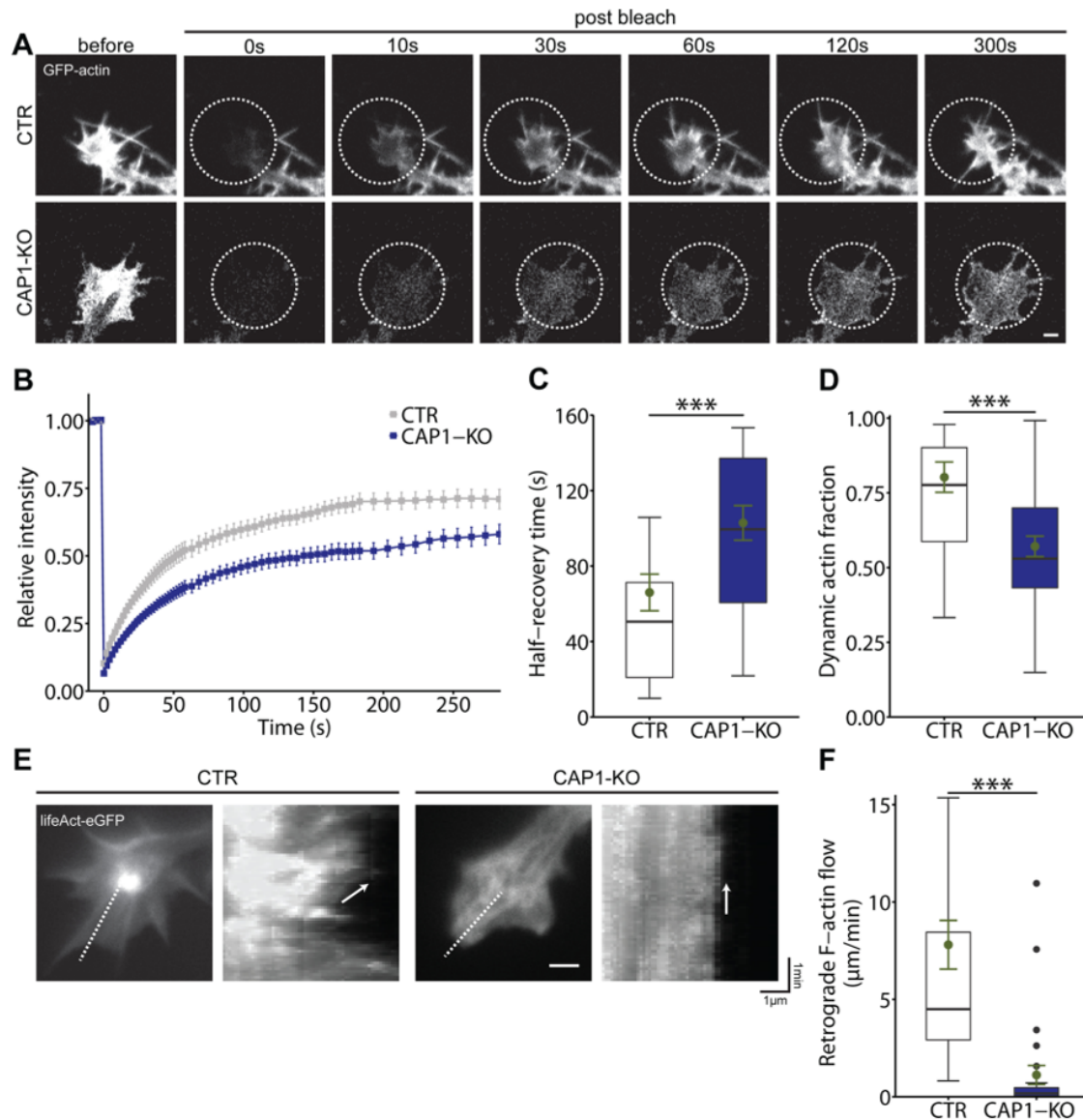
Fig. 5. CAP1 controls F-actin dynamics in growth cones. (A) Image sequence of GFP-actin in CTR and CAP1-KO growth cones during FRAP experiments. Dashed lines encircle bleached areas. **(B)** Recovery curves for GFP-actin in growth cones from CTR and CAP1-KO neurons. **(C)** Half-recovery time for GFP-actin in growth cones from CTR and CAP1-KO neurons. **(D)** Dynamic actin fraction in growth cones from CTR and CAP1-KO neurons. **(E)** Representative micrographs of growth cones from LifeAct-GFP-expressing CTR and CAP1-KO neurons. Dashed lines indicate where kymographs (shown on the right) have been generated from. Arrows in kymographs indicate retrograde F-actin flow. **(F)** Velocity of retrograde F-actin flow in growth cones from CTR and CAP1-KO neurons. Scale bars (in μm): 2 (A, E); ***: P < 0.001.

peripheral domain (Gomez and Letourneau, 2014; Omotade et al., 2017), we hypothesized that its activity was increased in CAP1-KO neurons. To test this hypothesis, we treated neurons with the Arp2/3 complex inhibitor CK-666 (Yang et al., 2012). As expected, CK-666 changed morphology of CTR growth cones (Fig. 4D-F). Compared to DMSO-treated CTR, circularity was reduced by 36 % and solidity by 12 % (circularity: DMSO: 0.22 ± 0.01, CK-666: 0.14 ± 0.01, P < 0.01; solidity: DMSO: 0.57 ± 0.02, CK-666: 0.50 ± 0.02, P < 0.001; n = 30/3). Similarly, CK-666 altered morphology of CAP1-KO growth cones as deduced from a 40 % reduction in circularity and a 21 % reduction in solidity when compared to DMSO-treated CAP1-KO (circularity: DMSO: 0.40 ± 0.02, CK-666: 0.24 ± 0.01, P < 0.001; solidity: DMSO: 0.82 ± 0.01, CK-666: 0.65 ± 0.02, P < 0.001; n = 30/3). Of note, both shape indices were still higher in CK-666-treated CAP1-KO neurons when compared to CK-666-treated CTR neurons (P < 0.001 for both parameters). Upon CK-666 treatment, circularity in CAP1-KO growth cones was not different from DMSO-treated CTR (P = 0.13) and solidity increased by only 13 % (P < 0.001). Hence, inhibition of the Arp2/3 complex partially rescued altered morphology of CAP1-KO growth cones.

Next, we examined whether actin dynamics was altered in CAP1-KO growth cones. We therefore performed fluorescence recovery after photobleaching (FRAP) experiments in GFP-actin-expressing neurons to determine actin turnover within a time frame of 300 s upon bleaching

(Movies S3, S4). In CTR growth cones, GFP-actin rapidly recovered with a mean half-recovery time ($t_{1/2}$) of 65.99 ± 9.72 s (Fig. 5A-C). Fluorescence recovery was much slower in CAP1-KO growth cones as indicated by a roughly 60 % increase in $t_{1/2}$ (102.88 ± 9.17 s, n = 40/3, P < 0.001). Moreover, the dynamic actin fraction that recovered within 300 s was reduced by 30 % in CAP1-KO growth cones (Fig. 5D; CTR: 0.80 ± 0.05, CAP1-KO: 0.57 ± 0.03, P < 0.001). We also expressed LifeAct-GFP to visualize F-actin in living neurons (Riedl et al., 2008). Compared to CTR neurons, F-actin appeared less dynamic in CAP1-KO growth cones (Movies S5, S6). Kymograph analysis allowed us to determine retrograde F-actin flow and, hence, to quantify F-actin dynamics in growth cones (Flynn et al., 2012). In CTR growth cones, the average retrograde flow velocity was 7.81 ± 1.25 μm/min (Fig. 5E-F), while in CAP1-KO neurons the velocity was seven-fold reduced (1.12 ± 0.49 μm/min, n = 25/3, P < 0.001). Slower actin turnover in FRAP experiments as well as reduced F-actin retrograde flow velocity revealed impaired actin dynamics in CAP1-KO growth cones. In summary, our data demonstrated a crucial role for CAP1 in growth cone F-actin organization and dynamics.

2.6. CAP1 controls growth cone size downstream of guidance cues

Guidance cues act upstream of growth cone actin dynamics and thereby control neurite outgrowth and neuron connectivity. Next, we
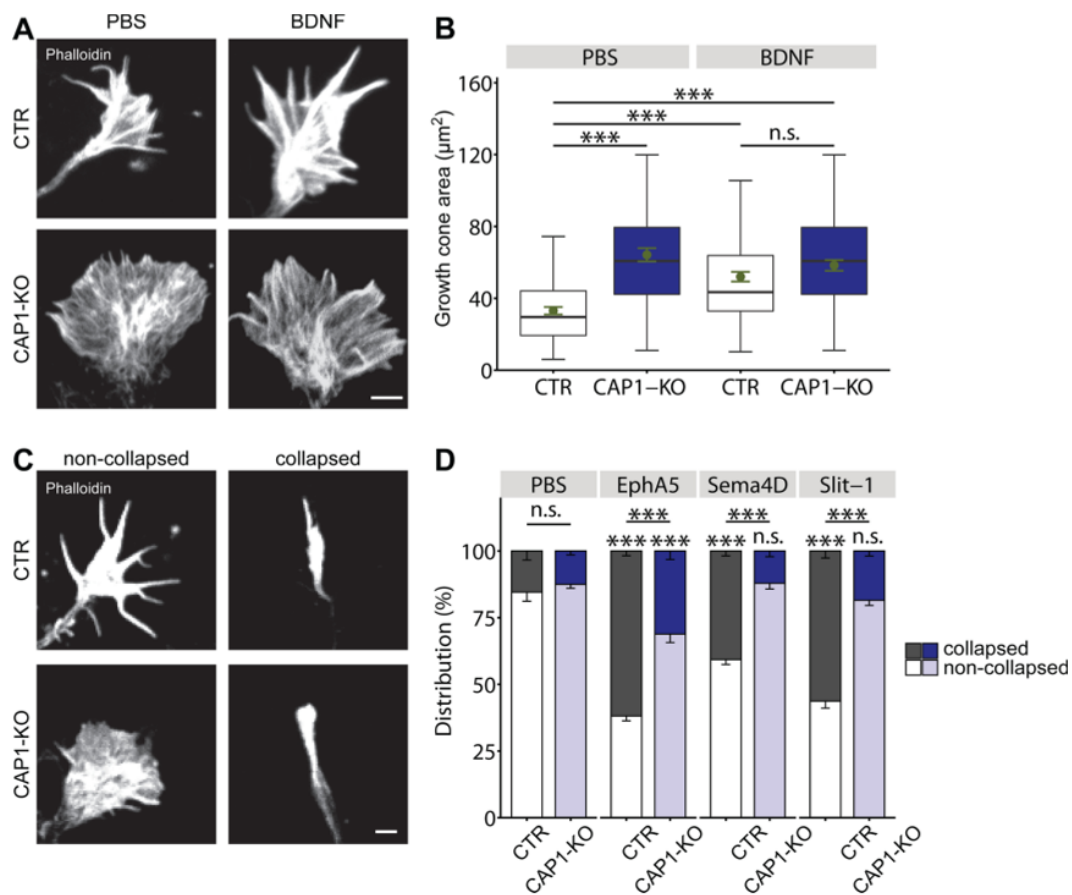

Fig. 6. CAP1 acts downstream of guidance cues in growth cones. (A) Phalloidin-labeled growth cones from CTR and CAP1-KO neurons treated with either PBS or BDNF. **(B)** Growth cone size in CTR and CAP1-KO neurons treated with either PBS or BDNF. **(C)** Phalloidin-stained non-collapsed and collapsed growth cones from CTR and CAP1-KO neurons. **(D)** Fraction of collapsed and non-collapsed growth cones from CTR and CAP1-KO neurons treated with either PBS or the repellent cues EphrinA5 (EphA5), Semaphorin D (Sema4D) or Slit-1. Comparisons between PBS-treated control conditions and treatment with either EphA5, Sema4D or Slit-1 are indicated by n.s. or asterisks directly above bars. Scale bars (in μm): 2 (A, C); n.s.: P ≥ 0.05, *: P < 0.05, ***: P < 0.001.

tested whether CAP1 was relevant for guidance cue-induced morphological changes in growth cones. We therefore determined growth cones upon treatment with either the attractant brain-derived neurotrophic factor (BDNF) or the repellent cues Ephrin A5 (EphA5), Semaphorin 4D (Sema4D) and Slit-1. Compared to PBS-treated neurons, CTR growth cones were enlarged by 60 % upon BDNF treatment (Fig. 6A-B; (in μm^2) PBS: 33.09 ± 2.08, BDNF: 52.02 ± 2.68, P < 0.001, n = 80/3). Instead, BDNF did not enlarge CAP1-KO growth cones ((in μm^2) PBS: 64.24 ± 3.70, BDNF: 58.33 ± 3.03, P = 0.20, n = 60/3), and growth cone size was similar in CTR and CAP1-KO neurons upon BDNF treatment (P = 0.20). Hence, CAP1-KO growth cones failed in responding to the attractant cue BDNF.

CAP1-KO neurons were also impaired in growth cone collapse downstream of the repellent cues EphA5, Sema4D and Slit-1. EphA5 fourfold increased the fraction of collapsed growth cones in CTR neurons (Fig. 6C-D; (in %) PBS: 15.43 ± 3.41, EphA5: 61.87 ± 1.79, n = 200/3, P

< 0.001). EphA5 also increased the fraction of collapsed CAP1-KO growth cones ((in %) PBS: 12.52 ± 1.47, EphA5: 31.13 ± 3.20, n = 200/3, P < 0.001), but the EphA5 effect was smaller when compared to CTR (P < 0.001). Sema4D and Slit-1 both induced growth cone collapse in CTR neurons and increased the collapsed growth cone fraction by a factor of 2.6 and 3.7, respectively (Sema4D: 40.70 ± 1.85, P < 0.001; Slit-1: 56.29 ± 2.64, P < 0.001). Conversely, neither Sema4D nor Slit-1 increased the collapsed growth cone fraction in CAP1-KO neurons (Sema4D: 12.12 ± 2.13, P = 0.85; Slit-1: 18.50 ± 1.93, P = 0.42). Together, CAP1 acts downstream of BDNF and the repellent cues EphA5, Sema4D and Slit-1, thereby implicating CAP1 in signaling cascades that are relevant for directed neurite outgrowth and neuron connectivity in the mammalian brain (Lowery and Van Vactor, 2009).
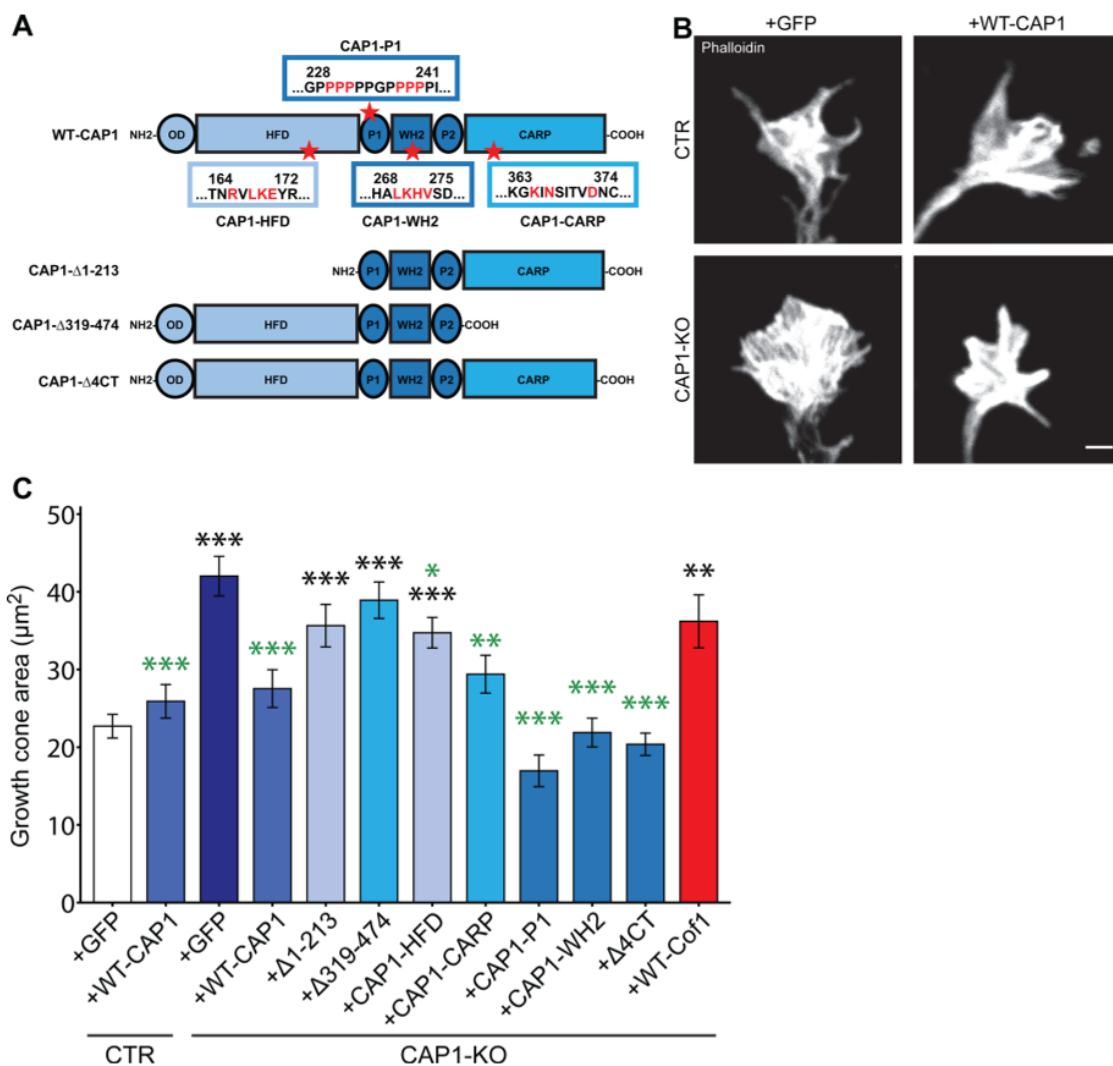
Fig. 7. Helical-folded domain is relevant for CAP1 function in growth cones. (A) Upper scheme showing protein domains of CAP1. HFD: helical folded domain, P1: proline-rich stretch 1, WH2: Wiscott-Aldrich homology 2 domain, P2: proline-rich stretch 2, CARP domain. Amino acid residues shown in red were replaced by alanine in CAP1 mutant constructs. Lower schemes show CAP1 deletion mutants. **(B)** Representative micrographs of phalloidin-stained growth cones from stage 2 CTR and CAP1-KO neurons expressing GFP or GFP-tagged WT-CAP1. **(C)** Growth cone size in CTR and CAP1-KO neurons that express either GFP, WT-CAP1, CAP1 deletion constructs (Δ1-213, Δ319-474, Δ4CT), CAP1 mutant constructs (CAP1-HFD, CAP1-CARP, CAP1-WH2, CAP1-P1) or WT-cofilin1 (Cof1). Black asterisks above columns indicate conditions significantly different from GFP-expressing CTR neurons, green asterisks indicate conditions significantly different from GFP-expressing CAP1-KO neurons. Scale bars (in μm): 2 (B); *: P < 0.05, **: P < 0.01, ***: P < 0.001.

2.7. The helical folded domain is critical for CAP1 function in growth cones

CAP1 is a multi-domain protein comprising several conserved domains capable of binding actin or ABP (Fig. 7A). By expressing CAP1 mutants in CAP1-KO neurons, we next tested which domain was relevant in growth cones. In these experiments, we used growth cone size as a readout, which showed the most robust difference between CTR and CAP1-KO neurons (Fig. 3). In control experiments, we expressed GFP-tagged wild-type (WT) CAP1, which did not change growth cone size in CTR, but normalized size in CAP1-KO neurons (Fig. 7B-C; (in μm^2): CTR: GFP: 22.71 ± 1.52, WT-CAP1: 25.90 ± 2.16, n = 100/3, P = 0.38; CAP1-KO: GFP: 42.02 ± 2.55, WT-CAP1: 27.54 ± 2.43, n = 80/3, P < 0.001). Unlike WT-CAP1, deletion constructs lacking either the N-terminal 213 amino acid (aa) residues ($\Delta 1-213$) or the last 156 residues ($\Delta 319-474$) did not normalize growth cone size in CAP1-KO neurons ($\Delta 1-213$: 35.64 ± 2.74, n = 80/3, P = 0.09; $\Delta 319-474$: 38.92 ± 2.34, n = 70/3, P = 0.46). To narrow down CAP1 domains relevant in growth cones, we mutated CAP1's i) helical folded domain (HFD), ii) proline-rich stretch (P1), iii) Wiscott-Aldrich homology 2 (WH2) domain and iv) β-sheets within the CARP domain (Kotila et al., 2018, 2019). Further, we deleted the last four aa residues ($\Delta 4CT$), which have been implicated in actin dynamics recently (Kotila et al., 2018). Similar to WT-CAP1 and both deletion constructs, all mutant CAP1 variants were located in growth cones (Fig. S3A). Expression of CAP1-P1, CAP1-WH2 or CAP1-CARP mutants or of $\Delta 4CT$ normalized CAP1-KO growth cone size (P1: 16.96 ± 2.04, n = 50/3, P < 0.001; WH2: 21.88 ± 1.85, n = 50/3, P < 0.001; CARP: 29.40 ± 2.43, n = 75/3, P < 0.001; $\Delta 4CT$: 20.38 ± 1.44, n = 80/3, P < 0.001). Instead, CAP1-HFD expression only slightly reduced growth cone size in CAP1-KO neurons (34.73 ± 1.97, n = 100/3, P < 0.05), which was still larger when compared to CTR neurons or WT-CAP1-expressing CAP1-KO neurons (P < 0.001 and <0.05, respectively). Together, our data identified HFD to be relevant for CAP1 in growth cones. Since previous studies revealed an interaction of HFD with ADF/cofilin-actin-complexes (Kotila et al., 2019; Shekhar et al., 2019), we hypothesized that CAP1 interacts with ADF/cofilin in growth cones.

2.8. Acute CAP1 inactivation impaired growth cone size and actin dynamics

The ADF/cofilin family comprises the family members ADF, cofilin1 and cofilin2. All three are expressed in the mouse brain, but analyses of gene targeted mice identified cofilin1 as the major family member during brain development (Bellenchi et al., 2007; Görlich et al., 2011; Flynn et al., 2012; Gurniak et al., 2014). Moreover, cofilin1 has been located in growth cones and implicated in actin dynamics downstream of guidance cues (Dent et al., 2011; Flynn et al., 2012; Garvalov et al., 2007; Wang et al., 2016). We therefore hypothesized that CAP1 co-operates with cofilin1 in growth cones. To test this hypothesis, we chose a genetic approach and compared under identical experimental conditions growth cones from neurons lacking either CAP1 or cofilin1 or both ABP. To do so, we isolated hippocampal neurons from i) CAP1$^{flx/flx}$ mice, ii) Cfl1$^{flx/flx}$ mice (Bellenchi et al., 2007) and iii) double transgenic mice (CAP1$^{flx/flx}$/Cfl1$^{flx/flx}$) at E18.5. Gene inactivation in isolated neurons was achieved by expression of mCherry-tagged Cre (Cre), neurons expressing a catalytic inactive mCherry-Cre (Cre-mut) served as CTR (Kullmann et al., 2020b). Immunocytochemistry confirmed CAP1 inactivation upon Cre expression, but not upon Cre-mut expression (Fig. S5). We reset neurons into an undifferentiated stage by re-plating them at DIV2 (Biswas and Kalil, 2018), and investigated growth cones 24 h later. First, we tested whether acute CAP1 inactivation compromised actin dynamics in growth cones. To do so, we performed FRAP experiments in GFP-actin-expressing neurons, and we determined retrograde F-actin flow in LifeAct-GFP-expressing neurons, similar to our analyses in neurons from CAP1-KO mice (Fig. 5). Compared to Cre-mut-expressing

neurons, third-recovery time ($t_{1/3}$) of photobleached GFP-actin was increased and the dynamic actin fraction was reduced in Cre-expressing CAP1$^{flx/flx}$ neurons (Fig. 8A-D, Movies S7−8; $t_{1/3}$ (in s): Cre-mut: 27.89 ± 2.87, Cre: 54.77 ± 7.31, n = 19/3, P < 0.05; dynamic fraction: Cre-mut: 0.74 ± 0.03, Cre: 0.56 ± 0.04, n = 19/3, P < 0.001). Moreover, retrograde F-actin flow was reduced in Cre-expressing CAP1$^{flx/flx}$ neurons (Fig. 8E-F, Movies S9−10; (in μm/min) Cre-mut: 6.91 ± 0.52, Cre: 0.22 ± 0.07, n = 32/3, P < 0.001). Hence, actin dynamics was impaired in Cre-expressing CAP1$^{flx/flx}$ neurons, and growth cone actin defects were associated with a 41 % increase in growth cone size (Fig. 9A-B; (in μm^2) Cre-mut: 19.60 ± 1.44, Cre: 27.72 ± 2.12, n = 90/3, P < 0.05). Together, acute CAP1 inactivation in hippocampal neurons caused growth cone defects similar to those we reported for neurons from CAP1-KO mice, thereby proving suitability of the experimental approach.

2.9. Cofilin1 inactivation caused growth cone defects similar to CAP1 inactivation

Next, we performed identical experiments with neurons from Cfl1$^{flx/flx}$ mice. Compared to Cre-mut-expressing neurons, actin dynamics in growth cones was impaired upon Cre expression in Cfl1$^{flx/flx}$ neurons as judged from an increased $t_{1/3}$ and reduced dynamic actin fraction in FRAP experiments (Fig. 8A-D, Movie S11; $t_{1/3}$ (in s): 55.17 ± 11.94, n = 21/3, P < 0.05; dynamic fraction: 0.58 ± 0.05, n = 21/3, P < 0.01) as well as from reduced retrograde F-actin flow (Fig. 8E-F, Movie S12; (in μm/min) 1.42 ± 0.25, n = 30/3, P < 0.001). Moreover, growth cones were enlarged by 42 % upon cofilin1 inactivation (Fig. 9A-B; (in μm^2) Cre-mut: 21.93 ± 1.51, Cre: 31.21 ± 2.43, n = 70/3, P < 0.05). While overexpression of WT-cofilin1 rescued growth cone size in Cre-expressing Cfl1$^{flx/flx}$ neurons (Fig. 9A-B; (in μm^2) 24.22 ± 1.75, n = 75/3, P < 0.05), overexpression of a phospho-mimetic cofilin1 mutant (cofilin1-S3D) that cannot bind actin failed in reducing growth cone size, but instead enlarged growth cones (44.27 ± 4.51, n = 70/3, P < 0.001). Together, impairment in actin dynamics and growth cone enlargement in cofilin1-deficient neurons was very similar to neurons lacking CAP1.

We next tested, whether CAP1 or cofilin1 were able to compensate each other's inactivation in growth cones. We therefore overexpressed WT-CAP1 in Cre-expressing Cfl1$^{flx/flx}$ neurons and, *vice versa*, WT-cofilin1 in Cre-expressing CAP1$^{flx/flx}$ neurons and determined growth cone size as a readout. Overexpression of WT-CAP1 did not reduce growth cone size in cofilin1-deficient neurons (Fig. 9B; (in μm^2) 33.25 ± 3.26, n = 70/3, P = 0.64), similar to WT-cofilin1 overexpression in CAP1-KO neurons (Fig. 7C; (in μm^2) 36.20 ± 3.41, n = 50/3, P = 0.23). Together, inactivation of CAP1 and cofilin1 induced similar defects in growth cone actin dynamics and size, demonstrating that they are of equal importance in growth cones. Further, both actin regulators were not able to compensate each other's inactivation in growth cones.

2.10. CAP1 cooperates with cofilin1 in growth cones

Finally, we set out to test whether CAP1 and cofilin1 cooperate in growth cones or control growth cone size via independent pathways. We therefore examined growth cones in Cre-expressing CAP1$^{flx/flx}$/Cfl1$^{flx/flx}$ neurons (termed double knockout (dKO)). FRAP experiments revealed a strong slowdown in actin turnover in dKO neurons as deduced from increased $t_{1/3}$ (Fig. 8A-C, Movie S13; $t_{1/3}$ (in s) 103.77 ± 20.56, n = 22/3, P < 0.01). Impaired actin turnover was associated with a reduced fraction of dynamic actin (Fig. 8D; 0.44 ± 0.04, n = 22/3, P < 0.001). Likewise, retrograde F-actin flow was reduced in dKO (Fig. 8E-F; Movie S14; (in μm/min) 0.21 ± 0.06, n = 30/3, P < 0.001). Further, we found growth cone size increased by roughly 50 % in dKO neurons (Fig. 9A, C; (in μm^2) CTR: 19.71 ± 1.13, dKO: 30.78 ± 1.74, n = 80/3, P < 0.001). Notably, growth cone size in dKO neurons was not different from single KO neurons lacking either CAP1 or cofilin1 (P = 0.31 or 0.97, respectively).
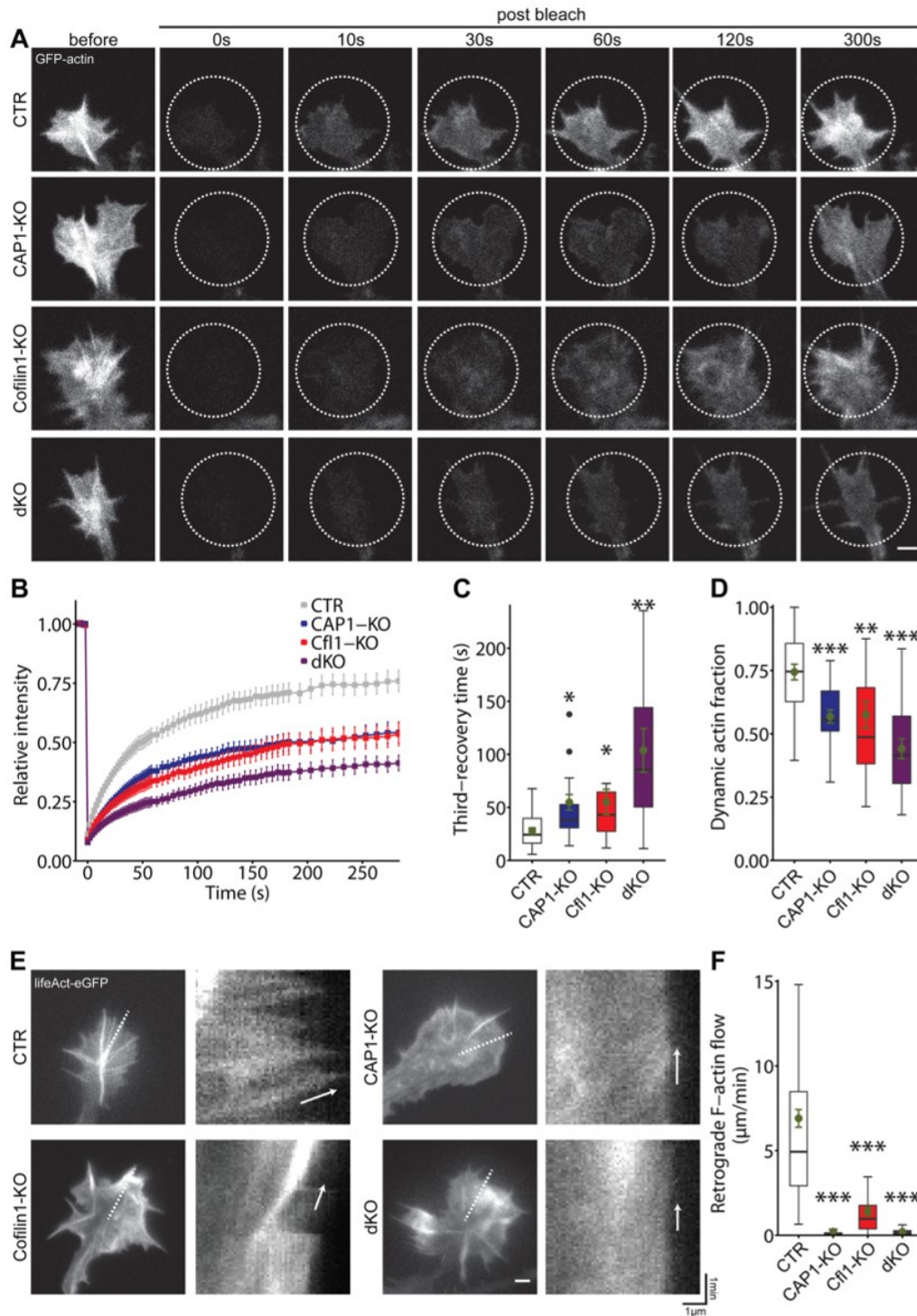
Fig. 8. Impaired actin dynamics in neurons lacking either CAP1, cofilin1 or both ABPs. (A) Image sequence of GFP-actin in growth cones from control neurons (CTR) expressing catalytic inactive Cre (Cre-mut) or Cre-expressing neurons from CAP1$^{flx/flx}$ (CAP1-KO), Cfl1$^{flx/flx}$ (cofilin1-KO), and CAP1$^{flx/flx}$/Cfl1$^{flx/flx}$ mice (dKO). Dashed lines encircle bleached areas. (B) Recovery curves for GFP-actin in growth cones from control and mutant neurons. (C) Third-recovery time for GFP-actin in growth cones from control and mutant neurons. (D) Dynamic actin fraction in growth cones from control and mutant neurons. (E) Representative micrographs of growth cones from LifeAct-GFP-expressing control and mutant neurons. Dashed lines indicate where kymographs (shown on the right) have been generated from. Arrows in kymographs indicate retrograde F-actin flow. (F) Velocity of retrograde F-actin flow in growth cones from control and mutant neurons. Asterisks above box plots in C, D and F indicate significance of differences when compared to CTR. Scale bars (in μm): 2 (A, E); *: $P < 0.05$, **: $P < 0.01$, ***: $P < 0.001$.
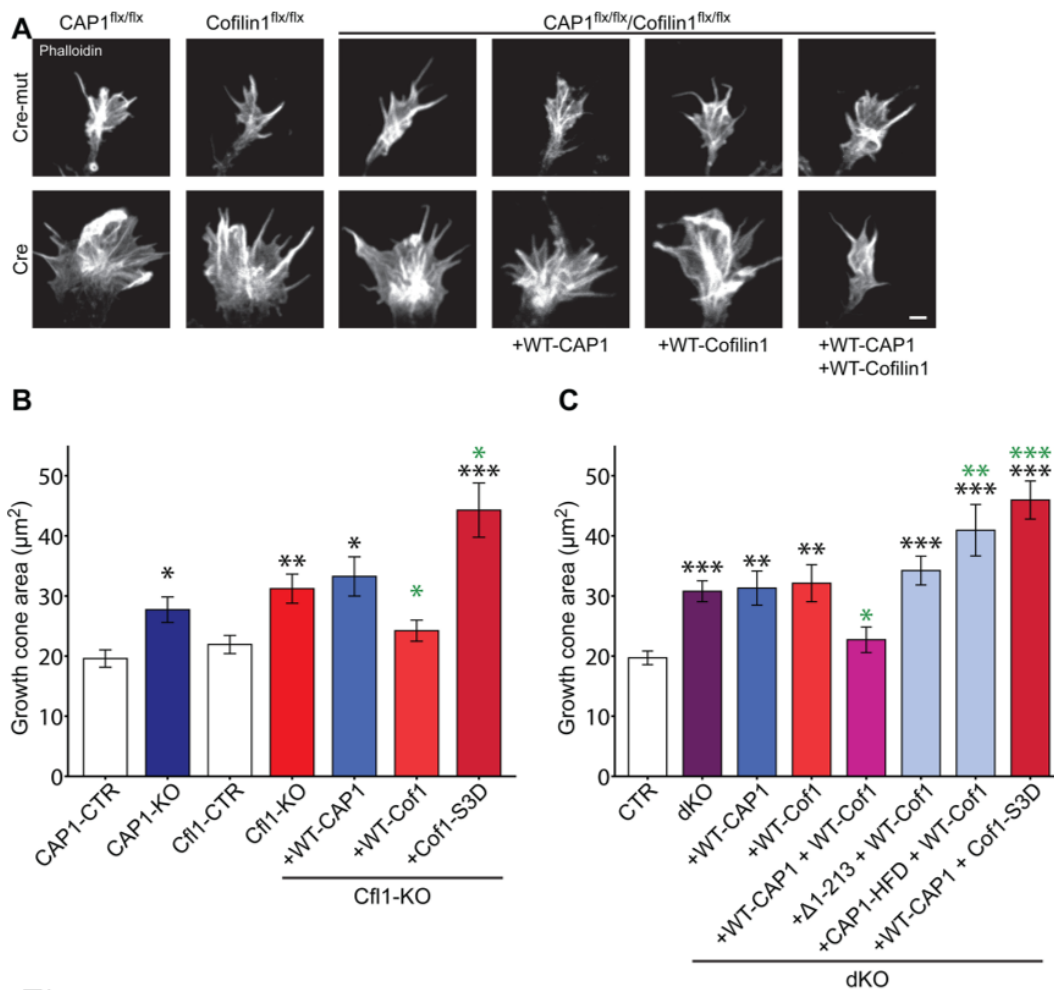
Fig. 9. CAP1 and cofilin1 synergistically control growth cone size. (A) Representative micrographs of phalloidin-stained growth cones from CAP1$^{flx/flx}$ and Cfl1$^{flx/flx}$ neurons expressing either Cre-mut (CTR) or Cre (KO) as well as from CAP1$^{flx/flx}$/Cfl1$^{flx/flx}$ neurons transfected with either Cre-mut (CTR) or Cre (KO) together with CAP1, Cofilin1 or both ABPs. (B) Growth cone size in CAP1$^{flx/flx}$ and Cfl1$^{flx/flx}$ neurons expressing either Cre-mut (CTR) or Cre (KO) as well as in Cre-expressing Cfl1$^{flx/flx}$ neurons that additional express WT-CAP1, WT-cofilin1 or cofilin1-S3D. Black asterisks indicate conditions significantly different from GFP-expressing CTR neurons, green asterisks indicate conditions significantly different from GFP-expressing cofilin1-KO neurons. (C) Growth cone size in CAP1$^{flx/flx}$/Cfl1$^{flx/flx}$ neurons expressing either Cre-mut (CTR) or Cre (dKO) as well as in dKO neurons additional transfected with indicated constructs. Black asterisks indicate conditions significantly different from GFP-expressing CTR neurons, green asterisks indicate conditions significantly different from GFP-expressing dKO neurons. Scale bars (in μm): 2 (A); n.s.: P ≥ 0.05, *: P < 0.05, **: P < 0.01, ***: P < 0.001.

To finally test whether CAP1 and cofilin1 cooperated in growth cones, we expressed WT-CAP1, WT-cofilin1 or both ABP in dKO neurons. Growth cone size in dKO neurons was unchanged upon expression of either WT-CAP1 or WT-cofilin1 ((in μm^2) WT-CAP1: 31.30 ± 2.84, n = 70/3, P = 0.89; WT-cofilin1: 32.12 ± 3.08, n = 100/3, P = 0.69). Instead, compound expression of WT-CAP1 and WT-cofilin1 normalized growth cone size in dKO neurons ((in μm^2) 22.71 ± 2.13, n = 90/3, P < 0.05). Growth cone size in these neurons was not different from CTR (P = 0.39). While expression of WT-cofilin1 together with WT-CAP1 normalized growth cone size in dKO neurons, expression of WT-cofilin1 together with CAP1 variants either possessing a mutated HFD or lacking the HFD (Δ1−213) failed in rescuing growth cone size ((in μm^2) HFD: 40.93 ± 4.29, n = 80/3, P < 0.01; Δ1−213: 34.22 ± 2.40, n = 120/3, P = 0.28). Moreover, growth cone size in dKO neurons was not reduced upon expression of WT-CAP1 together with cofilin1-S3D, but instead increased ((in μm^2) 45.95 ± 3.17, n = 100/3, P < 0.001). Together, these data demonstrated that CAP1 and cofilin1 cooperate in growth cones. Further, they revealed that CAP1′s HFD as well as

cofilin1′s interaction with actin is crucial for this cooperative activity.

3. Discussion

The present study aimed at deciphering the role of CAP1 for mammalian brain development, which we found expressed during neuron differentiation and enriched in growth cones. By generating a conditional mouse strain and by exploiting primary hippocampal neurons from brain-specific CAP1-KO mice, we identified CAP1 as a novel regulator of F-actin organization and dynamics in growth cones, which was relevant for growth cone morphology, motility and response to guidance cues. Growth cone defects in CAP1-KO neurons were associated with retarded neuron differentiation and impaired neuron connectivity in CAP1-KO brains. Rescue experiments in CAP1-KO neurons, and the analysis of dKO neurons lacking CAP1 and the key actin regulator cofilin1 revealed functional interdependence of both ABP in neuronal actin dynamics and growth cone function.

While CAPs have been recognized as ABPs almost two decades ago

12

(Balcer et al., 2003; Bertling et al., 2004; Freeman and Field, 2000; Hubberstey and Mottillo, 2002), significant progress in their molecular functions has been achieved just recently (Jansen et al., 2014; Johnston et al., 2015; Kotila et al., 2018, 2019; Mu et al., 2019; Shekhar et al., 2019). These studies, which either exploited recombinant proteins or have been performed in yeast, implicated CAP1 and CAP2, but also their yeast homolog Srv2 (suppressor of Ras2-Val19) in actin dynamics (for review: Rust et al., 2020). In good agreement with these studies, our live cell imaging data unraveled an important role for CAP1 in actin dynamics of growth cones. However, despite the substantial advancements of their molecular activities, the physiological functions of mammalian CAPs largely remained elusive, also because appropriate mouse models were lacking. This holds true specifically for CAP1 (Jang et al., 2019), while recent mouse studies implicated CAP2 in heart physiology, myofibril differentiation and dendritic spine morphology (Peche et al., 2012; Field et al., 2015; Kepser et al., 2019; Pelucchi et al., 2020). Our conditional mouse model allowed us to study the brain function of CAP1. We found that CAP1 controls actin dynamics in differentiating neurons, which was relevant for growth cone morphology and function. We showed that growth cone motility, and consequently its exploratory behavior, was severely disturbed in CAP1-KO neurons and that CAP1-KO growth cones were strongly impaired in responding to attractant and repellent cues. As expected for defective growth cone actin dynamics (Gomez and Letourneau, 2014), neurite formation and morphology as well as the microtubule cytoskeleton was altered in CAP1-KO neurons, and neuron connectivity was compromised in CAP1-KO brains. Instead, neuron layering and brain anatomy was largely preserved in CAP1-KO mice, demonstrating that CAP1 was dispensable for various important aspects of brain development such as neural stem cell proliferation and differentiation, neuron production and migration or layer formation in the cerebral cortex – different from other ABP that control neuronal actin dynamics during brain development (Bellenchi et al., 2007; Flynn et al., 2012; Kullmann et al., 2020a). Hence, our data led us suggest that CAP1 acquired a specific function in neuron differentiation and in establishing neuron connectivity. The latter is in good agreement with a previous study that implicated the Drosophila homolog capulet (also known as act up) in axonal midline crossing (Wills et al., 2002).

Although numerous ABPs have been implicated in growth cone motility (Dent et al., 2011), knowledge about the mechanisms that control actin dynamics in growth cones is still fragmented (Gomez and Letourneau, 2014; Omotade et al., 2017). Our data add CAP1 to the list of actin regulators in growth cones. By live cell imaging, we showed that CAP1 is relevant for dynamizing the growth cone actin cytoskeleton, and our pharmacological data revealed that CAP1 acts downstream of guidance cues such as BDNF, EphA5, Sema4D or Slit-1. Further, our rescue experiments identified CAP1′s HFD to be relevant in growth cones. Instead, expression of mutant CAP1 variants i) in which either the P1 or the WH2 domain were mutated or ii) which lacked the C-terminal four aa residues restored growth cone morphology in CAP1-KO neurons, very similar to WT-CAP1. We therefore concluded that CAP1′s interaction with ADF/cofilin-actin complexes was crucial in growth cones (Kotila et al., 2019; Moriyama and Yahara, 2002; Quintero-Monzon et al., 2009; Shekhar et al., 2019). Instead, CAP1′s nucleotide exchange activity on G-actin that depends on its WH2 domain as well as C-terminal four aa residues seems to be dispensable in growth cones, very much alike CAP1′s interaction with actin regulators such as profilin or Abl1 that depends on P1 (Bertling et al., 2007; Chaudhry et al., 2010; Kotila et al., 2018; Makkonen et al., 2013; Mattila et al., 2004; Nomura and Ono, 2013). Indeed, we confirmed the relevance of the CAP1-cofilin1 interaction in growth cones in a genetic approach, in which i) we found similar defects in growth cone actin dynamics upon inactivation of either CAP1, cofilin1 or both ABPs, ii) we found a similar increase in growth cone size in both single KO neurons and dKO neurons, iii) growth cone size in dKO neurons was normalized upon expression of WT-CAP1 together with WT-cofilin1, but not upon expression of

WT-CAP1 or WT-cofilin1 alone, and iv) growth cone size in dKO was not normalized upon expression of WT-cofilin1 together with CAP1 variants possessing a mutated HFD or upon expression of WT-CAP1 with actin-binding-deficient cofilin1-S3D. We therefore conclude that i) CAP1 cooperates with cofilin1 in growth cone actin dynamics and ii) CAP1 is mandatory for cofilin1 activity in growth cones and *vice versa*. Cofilin1 is a key regulator of the neuronal actin cytoskeleton (Rust, 2015). By exploiting gene targeted mice, we and others previously demonstrated that cofilin1 is important for brain development and function (Bellenchi et al., 2007; Flynn et al., 2012; Rust et al., 2010; Wolf et al., 2015; Zimmermann et al., 2015). Moreover, several studies implicated cofilin1 in growth cone motility and revealed a complex and context-dependent function in growth cone dynamics (Dent et al., 2011; Gomez and Letourneau, 2014; Omotade et al., 2017; Wang et al., 2016; Zhang et al., 2019). Very similar to CAP1, cofilin1 acts downstream of repellent cues in growth cone collapse (Grintsevich et al., 2016; Hsieh et al., 2006; Piper et al., 2006; Wen et al., 2007). A cooperation of CAP1 and cofilin1 as demonstrated here is in line with these studies. Moreover, it fits well to previous studies that either exploited recombinant proteins or have been performed in yeast (Bertling et al., 2004; Jansen et al., 2014; Johnston et al., 2015; Kotila et al., 2019; Moriyama and Yahara, 2002; Quintero-Monzon et al., 2009; Shekhar et al., 2019). These studies suggested that CAP1 and cofilin1 synergistically control actin dynamics and that CAP1 releases cofilin1 from its complex with G-actin, thereby allowing a new cycle of actin depolymerization (for review: Rust et al., 2020). However, these studies further implicated CAP1 in nucleotide exchange on G-actin that recycles G-actin for F-actin assembly. Our data suggest that G-actin recycling in growth cones does not depend on CAP1 and might be carried out by other ABPs such as profilin, for which such a function in growth cones has been proposed earlier (Gomez and Letourneau, 2014; Omotade et al., 2017; Vitriol and Zheng, 2012). Interestingly, inhibition of Arp2/3 complex by CK-666 partially rescued growth cone morphology in CAP1-KO neurons, suggesting increased Arp2/3 complex activity in CAP1-KO neurons. We speculate that F-actin disassembly mediated by CAP1 together with cofilin1 counteracts Arp2/3 complex-dependent F-actin assembly in growth cones. Accordingly, compromised F-actin disassembly (e.g. by CAP1 inactivation) causes increased activity of the Arp2/3 complex in growth cones. Such opposing functions of Arp2/3 complex and F-actin disassembly factors have been proposed earlier in dendritic spines (Spence and Soderling., 2015).

In summary, we identified CAP1 as a novel regulator of actin dynamics in growth cones that is relevant for growth cone function, neuron differentiation and neuron connectivity in the mouse brain and that cooperates with cofilin1 in neuronal actin dynamics and growth cone function.

4. Material and methods

4.1. Transgenic mice

Brain-specific deletion of CAP1 was achieved by crossing mice carrying conditional CAP1 alleles (CAP1$^{flx/flx}$) with CAP1$^{+/flx}$ mice that additionally express a Cre transgene under control of the nestin promoter (Tronche et al., 1999). Cfl1$^{flx/flx}$ mice have been generated previously (Bellenchi et al., 2007) and CAP1$^{flx/flx}$/Cfl1$^{flx/flx}$ mice were generated by crossing a CAP1$^{flx/flx}$ mice with Cfl1$^{flx/flx}$ mice. Mice were housed in the animal facility of the University of Marburg on 12 -h dark-light cycles with food and water available *ad libitum*. Treatment of mice was in accordance with the German law for conducting animal experiments and followed the guidelines for the care and use of laboratory animals of the U.S. National Institutes of Health. Killing of mice has been approved by internal animal welfare authorities at Marburg University (references: AK-5−2014-Rust, AK-6−2014-Rust, AK-5−2018-Rust). Generation and breeding of gene targeted mice has been approved by the Regierungspräsidium Giessen (references:

V54−19c2015h01MR20/30 #83/2015, V54−19c2015h01MR20/29 #G22/2016) and by the Thüringer Landesamt für Verbraucherschutz (222684−04-02−060/14).

4.2. Cell culture and transfection

Primary hippocampal neurons from embryonic day 18 (E18) mice were prepared as previously described (Antoniou et al., 2018). Briefly, hippocampi were dissociated individually to keep their genetic identity and seed with a density of 31,000 neurons per cm^2 on 0.1 mg/mL poly-L-lysine-coated coverslips (15,500 neurons for each genotype per cm^2 in mixed cultures). Neurons were maintained for 5 h to 3 d in a humidified incubator at 37 °C with 5% CO$_2$ in Neurobasal medium containing 2% B27, 2 mM GlutaMax, 100 µg/mL streptomycin, and 100 U/mL penicillin (Gibco, Invitrogen). For overexpression of plasmids, neurons were nucleofected prior to plating with Amaxa nucleofector system (Lonza) according to manufacturer's protocol. For each nucleofection, 3 µg plasmid was transfected into 250,000 neurons, which were then plated at a density of 66,000 neurons per cm^2. For re-plating, neurons were seeded in wells coated with 0.05 mg/mL poly-L-lysine and detached with TrypLE™ Express (Gibco) at DIV2, similar to previous studies (Biswas and Kalil, 2018). Thereafter, neurons were pelleted at 7000 rpm for 7 min, plated on 0.1 mg/mL poly-L-lysine-coated coverslips and fixed 24 h later. Following constructs were used: C-terminal GFP-tagged WT-CAP1 or mutant CAP1 variants (see scheme in Fig. 7A) including a linker consisting of Gly-Gly-Arg between CAP1 and GFP, N-terminal myc-tagged CAP1 deletion constructs including a linker consisting of Leu-Met-Ala-Met-Glu-Ala-Arg-Ile-Arg-Ser-Thr between myc and CAP1, GFP (GenScript), GFP-actin and LifeAct-GFP (Robert Grosse lab), GFP-cofilin1 and GFP-cofilin1-S3D (Rehklau et al., 2017), mCherry-Cre and mCherry-Cre-mutant (Kullmann et al., 2020b).

4.3. Immunocytochemistry

Cultured neurons were fixed for 10 min in 4% paraformaldehyde (PFA) in PBS under cytoskeleton preserving conditions. After 5 min incubation with 0.4 % gelatin with 0.5 % Triton-X100 in PBS (carrier solution), neurons were incubated with following primary antibodies (in carrier solution): mouse anti-CAP1 (1:100, Abnova), rabbit anti-doublecortin (1:500, Abcam), rabbit anti-GFP (1:1,000, ThermoFisher Scientific), mouse anti tau-1 (1:200, Merck Millipore), mouse anti-c-Myc (1:200, ThermoFisher Scientific) and chicken anti-mCherry (1:500, Abcam). Thereafter, neurons were washed in PBS and incubated with the following secondary antibodies (in carrier solution): anti-mouse and anti-rabbit IgG coupled to either AlexaFluor488, AlexaFluor546 or AlexaFluor647 (1:500, Invitrogen) and AlexaFluor555-coupled anti-chicken IgG (1:500, Invitrogen). F-actin was visualized by staining with phalloidin coupled to either AlexaFluor488 (1:100, Invitrogen) or AlexaFluor647 (1:100, Cell Signaling Technologies). In each experiment, neurons were stained with the DNA dye Hoechst (1:1,000, Invitrogen). Image acquisition was done with a Leica TCS SP5 II confocal microscope setup, and image analysis was performed with ImageJ (Schindelin et al., 2012).

4.4. Growth cone morphology

Growth cone morphology was assessed by determining growth cone solidity (growth cone area divided by hull area), similar to previous studies (Chitsaz et al., 2015).' Hand-shaped' growth cones were defined as growth cones with visible filopodia protruding out of the lamellipodium, while smooth growth cones were lacking these protruding filopodia.

4.5. Live cell imaging

For fluorescence recovery after photobleaching (FRAP), GFP-actin transfected neurons were seeded in a 22 mm glass-bottom dish either directly after nucleofection or after re-plating and cultured for 1 d. Neurons were imaged with a Leica TCS SP5 II in a chamber heated to 35 °C and the medium was exchanged with CO$_2$-saturated HBS solution. For pre-bleaching condition, 5 images were acquired and in total 65 images for the fluorescence recovery over a time course of 5 min. Images were analyzed with ImageJ (Schindelin et al., 2012) and recovery curve calculated with R. The retrograde F-actin flow was measured on neurons, which were transfected with LifeAct-GFP and cultured in a 22 mm glass-bottom dish either directly after nucleofection or after re-plating for 1 d. Neurons were imaged in CO$_2$-regulated incubation chamber maintained at 37 °C with Leica DMi8 Thunder microscope system and a Leica DFC9000 GTC camera. Images were acquired every 5 s for 5 min. Generation and analysis of kymograph was performed with ImageJ (Schindelin et al., 2012). For DIC imaging, neurons were cultured as described above and imaged in a chamber maintained at 37 °C and the medium was exchanged with CO$_2$-saturated HBS solution. Images were acquired every 5 s for 10 min at a Leica DMi8 setup.

4.6. Growth cone collapse assay and pharmacological inhibition

Neurons were cultured for 1 d before incubation with 100 µM CK-666 (Sigma Aldrich), 100 µM BDNF (PeproTech), 1 µg/µl Ephrin A5 (R&D System), 50 nM Semaphorin 4D (Thomas Worzfeld lab) or 1 µg/µl Slit-1 (R&D System) for 60 min. Neurons were imaged with a Leica TCS SP5 II microscope system and analyzed with ImageJ (Schindelin et al., 2012). Collapsed and non-collapsed growth cones were defined according to previous studies (Muller et al., 1990). For BDNF-treated neurons only growth cone size was measured.

4.7. dSTORM

Neurons were plated in a µ-Slide 8 Well chamber (ibidi) at a density of 30,000 cells per well. 24 h after plating, neurons were fixed with 1% PFA and 0.05 % Triton-X for 1 min followed by 3% PFA for 10 min. After washing, samples were quenched with 1 mg/mL NaBH$_4$ for 10 min and washed again. For staining, cells were blocked with 100 µM L-lysine in Image-iT™ FX Signal Enhancer solution (Thermo Fisher Scientific) for 1 h and then stained with Phalloidin-AF647 (1:50 in PBS, Cell Signal Technology) for 48 h at 4 °C. Neurons were post-fixed with 4% PFA for 10 min, washed with 0.05 % Tween20 in PBS and incubated again with Phalloidin-AF647 (1:50 in PBS) for 24 h at 4 °C. Neurons were post-fixed for a second time with 4% PFA for 10 min, washed with 0.05 % Tween20 in PBS and stored in PBS at 4 °C until imaging.

For dual-color staining cell were blocked in 0.4 % gelatin with 0.5 % Triton-X100 in Image-iT™ FX Signal Enhancer solution (Thermo Fisher Scientific) for 1 h and afterwards incubated with primary antibodies diluted in carrier solution: mouse anti-CAP1 (1:100, Abnova) and mouse anti-c-Myc (1:200, ThermoFisher Scientific) or mouse anti-α-tubulin (1:200, Sigma Aldrich), respectively. After washing, cells were incubated with secondary antibody anti-mouse coupled to CF680 (1:300, Biotium) in carrier solution for 60 min. Secondary antibody solution was then replaced by 500 nM Phalloidin-AF647 and incubated overnight at 4 °C.

Single-color image was carried out on a customized single-molecule localization microscope as described before (Virant et al., 2018). Before imaging, samples were incubated with infrared beads (FluoSpheres infrared fluorescent Carboxylate-Modified Microspheres, ThermoFisher, USA; ex/em 715/755 nm; 1:2,000 in PBS) for 10 min and then PBS was exchanged with dSTORM buffer containing 100 mM mercaptoethylamine (MEA) with a glucose oxygen scavenger system (van de Linde et al., 2011). The sample was illuminated in HILO (Highly Inclined and Laminated Optical sheet) mode and growth cones were recorded at 20 Hz for 30,000 frames with a final intensity of the 640 nm laser adjusted to 1−2 kW cm^{-2} adapted from the parameters of the dSTORM recordings (Baarlink et al., 2017; Tokunaga et al., 2008). Recorded

fluorescent single molecule spots from the image acquisition were localized using ThunderSTORM (Ovesny et al., 2014) and further processed using customized Python scripts, kindly provided by Dr. Bartosz Turkowyd. The localization files were filtered for out-of-focus signals (80 nm < PSF sigma < 200 nm, uncertainty in xy < 50 nm) and corrected for sample drift during image acquisition using the infrared beads in the sample as described before (Balinovic et al., 2019). The final experimental localization precision in the processed localization files was determined by calculating the NeNA precision value (Endesfelder et al., 2014). Using RapidSTORM 3.0 (Wolter et al., 2012), super-resolved images were reconstructed from the localization files with a pixel size of 10 nm and were overlaid with a Gaussian blur according to the individual NeNA localization precision using ImageJ (Schindelin et al., 2012). The number of phalloidin-AlexaFluor647 localizations per growth cone area was measured with the software swift (written in C++, Endesfelder group, unpublished) by selecting the growth cone and normalized to the growth cone area. Filopodia were counted with ImageJ (Schindelin et al., 2012).

Dual-color dSTORM imaging was performed using a commercial SAFe 360 setup (abbelight, France). In brief, an inverted IX83 microscope (Olympus, Japan) with a 100 × 1.49NA objective was equipped with a 640 nm laser (LPX-640−500-CSB, Oxxius, France) and a 638 nm laser (ELERA from Errol, France). The laser line was coupled into the microscope via the ASTER technology for homogeneous TIRF and HILO illumination (abbelight, France) and was reflected onto the objective with a quad-band dichroic mirror (Di03-R405/488/532/635-t1−25 × 36 from Semrock, USA). The emitted light was filtered with a quadband bandpass filter (FF01−446/510/581/703−25 BrightLine quad-band bandpass filter, Semrock, USA) and split with a 700 nm longpass dichroic (T700lpxr, Chroma, Germany) into two detection paths. The fluorophore emissions were recorded with two 2048 × 2048 pixel sCMOS cameras (orca-fusion C1440−20UP, Hamamatsu, Japan) with an optical pixel size of 97 nm using an additional set of quadband bandpass filters (FF01−446/510/581/703−23.3-D BrightLine quad-band bandpass filter, Semrock, USA) right in front of the cameras.

Before imaging, cells were washed twice with PBS and then incubated in dSTORM buffer described above. Image acquisition was performed at 50 Hz for 30,000 frames with a laser power of approximately 40 mW after the objective controlled by the imaging software Neo-Imaging (abbelight, France). Movies were localized and corrected for lateral drift using the cross-correlation drift correction algorithm within the acquisition software NeoAnalysis (abbelight, France). The resulting localization files, merged from both cameras, were loaded into the 3D viewer part of NeoAnalysis and filtered for out-of-focus-signal (localization uncertainty < 25 nm). Spectral demixing (Winterflood et al., 2015) was used to assign each localization to a color channel. The spectral demixing thresholds used in NeoAnalysis were λ_1 lim. inf. = 0.2, λ_1 lim. sup. = 0.35, λ_2 lim. inf. = 0.55, λ_2 lim. sup. = 0.75 for actin-tubulin dual-color imaging, and λ_1 lim. inf. = 0, λ_1 lim. sup. = 0.429, λ_2 lim. inf. = 0.55, λ_2 lim. sup. = 1 for actin-CAP1 dual-color imaging. The parameters were slightly adjusted for both target sets from a calibration file that was derived from single-color stainings of phalloidin-AF647 and tubulin-ab-CF680, respectively. Localization files and reconstructed images with a pixel size of 10 nm were saved for both channels. Super-resolved images of both channels were opened in ImageJ, adjusted with individually optimized intensity ranges and overlaid with a Gaussian blur according to their individual NeNA localization precision. For dual-color images, lookup tables of redhot (for AF647) and cyanhot (for CF680) were added. Filopodia were counted in ImageJ (Schindelin et al., 2012).

CAP1 and Phalloidin localization density was quantified using a custom-written script in MATLAB (R2018b, MathWorks, Inc.).

4.8. Protein analysis

Cortices of E18.5 mice were homogenized in 500 μL RIPA buffer containing 50 mM Tris HCl (pH7.5), 150 mM NaCl, 0.5 % NP40, 0.1 % SDS and protease inhibitor (Complete, Roche). After centrifugation at 14,000 rpm for 10 min at 4 °C, samples were boiled for 5 min at 95 °C in Laemmli buffer including 6% DTT. Equal protein amounts were separated by SDS PAGE and blotted onto a polyvinylidene difluoride membrane (Merck) by using a Wet/Tank Blotting System (Biorad). Membranes were blocked in Tris-buffered saline (TBS) containing 5% milk powder, 0.5 % Tween-20 and 0.02 % sodium acid for 1 h and afterwards incubated with primary antibodies in blocking solution over night at 4 °C. As secondary antibodies, horseradish peroxidase (HRP)-conjugated antibodies (1:20,000, Thermo Fisher Scientific) were used and detected by chemiluminescence with ECL Plus Western Blot Detection System (GE Healthcare). Following primary antibodies were used: mouse anti-CAP1 (1:1,000, Abnova), mouse anti-GAPDH (1:1,000, R&D System). For secondary antibody, anti-mouse and anti-rabbit coupled to HRP (Thermo Fisher Scientific) were used and the blots were developed with ECL Prime Western Blotting Detection Reagent (GE Healthcare).

4.9. Histology and immunohistochemistry

Nissl staining and immunohistochemical staining was performed as described previously (Kullmann et al., 2020a). Briefly, E18.5 mice were killed by decapitation and brains were fixed for 2 h in PBS containing 4 % PFA. Thereafter, 25 μm transversal brain sections were generated by a Leica CM3050 S cryostat. For immunohistochemistry, brain sections were incubated for 1 h with 2% BSA, 3% goat serum, 10 % donkey serum and 0.5 % NP40 in PBS and stained over night at 4 °C with following primary antibodies in 2% BSA and 0.5 % NP40 in PBS: rat anti-Ctip2 (1:1,000, Abcam), rabbit anti-Neurofilament200 (1:80, Sigma-Aldrich), rabbit anti-Tbr1 (1:200, Abcam). As secondary antibodies, AlexaFluor488 anti-rabbit, AlexaFluor488 anti-rat and Alexa-Fluor546 anti-rabbit IgG was used. For Nissl staining, brains sections were incubated in staining solution according to the manufacturer's instructions. Image acquisition was done with a Leica TCS SP5 II confocal microscope setup and Leica M80 equipped with a Leica DFC295 camera. Quantification of hippocampi was performed with ImageJ (Schindelin et al., 2012).

4.10. DiI axonal tracing

Brains of E18.5 mice were fixed for 24 h in 4 % PFA. After fixation NeuroTrace® DiI tissue-labeling paste (Invitrogen) was applied along the midline on the surface of one hemisphere of the neocortex. Brains were incubated for 5 weeks at 37 °C in a humidified environment of 1% PFA in PBS. 250 μm transversal brain sections were obtained with a Leica VT 1000S and stained with the DNA dye Hoechst (1:1,000, Invitrogen) for 15 min. Images were acquired with a Leica TCS SP5 II confocal microscope.

4.11. Statistical analysis

Statistical tests were done in R or Sigma Plot. For comparing mean values between groups, student's *t*-test or Mann-Whitney *U* test was performed. Analyzing the rescue conditions, ANOVA with post-hoc test was used. Stage distribution ('hand shaped' vs. smooth, non-collapsed vs. collapsed) was tested for differences with χ2-test.

Author contributions

Blastocyst injection of CAP1 targeted ES cells was performed by CAH. Experiments were designed and results were discussed by FS, TAD, IM, JW, UE and MBR. Data were analyzed by FS, TAD, IM, JW, UE and MBR. Manuscript was written by MBR and FS.

Appendix A. The Peer Review Overview and Supplementary data

The Peer Review Overview and Supplementary data associated with this article can be found in the online version, at doi: https://doi.org/10.1016/j.pneurobio.2021.102050.

References

Antoniou, A., Khudayberdiev, S., Idziak, A., Bicker, S., Jacob, R., Schratt, G., 2018. The dynamic recruitment of TRBP to neuronal membranes mediates dendritogenesis during development. EMBO Rep. 19, e44853.

Baarlink, C., Plessner, M., Sherrard, A., Morita, K., Misu, S., Virant, D., Kleinschnitz, E. M., Harniman, R., Alibhai, D., Baumeister, S., Miyamoto, K., Endesfelder, U., Kaidi, A., Grosse, R., 2017. A transient pool of nuclear F-actin at mitotic exit controls chromatin organization. Nat. Cell Biol. 19, 1389–1399.

Balcer, H.I., Goodman, A.L., Rodal, A.A., Smith, E., Kugler, J., Heuser, J.E., Goode, B.L., 2003. Coordinated regulation of actin filament turnover by a high-molecular-weight Srv2/CAP complex, cofilin, profilin, and Aip1. Curr. Biol. 13, 2159–2169.

Balinovic, A., Albrecht, D., Endesfelder, U., 2019. Spectrally red-shifted fluorescent fiducial markers for optimal drift correction in localization microscopy. J. Phys. D Appl. Phys. 52, 204002.

Bellenchi, G.C., Gurniak, C.B., Perlas, E., Middei, S., Ammassari-Teule, M., Witke, W., 2007. N-cofilin is associated with neuronal migration disorders and cell cycle control in the cerebral cortex. Genes Dev. 21, 2347–2357.

Bertling, E., Hotulainen, P., Mattila, P.K., Matilainen, T., Salminen, M., Lappalainen, P., 2004. Cyclase-associated protein 1 (CAP1) promotes cofilin-induced actin dynamics in mammalian nonmuscle cells. Mol. Biol. Cell 15, 2324–2334.

Bertling, E., Quintero-Monzon, O., Mattila, P.K., Goode, B.L., Lappalainen, P., 2007. Mechanism and biological role of profilin-Srv2/CAP interaction. J. Cell. Sci. 120, 1225–1234.

Biswas, S., Kalil, K., 2018. The microtubule-associated protein tau mediates the organization of microtubules and their dynamic exploration of actin-rich lamellipodia and filopodia of cortical growth cones. J. Neurosci. 38, 291–307.

Chaudhry, F., Little, K., Talarico, L., Quintero-Monzon, O., Goode, B.L., 2010. A central role for the WH2 domain of Srv2/CAP in recharging actin monomers to drive actin turnover in vitro and in vivo. Cytoskeleton 67, 120–133.

Chitsaz, D., Morales, D., Law, C., Kania, A., 2015. An automated strategy for unbiased morphometric analyses and classifications of growth cones in vitro. PLoS One 10, e0140959.

Dent, E.W., Gupton, S.L., Gertler, F.B., 2011. The growth cone cytoskeleton in axon outgrowth and guidance. Cold Spring Harb. Perspect. Biol. 3.

Dotti, C.G., Sullivan, C.A., Banker, G.A., 1988. The establishment of polarity by hippocampal neurons in culture. J. Neurosci. 8, 1454–1468.

Dupraz, S., Hilton, B.J., Husch, A., Santos, T.E., Coles, C.H., Stern, S., Brakebusch, C., Bradke, F., 2019. RhoA controls axon extension independent of specification in the developing brain. Curr. Biol. 29, 3874–3886.

Endesfelder, U., Malkusch, S., Fricke, F., Heilemann, M., 2014. A simple method to estimate the average localization precision of a single-molecule localization microscopy experiment. Histochem. Cell Biol. 141, 629–638.

Field, J., Ye, D.Z., Shinde, M., Liu, F., Schillinger, K.J., Lu, M., Wang, T., Skettini, M., Xiong, Y., Brice, A.K., Chung, D.C., Patel, V.V., 2015. CAP2 in cardiac conduction, sudden cardiac death and eye development. Sci. Rep. 5, 17256.

Flynn, K.C., Hellal, F., Neukirchen, D., Jacob, S., Tahirovic, S., Dupraz, S., Stern, S., Garvalov, B.K., Gurniak, C., Shaw, A.E., Meyn, L., Wedlich-Soldner, R., Bamburg, J. R., Small, J.V., Witke, W., Bradke, F., 2012. ADF/Cofilin-mediated actin retrograde flow directs neurite formation in the developing brain. Neuron 76, 1091–1107.

Freeman, N.L., Field, J., 2000. Mammalian homolog of the yeast cyclase associated protein, CAP/Srv2p, regulates actin filament assembly. Cell Mot Cytoskeleton 45, 106–120.

Garvalov, B.K., Flynn, K.C., Neukirchen, D., Meyn, L., Teusch, N., Wu, X., Brakebusch, C., Bamburg, J.R., Bradke, F., 2007. Cdc42 regulates cofilin during the establishment of neuronal polarity. J. Neurosci. 27, 13117–13129.

Gomez, T.M., Letourneau, P.C., 2014. Actin dynamics in growth cone motility and navigation. J. Neurochem. 129, 221–234.

Görlich, A., Wolf, M., Zimmermann, A.M., Gurniak, C.B., Al Banchaabouchi, M., Sassoe-Pognetto, M., Witke, W., Friauf, E., Rust, M.B., 2011. N-cofilin can compensate for the loss of ADF in excitatory synapses. PLoS One 6, e26789.

Grintsevich, E.E., Yesilyurt, H.G., Rich, S.K., Hung, R.J., Terman, J.R., Reisler, E., 2016. F-actin dismantling through a redox-driven synergy between Mical and cofilin. Nat. Cell Biol. 18, 876–885.

Gurniak, C.B., Chevessier, F., Jokwitz, M., Jonsson, F., Perlas, E., Richter, H., Matern, G., Boyl, P.P., Chaponnier, C., Furst, D., Schroder, R., Witke, W., 2014. Severe protein aggregate myopathy in a knockout mouse model points to an essential role of cofilin2 in sarcomeric actin exchange and muscle maintenance. Eur. J. Cell Biol. 93, 252–266.

Hsieh, S.H., Ferraro, G.B., Fournier, A.E., 2006. Myelin-associated inhibitors regulate cofilin phosphorylation and neuronal inhibition through LIM kinase and Slingshot phosphatase. J. Neurosci. 26, 1006–1015.

Hubberstey, A.V., Mottillo, E.P., 2002. Cyclase-associated proteins: CAPacity for linking signal transduction and actin polymerization. FASEB J. 16, 487–499.

Jang, H.D., Lee, S.E., Yang, J., Lee, H.C., Shin, D., Lee, H., Lee, J., Jin, S., Kim, S., Lee, S. J., You, J., Park, H.W., Nam, K.Y., Lee, S.H., Park, S.W., Kim, J.S., Kim, S.Y., Kwon, Y.W., Kwak, S.H., Yang, H.M., Kim, H.S., 2019. Cyclase-associated protein 1 is a binding partner of proprotein convertase subtilisin/kexin type-9 and is required for the degradation of low-density lipoprotein receptors by proprotein convertase subtilisin/kexin type-9. Eur. Heart J. 41, 239–252.

Jansen, S., Collins, A., Golden, L., Sokolova, O., Goode, B.L., 2014. Structure and mechanism of mouse cyclase-associated protein (CAP1) in regulating actin dynamics. J. Biol. Chem. 289, 30732–30742.

Johnston, A.B., Collins, A., Goode, B.L., 2015. High-speed depolymerization at actin filament ends jointly catalysed by Twinfilin and Srv2/CAP. Nat. Cell Biol. 17, 1504–1511.

Kepser, L.J., Damar, F., De Cicco, T., Chaponnier, C., Proszynski, T.J., Pagenstecher, A., Rust, M.B., 2019. CAP2 deficiency delays myofibril actin cytoskeleton differentiation and disturbs skeletal muscle architecture and function. Proc. Natl. Acad. Sci. U.S.A. 116, 8397–8402.

Kotila, T., Kogan, K., Enkavi, G., Guo, S., Vattulainen, I., Goode, B.L., Lappalainen, P., 2018. Structural basis of actin monomer re-charging by cyclase-associated protein. Nat. Commun. 9, 1892.

Kotila, T., Wioland, H., Enkavi, G., Kogan, K., Vattulainen, I., Jegou, A., Romet-Lemonne, G., Lappalainen, P., 2019. Mechanism of synergistic actin filament pointed end depolymerization by cyclase-associated protein and cofilin. Nat. Commun. 10, 5320.

Kullmann, J.A., Meyer, S., Pipicelli, F., Kyrousi, C., Schneider, F., Bartels, N., Cappello, S., Rust, M.B., 2020a. Profilin1-dependent F-Actin assembly controls division of apical radial glia and neocortex development. Cereb. Cortex 30, 3467–3482.

Kullmann, J.A., Trivedi, N., Howell, D., Laumonnerie, C., Nguyen, V., Banerjee, S.S., Stabley, D.R., Shirinifard, A., Rowitch, D.H., Solecki, D.J., 2020b. Oxygen tension and the VHL-Hif1alpha pathway determine onset of neuronal polarization and cerebellar granule zone exit. Neuron 106, 607–623.

Lowery, L.A., Van Vactor, D., 2009. The trip of the tip: understanding the growth cone machinery. Nat. Rev. Mol. Cell Biol. 10, 332–343.

Makkonen, M., Bertling, E., Chebotareva, N.A., Baum, J., Lappalainen, P., 2013. Mammalian and malaria parasite cyclase-associated proteins catalyze nucleotide exchange on G-actin through a conserved mechanism. J. Biol. Chem. 288, 984–994.

Mattila, P.K., Quintero-Monzon, O., Kugler, J., Moseley, J.B., Almo, S.C., Lappalainen, P., Goode, B.L., 2004. A high-affinity interaction with ADP-actin monomers underlies the mechanism and in vivo function of Srv2/cyclase-associated protein. Mol. Biol. Cell 15, 5158–5171.

Melak, M., Plessner, M., Grosse, R., 2017. Actin visualization at a glance. J. Cell. Sci. 130, 525–530.

Moriyama, K., Yahara, I., 2002. Human CAP1 is a key factor in the recycling of cofilin and actin for rapid actin turnover. J. Cell. Sci. 115, 1591–1601.

Mu, A., Fung, T.S., Kettenbach, A.N., Chakrabarti, R., Higgs, H.N., 2019. A complex containing lysine-acetylated actin inhibits the formin INF2. Nat. Cell Biol. 21, 592–602.

Muller, B., Stahl, B., Bonhoeffer, F., 1990. In vitro experiments on axonal guidance and growth-cone collapse. J. Exp. Biol. 153, 29–46.

Nomura, K., Ono, S., 2013. ATP-dependent regulation of actin monomer-filament equilibrium by cyclase-associated protein and ADF/cofilin. Biochem. J. 453, 249–259.

Omotade, O.F., Pollitt, S.L., Zheng, J.Q., 2017. Actin-based growth cone motility and guidance. Mol. Cell. Neurosci. 84, 4–10.

Ovesny, M., Krizek, P., Borkovec, J., Svindrych, Z., Hagen, G.M., 2014. ThunderSTORM: a comprehensive ImageJ plug-in for PALM and STORM data analysis and super-resolution imaging. Bioinformatics 30, 2389–2390.

Peche, V.S., Holak, T.A., Burgute, B.D., Kosmas, K., Kale, S.P., Wunderlich, F.T., Elhamine, F., Stehle, R., Pfitzer, G., Nohroudi, K., Addicks, K., Stockigt, F., Schrickel, J.W., Gallinger, J., Schleicher, M., Noegel, A.A., 2012. Ablation of cyclase-associated protein 2 (CAP2) leads to cardiomyopathy. Cell. Mol. Life Sci. 70, 527–543.

Pelucchi, S., Vandermeulen, L., Pizzamiglio, L., Aksan, B., Yan, J., Konietzny, A., Bonomi, E., Borroni, B., Padovani, A., Rust, M.B., Di Marino, D., Mikhaylova, M., Mauceri, D., Antonucci, F., Edefonti, V., Gardoni, F., Di Luca, M., Marcello, E., 2020.

CAP2 dimerization regulates Cofilin in structural plasticity and Alzheimer's disease. Brain Commun. In press.

Piper, M., Anderson, R., Dwivedy, A., Weinl, C., van Horck, F., Leung, K.M., Cogill, E., Holt, C., 2006. Signaling mechanisms underlying Slit2-induced collapse of Xenopus retinal growth cones. Neuron 49, 215–228.

Pollard, T.D., 2017. What we know and do not know about actin. Handb. Exp. Pharmacol. 235, 331–347.

Quintero-Monzon, O., Jonasson, E.M., Bertling, E., Talarico, L., Chaudhry, F., Sihvo, M., Lappalainen, P., Goode, B.L., 2009. Reconstitution and dissection of the 600-kDa Srv2/CAP complex: roles for oligomerization and cofilin-actin binding in driving actin turnover. J. Biol. Chem. 284, 10923–10934.

Ramón y Cajal, S., 1909. Histologie du System Nerveux de l'Homme et des Vertebres. Malonine, Paris.

Rehklau, K., Hoffmann, L., Gurniak, C.B., Ott, M., Witke, W., Scorrano, L., Culmsee, C., Rust, M.B., 2017. Cofilin1-dependent actin dynamics control DRP1-mediated mitochondrial fission. Cell Death Dis. 8, e3063.

Riedl, J., Crevenna, A.H., Kessenbrock, K., Yu, J.H., Neukirchen, D., Bista, M., Bradke, F., Jenne, D., Holak, T.A., Werb, Z., Sixt, M., Wedlich-Soldner, R., 2008. Lifeact: a versatile marker to visualize F-actin. Nat. Methods 5, 605–607.

Rust, M.B., 2015. ADF/cofilin: a crucial regulator of synapse physiology and behavior. Cell. Mol. Life Sci. 72, 3521–3529.

Rust, M.B., Gurniak, C.B., Renner, M., Vara, H., Morando, L., Gorlich, A., Sassoe-Pognetto, M., Banchaabouchi, M.A., Giustetto, M., Triller, A., Choquet, D., Witke, W., 2010. Learning, AMPA receptor mobility and synaptic plasticity depend on n-cofilin-mediated actin dynamics. EMBO J. 29, 1889–1902.

Rust, M.B., Khudayberdiev, S., Pelucchi, S., Marcello, E., 2020. CAPt'n of actin dynamics: recent advances in the molecular, developmental and physiological functions of cyclase-associated protein (CAP). Front. Cell Dev. Biol. 8, 586631.

Schindelin, J., Arganda-Carreras, I., Frise, E., Kaynig, V., Longair, M., Pietzsch, T., Preibisch, S., Rueden, C., Saalfeld, S., Schmid, B., Tinevez, J.Y., White, D.J., Hartenstein, V., Eliceiri, K., Tomancak, P., Cardona, A., 2012. Fiji: an open-source platform for biological-image analysis. Nat. Methods 9, 676–682.

Shekhar, S., Chung, J., Kondev, J., Gelles, J., Goode, B.L., 2019. Synergy between Cyclase-associated protein and Cofilin accelerates actin filament depolymerization by two orders of magnitude. Nat. Commun. 10, 5319.

Spence, E.F., Soderling, S.H., 2015. Actin out: regulation of the synaptic cytoskeleton. J. Biol. Chem. 290, 28613–28622.

Tokunaga, M., Imamoto, N., Sakata-Sogawa, K., 2008. Highly inclined thin illumination enables clear single-molecule imaging in cells. Nat. Methods 5, 159–161.

Tronche, F., Kellendonk, C., Kretz, O., Gass, P., Anlag, K., Orban, P.C., Bock, R., Klein, R., Schutz, G., 1999. Disruption of the glucocorticoid receptor gene in the nervous system results in reduced anxiety. Nature Genet 23, 99–103.

van de Linde, S., Loschberger, A., Klein, T., Heidbreder, M., Wolter, S., Heilemann, M., Sauer, M., 2011. Direct stochastic optical reconstruction microscopy with standard fluorescent probes. Nat. Protoc. 6, 991–1009.

Virant, D., Traenkle, B., Maier, J., Kaiser, P.D., Bodenhofer, M., Schmees, C., Vojnovic, I., Pisak-Lukats, B., Endesfelder, U., Rothbauer, U., 2018. A peptide tag-specific nanobody enables high-quality labeling for dSTORM imaging. Nat. Commun. 9, 930.

Vitriol, E.A., Zheng, J.Q., 2012. Growth cone travel in space and time: the cellular ensemble of cytoskeleton, adhesion, and membrane. Neuron 73, 1068–1081.

Wang, W., Rai, A., Hur, E.M., Smilansky, Z., Chang, K.T., Min, K.T., 2016. DSCR1 is required for both axonal growth cone extension and steering. J. Cell Biol. 213, 451–462.

Wen, Z., Han, L., Bamburg, J.R., Shim, S., Ming, G.L., Zheng, J.Q., 2007. BMP gradients steer nerve growth cones by a balancing act of LIM kinase and Slingshot phosphatase on ADF/cofilin. J. Cell Biol. 178, 107–119.

Wills, Z., Emerson, M., Rusch, J., Bikoff, J., Baum, B., Perrimon, N., Van Vactor, D., 2002. A Drosophila homolog of cyclase-associated proteins collaborates with the Abl tyrosine kinase to control midline axon pathfinding. Neuron 36, 611–622.

Winterflood, C.M., Platonova, E., Albrecht, D., Ewers, H., 2015. Dual-color 3D superresolution microscopy by combined spectral-demixing and biplane imaging. Biophys. J. 109, 3–6.

Wolf, M., Zimmermann, A.M., Gorlich, A., Gurniak, C.B., Sassoe-Pognetto, M., Friauf, E., Witke, W., Rust, M.B., 2015. ADF/Cofilin controls synaptic actin dynamics and regulates synaptic vesicle mobilization and exocytosis. Cereb. Cortex 25, 2863–2875.

Wolter, S., Loschberger, A., Holm, T., Aufmkolk, S., Dabauvalle, M.C., van de Linde, S., Sauer, M., 2012. rapidSTORM: accurate, fast open-source software for localization microscopy. Nat. Methods 9, 1040–1041.

Yang, Q., Zhang, X.F., Pollard, T.D., Forscher, P., 2012. Arp2/3 complex–dependent actin networks constrain myosin II function in driving retrograde actin flow. J. Cell Biol. 197, 939–956.

Zhang, X.F., Ajeti, V., Tsai, N., Fereydooni, A., Burns, W., Murrell, M., De La Cruz, E.M., Forscher, P., 2019. Regulation of axon growth by myosin II-dependent mechanocatalysis of cofilin activity. J. Cell Biol. 218, 2329–2349.

Zimmermann, A.M., Jene, T., Wolf, M., Gorlich, A., Gurniak, C.B., Sassoe-Pognetto, M., Witke, W., Friauf, E., Rust, M.B., 2015. Attention-Deficit/Hyperactivity disorder-like phenotype in a mouse model with impaired actin dynamics. Biol. Psychiatry 78, 95–106.
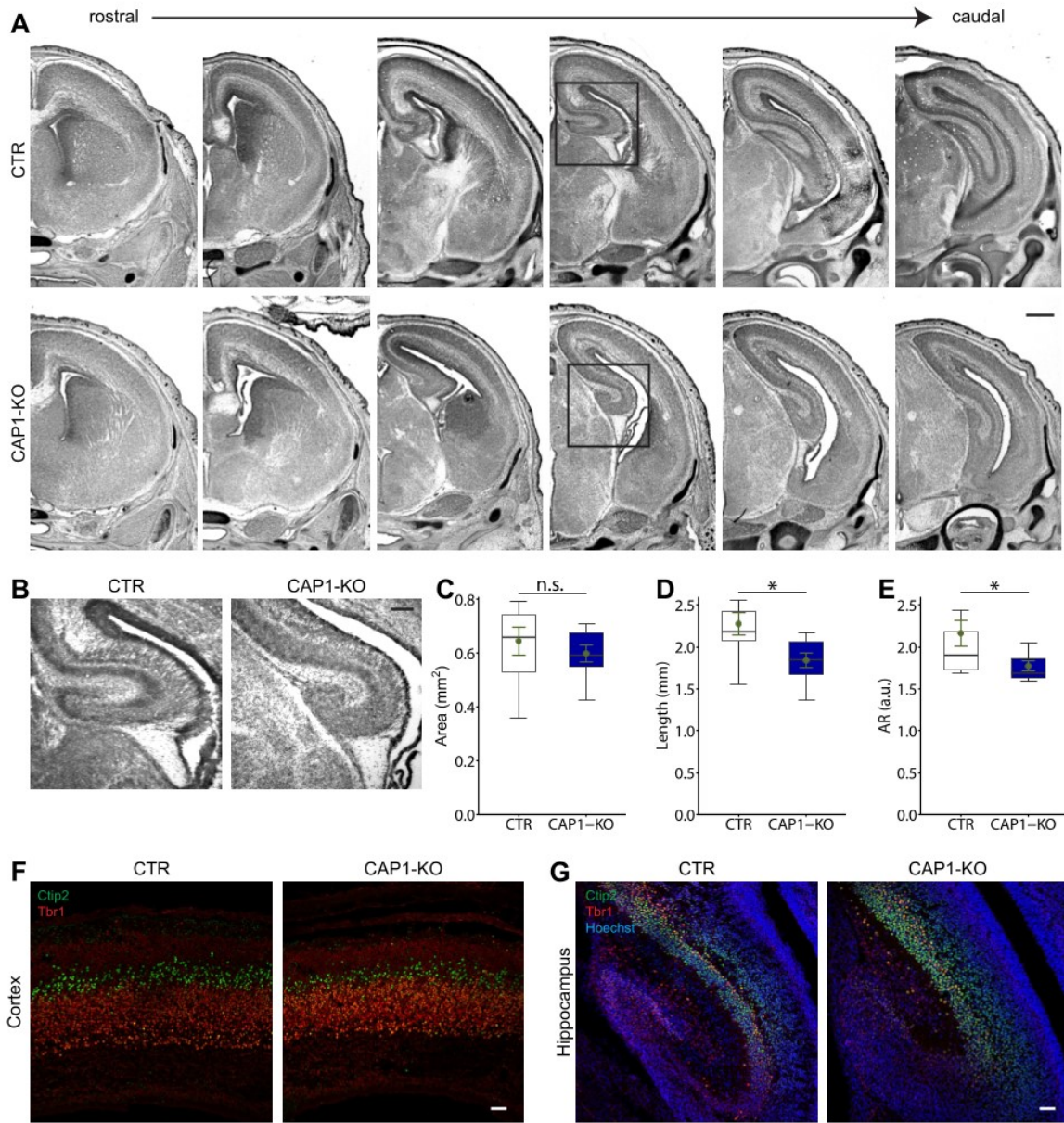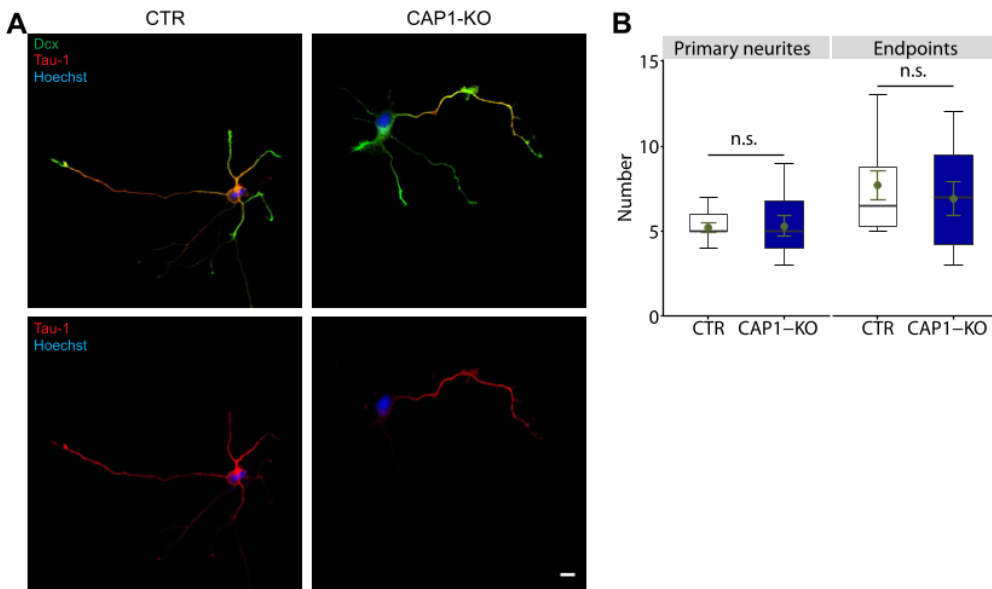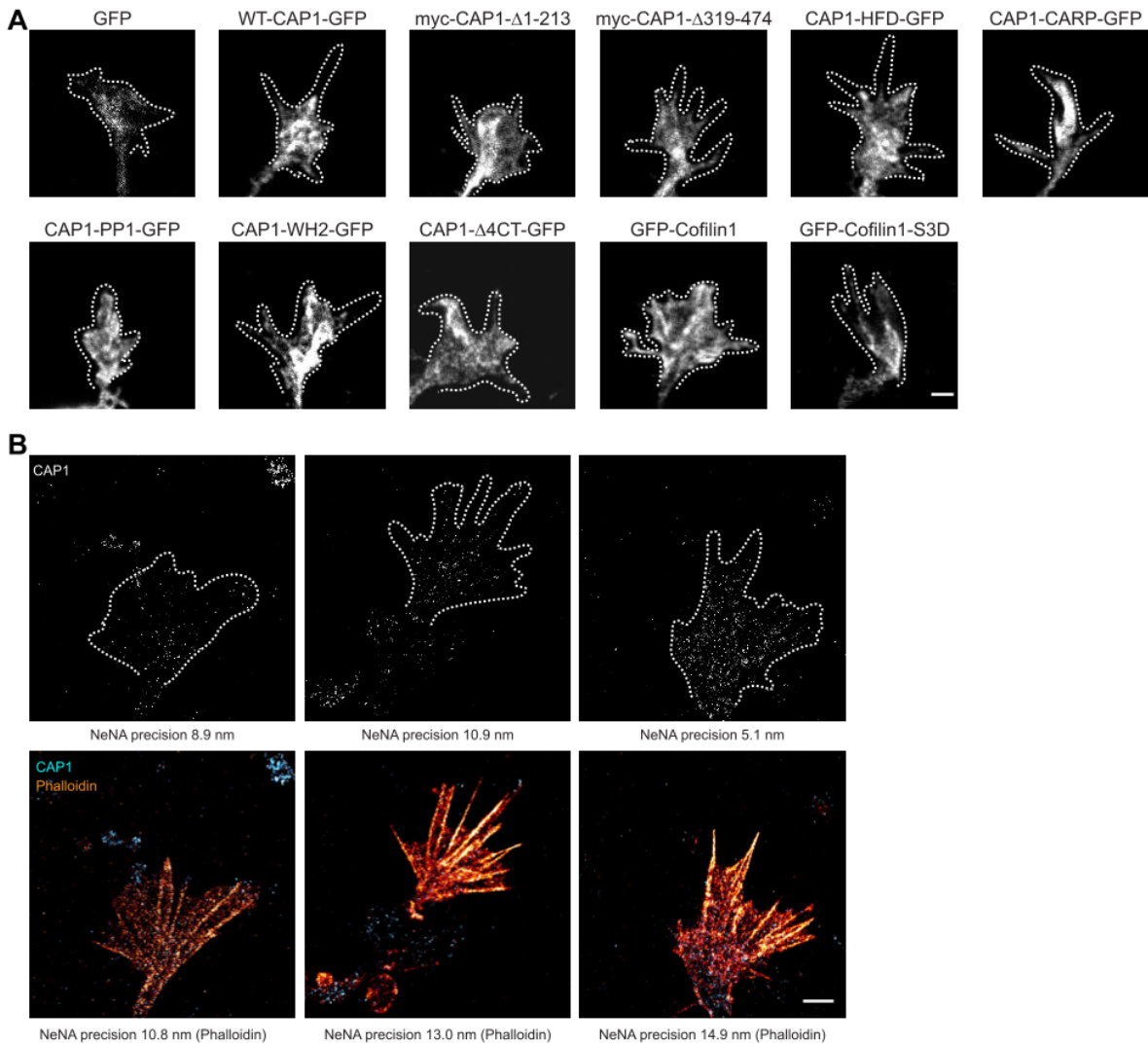
Figure S1

Figure S2

Figure S3

A

CTR — NeNA precision 12.4 nm | NeNA precision 12.4 nm | NeNA precision 13.7 nm

CAP1-KO — NeNA precision 13.7 nm | NeNA precision 13.7 nm | NeNA precision 11.5 nm

B

α-Tubulin

CTR — NeNA precision 11.6 nm | NeNA precision 13.0 nm (Phalloidin) | NeNA precision 14.6 nm | NeNA precision 18.2 nm (Phalloidin)

CAP1-KO — NeNA precision 12.9 nm | NeNA precision 17.0 nm (Phalloidin) | NeNA precision 11.1 nm | NeNA precision 9.5 nm (Phalloidin)

CTR — NeNA precision 12.3 nm | NeNA precision 16.7 nm (Phalloidin) | NeNA precision 11.8 nm | NeNA precision 14.2 nm (Phalloidin)

CAP1-KO — NeNA precision 12.0 nm | NeNA precision 11.6 nm (Phalloidin) | NeNA precision 12.0 nm | NeNA precision 15.2 nm (Phalloidin)

C

*** Microtubule   *** Actin bundles

CTR   CAP1−KO

D

No. of microtubule reaching leading edge

***

CTR   CAP1−KO

Figure S4

55

Figure S5

Legends to supplementary figures

Figure S1. (A) Nissl staining of transversal brain sections from E18.5 CTR and CAP1-KO mice. Boxes indicate areas shown at higher magnification in B. **(B)** Nissl-stained hippocampus from transversal brain sections E18.5 CTR and CAP1-KO mice. Graphs showing **(C)** hippocampal area, **(D)** length of the cornus ammonis and **(E)** hippocampal aspect ratio (AR) in transversal brain sections. **(F-G)** Antibody staining of transversal brain sections from E18.5 CTR and CAP1-KO mice against the neuronal markers Tbr1 (red) and Ctip2 (green). CTX: cerebral cortex, HIP: hippocampus. Sections were additionally stained with Hoechst (blue). Scale bars (in µm): 500 (A), 250 (B), 50 (F, G). n.s.: $P \geq 0.05$, *: $P < 0.05$.

Figure S2. (A) Stage 3 neurons stained with antibodies against the axon marker tau-1 (red) and Dcx (green). Neurons were additionally stained with Hoechst (blue). **(B)** Number of primary neurites and neurite endpoints in stage 3 CTR and CAP1-KO neurons. Scale bar (in µm): 10. n.s.: $P \geq 0.05$.

Figure S3. (A) Localization of GFP, GFP-WT-CAP1, mutant GFP-CAP1 variants, myc-tagged CAP1 deletion constructs and GFP-cofilin1 in DIV1 growth cones. Dashed lines outline growth cones as deduced from phalloidin labelling (not shown). **(B)** dSTORM-acquired micrographs showing growth cones from CTR neurons overexpressing myc-CAP1 stained with phalloidin (orange) and antibodies against CAP1 and myc (light blue). Scale bars (in µm): 2 (A, B).

Figure S4. (A) Micrographs of phalloidin-stained growth cones from CTR and CAP1-KO neurons acquired by dSTORM. Dashed line marks border between C domain and T zone. Crossed out box marks position of fiducial marker used for drift correction. **(B)** dSTORM-acquired micrographs showing growth cones from CTR and CAP1-KO neurons stained with phalloidin (orange) and an antibody against α-tubulin (blue). Graphs showing number of **(C)** microtubule and actin bundles per growth cone and **(D)** microtubule number approaching the leading edge. Scale bars (in µm): 2 (A, B). ***: $P < 0.001$.

1

Figure S5. Micrographs of phalloidin and CAP1-stained growth cones from CAP1[flx/flx] neurons either expressing Cre-mut or Cre. Dashed lines outline growth cones. Scale bar (in µm): 2.

Movie S1: Movie showing a CTR growth cone imaged by differential interference contrast (DIC) microscopy. Many protruding and retracting filopodia were present during image acquisition of 10 min. Scale bar: 2 µm.

Movie S2: Absence of filopodia and only low motility in a representative DIC imaged CAP1-KO growth cone. Acquisition time: 10 min, scale bar: 2 µm.

Movie S3: Movie showing GFP-actin recovery upon bleaching in a CTR growth cone. Upon bleaching fluorescence recovery was recorded over a time course of 3 min. Scale bar: 2 µm.

Movie S4: Movie showing GFP-actin recovery upon bleaching in a CAP1-KO growth cone. Upon bleaching fluorescence recovery was recorded over a time course of 3 min. Scale bar: 2 µm.

Movie S5: Movie showing a growth cone from a LifeAct-GFP-transfected CTR neuron. Images were acquired every 5 s for 5 min. Scale bar: 2 µm.

Movie S6: Movie showing a growth cone from a LifeAct-GFP-transfected CAP1-KO neuron. Images were acquired every 5 s for 5 min. Scale bar: 2 µm.

Movie S7: Movie showing GFP-actin recovery upon bleaching in a growth cone from a control neuron expressing catalytic inactive Cre (Cre-mut). Upon bleaching fluorescence recovery was recorded over a time course of 3 min. Scale bar: 2 µm.

2

Movie S8: Movie showing GFP-actin recovery upon bleaching in a growth cone from a Cre-expressing CAP1$^{flx/flx}$ neuron. Upon bleaching fluorescence recovery was recorded over a time course of 3 min. Scale bar: 2 μm.

Movie S9: Movie showing a growth cone from a LifeAct-GFP-transfected control neuron expressing catalytic inactive Cre (Cre-mut). Images were acquired every 5 s for 5 min. Scale bar: 2 μm.

Movie S10: Movie showing a growth cone from a LifeAct-GFP-transfected Cre-expressing CAP1$^{flx/flx}$ neuron. Images were acquired every 5 s for 5 min. Scale bar: 2 μm.

Movie S11: Movie showing GFP-actin recovery upon bleaching in a growth cone from a Cre-expressing Cfl1$^{flx/flx}$ neuron. Upon bleaching fluorescence recovery was recorded over a time course of 3 min. Scale bar: 2 μm.

Movie S12: Movie showing a growth cone from a LifeAct-GFP-transfected Cre-expressing Cfl1$^{flx/flx}$ neuron. Images were acquired every 5 s for 5 min. Scale bar: 2 μm.

Movie S13: Movie showing GFP-actin recovery upon bleaching in a growth cone from a Cre-expressing CAP1$^{flx/flx}$/Cfl1$^{flx/flx}$ neuron. Upon bleaching fluorescence recovery was recorded over a time course of 3 min. Scale bar: 2 μm.

Movie S14: Movie showing a growth cone from a LifeAct-GFP-transfected Cre-expressing CAP1$^{flx/flx}$/Cfl1$^{flx/flx}$ neuron. Images were acquired every 5 s for 5 min. Scale bar: 2 μm.

3

Neuron replating, a powerful and versatile approach to study early aspects of neuron differentiation, *Cells*, 2021

Novel Tools and Methods

Neuron Replating, a Powerful and Versatile Approach to Study Early Aspects of Neuron Differentiation

Felix Schneider,[1,2,3] Thuy-An Duong,[1] and ⓘMarco B. Rust[1,2,3]

[1]Molecular Neurobiology Group, Institute of Physiological Chemistry, University of Marburg, Marburg 35032, Germany, [2]Center for Mind, Brain and Behavior (CMBB), University of Marburg and Justus-Liebig-University Giessen, Marburg 35032, Germany, and [3]DFG Research Training Group, Membrane Plasticity in Tissue Development and Remodeling, GRK 2213, University of Marburg, Marburg 35032, Germany

Abstract

Neuron differentiation includes formation and outgrowth of neurites that differentiate into axons or dendrites. Directed neurite outgrowth is controlled by growth cones that protrude and retract actin-rich structures to sense environmental cues. These cues control local actin filament dynamics, steer growth cones toward attractants and away from repellents, and navigate neurites through the developing brain. Rodent hippocampal neurons are widely used to study the mechanisms underlying neuron differentiation. Genetic manipulation of isolated neurons including gene inactivation or reporter gene expression can be achieved by classical transfections methods, but these methods are restricted to neurons cultured for several days, after neurite formation or outgrowth. Instead, electroporation allows gene manipulation before seeding. However, reporter gene expression usually takes up to 24 h, and time course of gene inactivation depends on the half live of the targeted mRNA and gene product. Hence, these methods do not allow to study early aspects of neuron differentiation. In the present study, we provide a detailed protocol in which we combined electroporation-based gene manipulation of mouse hippocampal neurons before initial seeding with a replating step after 2 d *in vitro* (DIV) that resets neurons into an undifferentiated stage. By categorizing neurons according to their differentiation stage, thorough morphometric analyses, live imaging of actin dynamics in growth cones as well as guidance cue-mediated growth cone morphologic changes, we demonstrate that differentiation and function of replated neurons did not differ from non-replated neurons. In summary, we provide a protocol that allows to thoroughly characterize differentiation of mouse primary hippocampal neurons.

Key words: actin; cofilin; growth; neurite; neuron replating; replating

Significance Statement

Unraveling the molecular mechanisms that control neuron differentiation requires reporter gene expression or gene inactivation. In mouse primary hippocampal neurons, a widely used cellular system to study neuron differentiation, classical transfection methods are restricted to later stages of differentiation. Instead, electroporation allows genetic manipulation before seeding. However, time course of reporter gene expression or gene inactivation frequently hinders a full characterization of neuron differentiation, specifically of early stages. To circumvent this limitation, we combined electroporation-based genetic manipulation before initial seeding with a replating step after 2 d *in vitro* (DIV), which reset neurons into an undifferentiated stage. We show that replated neurons differentiated similar to non-replated neurons. We provide a detailed protocol that allows to comprehensively characterize the molecular mechanisms underlying neuron differentiation.

eNeuro

Introduction

During differentiation, neurons undergo striking morphologic changes from spheres to polar cells possessing an axon and a highly branched dendritic compartment (Dotti et al., 1988; da Silva and Dotti, 2002). Essential steps during early neuron differentiation include the formation and outgrowth of neurites, which later differentiate into axons or dendrites. Directed neurite outgrowth depends on growth cones, structures at neurite tips enriched in actin filaments (F-actin) that steer neurites toward attractants and away from repellent cues and, hence, navigate neurites through the developing brain (Gomez and Letourneau, 2014). Cultured hippocampal neurons isolated from mice or rats are widely used cellular systems to study neuron differentiation as they readily polarize on a two-dimensional substrate at very low densities (Dotti et al., 1988; da Silva and Dotti, 2002). Genetic manipulation including gene silencing, gene deletion or reporter gene expression provide powerful approaches to study virtually all biological processes in cellular systems, including neuron differentiation. Electroporation-based nucleofection as well as classical transfection procedures such as liposome-based transfection or calcium phosphate precipitation are the most commonly applied methods for gene transfer into cultured hippocampal neurons as they are far less labor-intensive when compared with virus infection (Dudek et al., 2001; Ohki et al., 2001; Zeitelhofer et al., 2009; Viesselmann et al., 2011; Sun et al., 2013). Unfortunately, efficiency of classical transfection procedures is rather low and these approaches are convenient only for hippocampal neurons cultured for several days, e.g., at around 6 d *in vitro* (DIV) or later. Instead, nucleofection allows genetic manipulation of hippocampal neurons before seeding. However, expression of reporter genes usually takes up to 24 h, and more importantly, time course and efficiency of gene silencing or gene deletion depends on the half live of the targeted mRNA and gene product. Consequently, nucleofection of hippocampal neurons does not allow a thorough analysis of neuron differentiation, specifically not of early processes during neuron differentiation. Thus, experimental approaches are needed to circumvent these limitations. We here report a protocol to reset primary hippocampal neurons from embryonic mice at DIV2 into an undifferentiated stage. Before initial seeding, these neurons can be manipulated genetically by means of nucleofection. We show that a combination of nucleofection and replating allows to study early aspects of neuron differentiation.

Materials and Methods

Mice

Generation of ADF−/−/Cfl1$^{flx/flx}$ mice has been reported before (Bellenchi et al., 2007; Wolf et al., 2015; Zimmermann et al., 2015). Mice were housed with food and water available *ad libitum* on 12/12 h light/dark cycles. Treatment of mice was in accordance with the German law for conducting animal experiments and followed the guidelines for the care and use of laboratory animals of the National Institutes of Health. Killing of mice has been approved by internal animal welfare authorities (references: AK-5-2014, AK-6-2014, AK-12-2020). Genetic inactivation of Cfl1 in neurons from ADF−/−/Cfl1$^{flx/flx}$ mice was achieved by nucleofection of catalytic active mCherry-Cre. ADF−/−/Cfl1$^{flx/flx}$ neurons expressing a mutant, catalytic inactive mCherry-Cre served as controls. Both constructs have been achieved from the Solecki lab (Kullmann et al., 2020).

Hippocampus dissection and neuron isolation

One day before neuron isolation, glass cover slips (13 mm in diameter, VWR) were placed into 24-well plates and coated overnight with 0.1 mg/ml poly-L-lysine hydrobromid (dilution of 1 mg/ml poly-L-lysine with 0.1 M boric acid at pH 8.5) in a humidified incubator at 37°C and 5% CO_2. For replating, 24-well plates without cover slips were coated with 0.05 mg/ml poly-L-lysine hydrobromid and similar incubated as above. On the day of neuron isolation, plates were washed twice with ddH_2O and equilibrated either with 500-µl nucleofection medium (DMEM-31966; Invitrogen) supplemented with 10% fetal bovine serum (FBS; Invitrogen) or for non-nucleofected neurons with neurobasal (NB; Invitrogen) medium. Mice of either sex were killed at embryonic day (E)18.5 by decapitation, and brains were dissected on ice in Leibovitz's L15-Medium with 7 mM HEPES (L15+H, Invitrogen). After removal of the meninges, hippocampi of each embryo were isolated and collected in a tube containing cooled L15+H. Thereafter, medium was replaced by 500-µl pre-warmed TrypLE Express (Invitrogen) per embryo and incubated for 6 min at 37°C. Subsequently, hippocampi were washed twice with NB medium containing 2% B27, 2 mM GlutaMax, 100 µg/ml streptomycin, and 100 U/ml penicillin (NB+, Invitrogen). After washing, neurons were triturated in 1 ml NB+ by pipetting seven times up and down with a P1000 pipette. Neuron solution was filled up to 1 ml NB+ medium per embryo and density was calculated by using a hemocytometer. Thereafter, neurons were plated at a density of 60,000 cells per well. 5 h after plating, medium was completely replaced by NB+ medium.

Electroporation of hippocampal neurons

In some experiments, neurons were electroporated before plating. In these experiments, electroporation was

eNeuro

performed according to manufacturer's protocol by using the Amaxa P3 Primary Cell 4D-Nucleofector X kit L (Lonza) and 4D-Nucleofector (Lonza). For nucleofection, 250,000 neurons were transfected with 3-μg plasmid and the entire neuron suspension was plated in a single well of a 24-well plate in nucleofection medium; 5 h after plating, medium was completely replaced by NB+ medium.

Replating of hippocampal neurons

At DIV2, neurons were detached and plated again (re-plated) on cover slips. Before replating, coverslips were prepared as described above. For replating, condition medium (350-μl medium from each well + 200 μl fresh NB+ medium for each well) was collected and kept in the water bath at 37°C. Remaining medium was aspirated, replaced with prewarmed 500-μl TrypLE Express per well and incubated for 15 min in the humidified incubator. To detach the cells after incubation, the bottom of the well was rinsed twice with the TrypLE Express, and 500-μl pre-warmed NB+ medium was added to stop enzymatic reaction. Again, the bottom of the well was rinsed twice with the medium-enzyme solution and then completely transferred in to 1.5-ml cups and centrifuged for 5 min with 7000 rpm. Thereafter, pelleted neurons were re-suspended in 500-μl condition medium and plated on cover slips in 24-well plates and incubated at 37°% with 5% CO_2 until further processing.

Immunocytochemistry

One or 2 d after seeding or replating, neurons were fixed for 10 min in 4% paraformaldehyde in PBS under cytoskeleton preserving conditions (pH 7–7.5). After washing with PBS, neurons were incubated with 0.4% gelatin with 0.5% Triton X-100 in PBS (carrier solution) for 5 min, followed by incubation with the primary antibody rabbit anti-Dcx (1:500, Abcam; in carrier solution). After 90 min incubation, neurons were washed with PBS and incubated with Alexa Fluor 488-coupled phalloidin (1:100, ThermoFisher Scientific) to visualize F-actin and the secondary antibody anti-rabbit IgG coupled to Alexa Fluor 546 (1:500, Invitrogen; in carrier solution). After 60 min of incubation, neurons were washed with PBS and nuclei were stained with the DNA dye Hoechst (1:1000 in PBS, Invitrogen). Neurons were imaged with a Leica TCS SP5 II confocal microscope setup.

Live cell imaging

For live cell imaging, neurons were seeded either directly after nucleofection or after replating in a poly-L-lysine hydrobromid-coated 22-mm glass-bottom dish and cultured for 1d. To measure actin turnover via fluorescence recovery after photobleaching (FRAP), neurons were transfected with GFP-actin (Robert Grosse lab) and imaged with a Leica TCS SP5 II in a chamber heated to 35°C. For imaging, neurons were washed once and then imaged in CO_2-saturated HBS solution (Invitrogen), supplemented with 4.16 mm $NaHCO_3$ and 2 mm $CaCl_2$. For prebleaching condition, five images of growth cones were acquired and in total 65 images over a time course of

5 min during fluorescence recovery. Images were analyzed with ImageJ (Schindelin et al., 2012) and recovery curve and parameters were calculated with R. To assess retrograde F-actin flow of growth cones neurons were transfected with LifeAct-GFP (Robert Grosse lab) and imaged in a CO_2-regulated chamber maintained at 37°C. Image acquisition was done with a Leica DMi8 Thunder microscope system and a Leica DFC9000 GTC camera, which acquired images every 5 s for 5 min. Kymograph generation and analysis was performed with ImageJ (Schindelin et al., 2012).

Growth cone collapse assay and BDNF treatment

Neurons were treated for 60 min with 100 ng/ml BDNF (PeproTech), 1 μg/μl Ephrin A5 (R&D Systems) or 1 μg/μl Slit-1 (R&D Systems) before fixation. Images were acquired with a Leica TCS SP5 II microscope system and analyses were done with ImageJ (Schindelin et al., 2012). Growth cone size was measured for determining BDNF effects, whereas repellent cues treated growth cones were categorized into collapsed and non-collapsed according to previous studies (Müller et al., 1990).

Statistics

Statistical tests were done in R or Sigma Plot. For comparing mean values between groups, Student's *t* test or Mann–Whitney *U* test was performed. Analyzing the rescue conditions, ANOVA with *post hoc* test was used. Stage distribution and non-collapsed versus collapsed growth cones were tested for differences with χ^2 test.

Results

Replating does not alter hippocampal neuron morphology

This study aimed at testing whether a combination of nucleofection and replating is a useful approach to study early aspects of hippocampal neuron differentiation. To do so, we isolated hippocampal neurons from C57Bl/6 mice at E18.5. Upon nucleofection, hippocampal neurons were seeded in 24-well plates and incubated at standard conditions (Fig. 1). After DIV2, we detached neurons by means of an enzymatic digest and mechanical treatment to reset them into an undifferentiated stage. Thereafter, hippocampal neurons were plated on cover slips and kept in culture, similar to non-replated neurons. To test whether this procedure affected neuron differentiation, we compared neurons 1 or 2 d after replating (DAR) with non-replated neurons at DIV1 or DIV2, respectively. We stained neurons with the F-actin marker phalloidin and an antibody against doublecortin (Dcx) that labeled neurites (Fig. 2A). This approach allowed us to categorize neurons according to their differentiation stage (Fig. 2B; Dotti et al., 1988). As expected, only a few non-replated DIV1 neurons remained in stage 1, i.e., they formed F-actin-enriched lamellipodia, but not yet neurites (Fig. 2C). The majority developed neurites, but not yet an axon and were assigned to stage 2, while a few neurons already possessed an axon and reached stage 3 (stage 1: $9.48 \pm 2.55\%$; stage 2: $79.95 \pm 4.43\%$, stage 3:
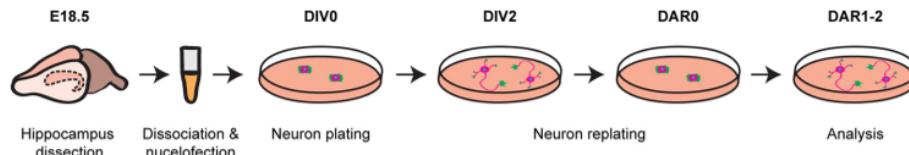
eNeuro

Figure 1. Scheme showing experimental procedure. Timeline and workflow of experimental approach including (1) isolation of hippocampal neurons from E18.5 mice; (2) nucleofection-based genetic manipulation before seeding that could be either reporter gene expression or gene inactivation; (3) culture of hippocampal neurons for 2 d; (4) replating of hippocampal neurons at DIV2 to reset them into an undifferentiated stage; (5) culture of replated neurons until further analyses.

$10.56 \pm 2.83\%$, $n > 180$ cells from three independent experiments). Very similar to non-replated DIV1 neurons, we found a few neurons in stage 1 and stage 3 at DAR1, while the majority were assigned to stage 2 (stage 1: $13.05 \pm 2.02\%$; stage 2: $77.59 \pm 2.90\%$, stage 3: $9.36 \pm 2.25\%$, $n > 340/3$). Comparison between DIV1 and DAR1 cultures revealed no difference in stage distribution ($p = 0.44$). At DIV2, the fraction of non-replated stage 3 neurons increased to roughly one third, and almost all other neurons were in stage 2 (stage 1: $4.81 \pm 2.22\%$, stage 2: $57.39 \pm 4.17\%$, stage 3: $37.80 \pm 3.10\%$; $n > 160/3$). We found a similar stage distribution among DAR2 neurons (stage 1: $5.32 \pm 1.59\%$, stage 2: $56.97 \pm 3.71\%$, stage 3: $37.71 \pm 4.56\%$; $n > 240/3$), with no difference when compared with DIV2 cultures ($p = 0.81$).

Antibody staining further allowed us to determine neuron morphology by counting the numbers of primary neurites and neurite endpoints and by calculating the ratio of primary neurites and neurite endpoints as a readout for neuron complexity. We determined these parameters in stage 2 neurons at DAR1 and DAR2 and compared them to non-replated neurons at DIV1 and DIV2, respectively. In DAR1 neurons, the numbers of primary neurites and neurite endpoints was not different from DIV1 neurons (neurites: DIV1: 5.11 ± 0.38, DAR1: 4.83 ± 0.25, $p = 0.54$; endpoints: DIV1: 5.50 ± 0.39, DAR1: 5.90 ± 0.33, $p = 0.44$; Fig. 2D,E). Instead, the neurite/endpoint ratio was slightly increased by roughly 10% in DAR1 neurons (DIV1: 1.10 ± 0.05, DAR1: 1.24 ± 0.05, $p < 0.05$; $n > 20/3$; Fig. 2F). Compared with DIV2 neurons, the neurite and endpoint numbers were slightly reduced by 8% and 30%, respectively, in DAR2 neurons (neurites: DIV2: 4.49 ± 0.26, DAR2: 4.12 ± 0.28, $p < 0.05$; endpoints: DIV2: 7.67 ± 0.70, DAR2: 5.38 ± 0.41, $p < 0.01$; $n > 20/3$; Fig. 2D,E). However, neuron complexity was similar to DIV2 neurons in DAR2 neurons (DIV2: 1.55 ± 0.11, DAR2: 1.33 ± 0.09, $p = 0.12$; Fig. 2F). Together, stage distribution did not differ between DAR1 and DIV1 cultures or between DAR2 and DIV2 cultures. Likewise, gross morphology of DAR1 and DAR2 neurons was similar to DIV1 and DIV2 neurons, respectively, and DAR2 neurons showed only minor changes in morphology.

Replating does not alter growth cone size or morphology

Next, we tested whether replating altered the morphology or function of growth cones, which are relevant for directed neurite outgrowth and neurite navigation through the developing brain. First, we exploited phalloidin-labeled neurons to determine growth cone size and morphology (Fig. 3A). For better comparison, we restricted this analysis to stage 2 neurons. In DIV1 and DIV2 neurons, growth cones size reached roughly 20 or 30 μm^2, respectively (DIV1: 23.05 ± 1.74 μm^2, $n > 70/3$; DIV2: 30.86 ± 2.25 μm^2, $n > 70/3$; Fig. 3B). Growth cone size did not differ from non-replated DIV1 or DIV2 neurons in neurons from DAR1 or DAR2 cultures, respectively (DAR1: 20.33 ± 1.00 μm^2, $n > 100/3$, $p = 0.18$; DAR2: 29.97 ± 1.95 μm^2, $n > 100/3$, $p = 0.76$). Growth cone morphology was assessed by determining growth cone circularity (area divided by perimeter) and solidity (growth cone area divided by hull area), similar to previous studies (Chitsaz et al., 2015; Dos-Santos Carvalho et al., 2020). Both parameters were not different between growth cones from DAR1 and DIV1 neurons (solidity: DIV1: 0.63 ± 0.02, $n > 70/3$, DAR1: 0.60 ± 0.01, $n > 90/3$, $p = 0.20$; circularity: DIV1: 0.22 ± 0.02, $n > 70/3$, DAR1: 0.25 ± 0.01, $n > 90/3$, $p = 0.33$; Fig. 3C). Together, replating neither affected growth cone size nor morphology.

Replating does not alter actin dynamics in growth cones

Next, as functional readouts, we assessed actin dynamics in replated neurons. We electroporated neurons before seeding to express GFP-actin that allowed us to determine actin turnover in growth cones by FRAP, similar to previous studies (Flynn et al., 2012). We performed FRAP experiments in growth cones from DAR1 neurons and compared actin turnover to growth cones from non-replated DIV1 neurons. In growth cones from DIV1 neurons, GFP-actin rapidly recovered with a mean half-recovery time ($t_{1/2}$) of 77.36 ± 12.29 s ($n > 20/3$; Fig. 4A–C; Movie 1). We noted a similar GFP-actin recovery in growth cones from DAR1 neurons, with no difference in $t_{1/2}$ (74.04 ± 10.00 s, $n > 20/3$, $p = 0.83$; Fig. 4A–C; Movie 2). Further, we calculated the stable actin fraction that did not recover within the time frame of 300 s. This fraction was not different between growth cones from DIV1 and DAR1 neurons (DIV1: 0.78 ± 0.03, DAR1: 0.75 ± 0.03, $p = 0.500$; Fig. 4D). Additionally, we electroporated neurons before plating to express LifeAct-GFP, which allowed us to visualize F-actin in living neurons (Riedl et al., 2008; Flynn et al., 2012). F-actin appeared similarly dynamic in growth cones from
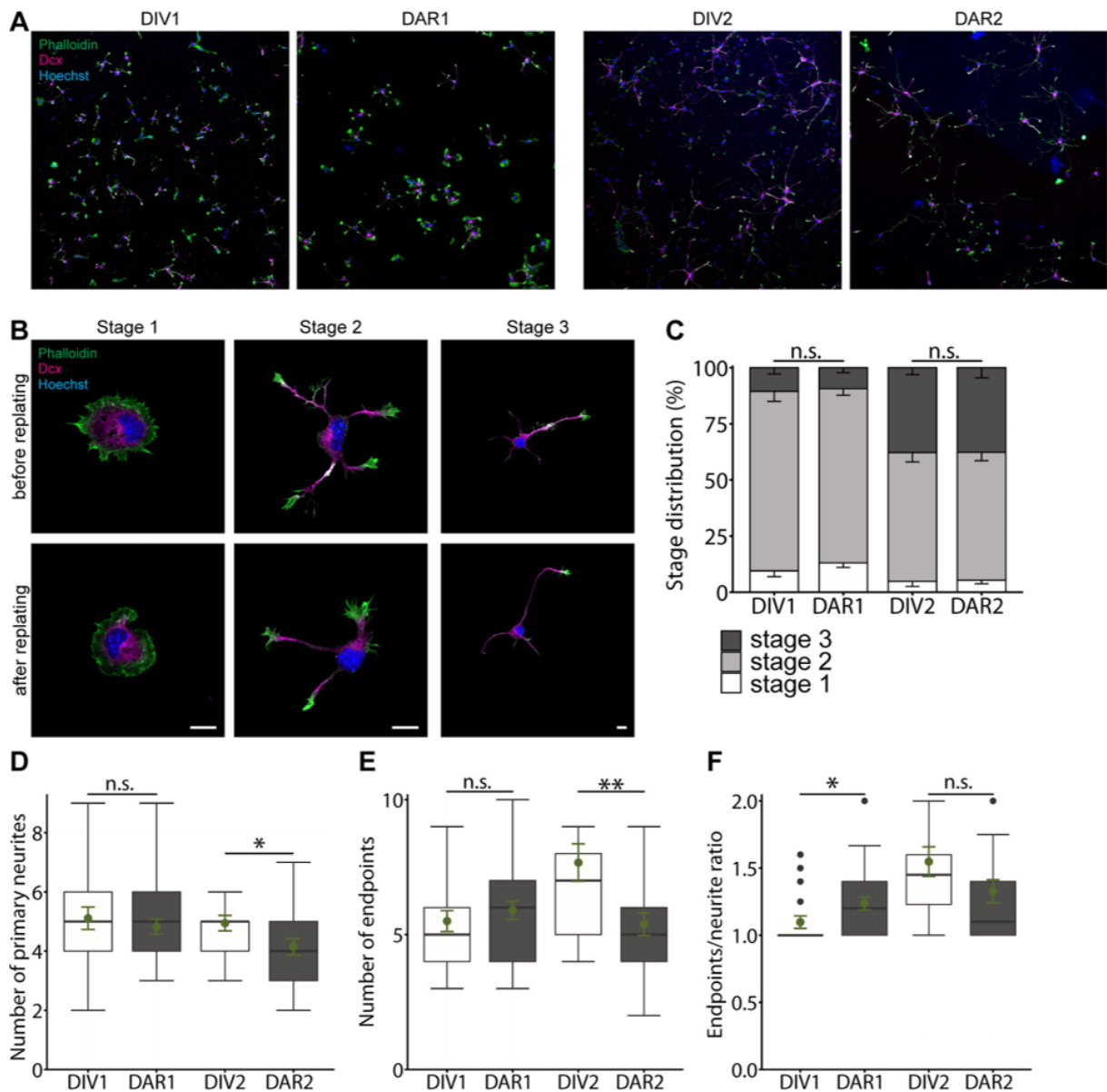
eNeuro

Figure 2. Replating neither alters differentiation nor gross morphology of hippocampal neurons. *A*, Representative micrographs of mouse non-replated hippocampal neurons at DIV1 and DIV2 as well as replated neurons at DAR1 and DAR2. Neurons were stained with the F-actin marker phalloidin (green), with an antibody against Dcx (magenta) and the intercalating dye Hoechst (blue). *B*, Representative micrographs of non-replated and replated stage 1, stage 2, and stage 3 neurons that have been used for morphometric analyses. *C*, Stage distribution of non-replated and replated neurons. Graphs showing (*D*) numbers of primary neurites, (*E*) numbers of neurite endpoints as well as (*F*) primary neurite/neurite endpoint ratio in non-replated and replated neurons. Scale bars: 50 µm (*A*) and 10 µm (*B*); ns: $p > 0.05$, $*p < 0.05$, $**p < 0.01$. Green dots indicate mean values with SEM.

DAR1 and DIV1 neurons (Movies 3, 4). Indeed, kymograph analysis revealed similar average retrograde flow velocity of F-actin in growth cones from both groups (DIV1: 8.18 ± 1.58 µm/min, $n > 20/3$, DAR1: 7.73 ± 0.82 µm/min, $n > 50/3$, $p = 0.80$; Fig. 4*E,F*). Together, replating neither affected actin turnover nor retrograde F-actin flow in growth cones.

Growth cones from replated neurons respond normally to guidance cues

Apart from studying actin dynamics, we tested whether growth cones from neurons of both groups respond differently to guidance cues. First, we determined growth cone size in phalloidin-stained DIV1 and DAR1 neurons on treatment with the neurotrophin brain-derived
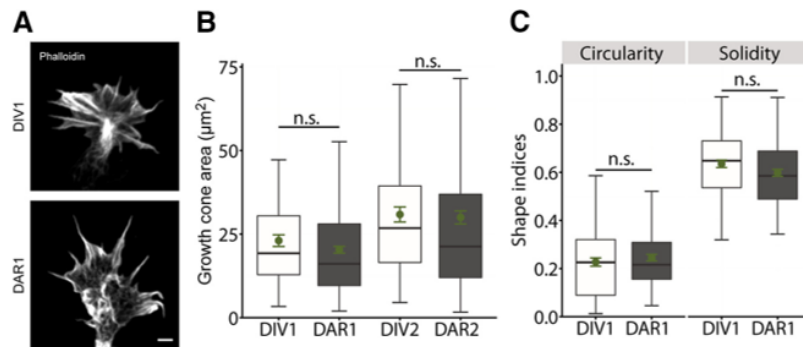
eNeuro

Figure 3. Replating does not alter growth cone size or morphology in hippocampal neurons. **A**, Representative micrographs of phalloidin-labeled growth cones from non-replated and replated stage 2 neurons. **B**, Growth cone size of non-replated and replated stage 2 neurons. **C**, Growth cone morphology (solidity, circularity) of non-replated and replated stage 2 neurons. Scale bar: 2 μm (**A**); ns: $p > 0.05$. Green dots indicate mean values with SEM.

neurotrophic factor (BDNF). As expected (Meier et al., 2011), BDNF increased growth cone size in non-replated neurons by 62% when compared with PBS-treated controls (PBS: 29.17 ± 1.35 μm^2, BDNF: 47.13 ± 2.40 μm^2, $p < 0.001$, $n > 130/3$; Fig. 5A,B). BDNF similarly increased growth cone size in DAR1 neurons (PBS: 31.30 ± 1.59 μm^2, BDNF: 56.45 ± 3.48 μm^2, $p < 0.001$, $n > 100/3$). Hence, growth cones from DIV1 and DAR1 neurons respond similarly to BDNF.

Second, we investigated the effects of two different repellent cues, namely Ephrin A5 (EphA5) and Slit-1, on growth cones from non-replated and replated neurons (Meier et al., 2011; Ye et al., 2019). As a readout, we determined the fraction of collapsed growth cones in phalloidin-stained neurons on treatment with either EphA5 or Slit-1 and compared these fractions to PBS-treated control neurons (Fig. 5C). In agreement with normal growth cone morphology in replated neurons, the fraction of collapsed growth cones did not differ between DIV1 and DAR1 neurons before guidance cue treatment (DIV1: $20.71 \pm 2.15\%$, DAR1: $20.20 \pm 2.19\%$, $p = 0.89$, $n > 200/3$; Fig. 5D). EphA5 and Slit-1 increased the fraction of collapsed growth cones roughly threefold in DIV1 neurons (EphA5: 60.95 ± 2.59, $p < 0.001$, $n > 300/3$; Slit-1: 53.67 ± 3.17, $p < 0.001$, $n > 300/3$). Similarly, both repellent cues strongly increased the fraction of collapsed growth cones in DAR1 neurons (EphA5: 58.80 ± 6.26, $p < 0.001$, $n > 210/3$; Slit-1: 50.80 ± 4.04, $p < 0.001$, $n > 200/3$). Together, growth cones from non-replated and replated neurons respond similarly to the neurotrophin BDNF as well as the repellent cues EphA5 and Slit-1.

Nucleofection-mediated gene inactivation allows to study early aspects of neuron differentiation in replated neurons

The aforementioned approaches to test growth cone actin dynamics in replated neurons were based on nucleofection-based reporter gene expression. To extend our characterization of replated neurons to gene inactivation, we exploited primary hippocampal neurons from gene targeted mice (ADF$-/-$/Cfl1$^{flx/flx}$) lacking the actin-

binding protein ADF and additionally carrying a floxed allele of the ADF homolog cofilin1 (Bellenchi et al., 2007). We chose this mouse model for a proof of concept, because actin-depolymerizing proteins of the ADF/cofilin family have been previously implicated in growth cone morphology (Gomez and Letourneau, 2014; Omotade et al., 2017), and because previous studies revealed redundant functions of ADF and cofilin1 in neurons (Zimmermann et al., 2015; Wolf et al., 2015; Flynn et al., 2012). To inactivate cofilin1, we electroporated ADF$-/-$/Cfl1$^{flx/flx}$ neurons before initial seeding with mCherry-tagged Cre recombinase (Cre), ADF$-/-$/Cfl1$^{flx/flx}$ neurons expressing a catalytically inactive mCherry-Cre variant (Cre-mut) served as controls (Kullmann et al., 2020). We fixed Cre-expressing and Cre-mut-expressing ADF$-/-$/Cfl1$^{flx/flx}$ neurons at either DIV1 or DAR1 and determined growth cone size on phalloidin staining (Fig. 6A). At DIV1, we found that growth cone size in Cre-expressing ADF$-/-$/Cfl1$^{flx/flx}$ neurons was not different from Cre-mut-expressing controls (Cre-mut: 26.5 ± 1.72 μm^2, Cre: 25.96 ± 1.95 μm^2, $p = 0.100$, $n > 30/3$; Fig. 6B). Instead, growth cone size was strongly increased in Cre-expressing ADF$-/-$/Cfl1$^{flx/flx}$ neurons at DAR1 when compared with Cre-mut-expressing controls (Cre-mut: 24.40 ± 2.2 μm^2, Cre: 48.50 ± 3.74 μm^2, $p < 0.001$, $n > 80/3$). Hence, ADF$-/-$/Cfl1$^{flx/flx}$ neurons displayed the expected increase in growth cone size on genetic inactivation of ADF and cofilin1 at DAR1, but not at DIV1. Together, our replating protocol together with nucleofection-based gene inactivation before initial seeding allowed us to study the relevance of a gene of interest for early processes of neuron differentiation, thereby highlighting the utility of our approach.

Discussion

In the present study we report a protocol to reset DIV2 primary mouse hippocampus neurons into an undifferentiated stage. We combined replating with nucleofection-based genetic manipulation (both reporter gene expression as well as gene inactivation by exploiting the Cre/loxP system) before initial seeding of primary neurons. This approach allows a thorough analysis of neuron
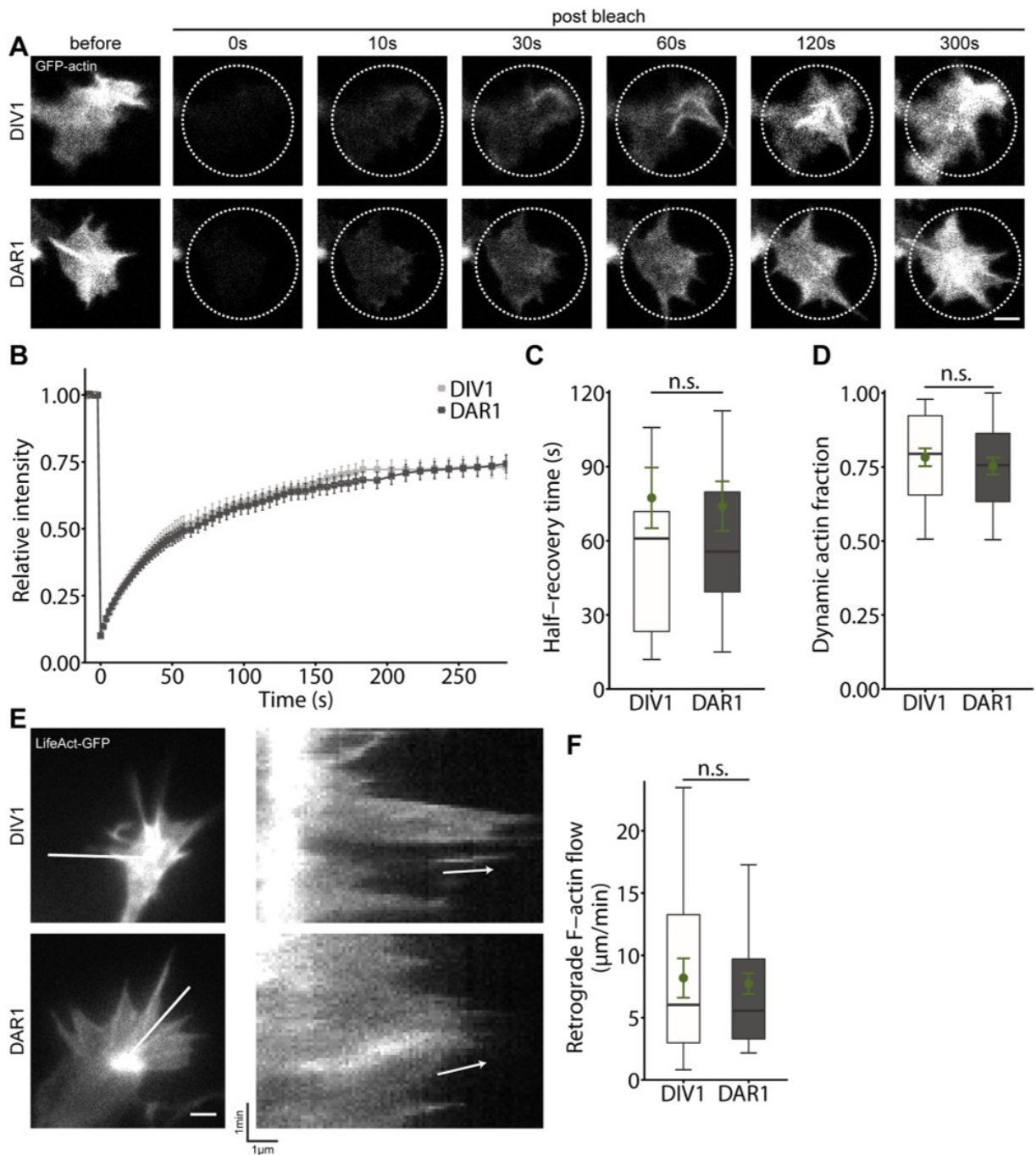
Figure 4. Replating does not impair actin dynamics in growth cones. **A**, Image sequence of growth cones from GFP-actin-expressing non-replated and replated stage 2 neurons during FRAP analysis. **B**, Recovery curves for GFP-actin in growth cones from stage 2 neurons at DIV1 and DAR1. **C**, Half-recovery time of GFP-actin in growth cones during FRAP experiment. **D**, Stable actin fraction in growth cones during FRAP experiments. **E**, Representative micrographs of growth cones from LifeAct-GFP-expressing non-replated and replated neurons. Lines indicate where kymographs (shown on the right) have been generated from. Arrows indicate the retrograde F-actin flow. **F**, Velocity of retrograde F-actin flow in growth cones. Scale bars: 2 μm (**A**, **D**); ns: $p > 0.05$. Green dots indicate mean values with SEM.
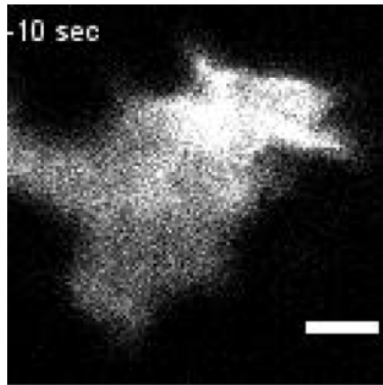
Movie 1. Movie showing GFP-actin recovery upon bleaching in the growth cone of a non-replated neuron at DIV1. Upon bleaching fluorescence recovery was recorded over a time course of 3 min. Scale bar: 2 μm. [View online]
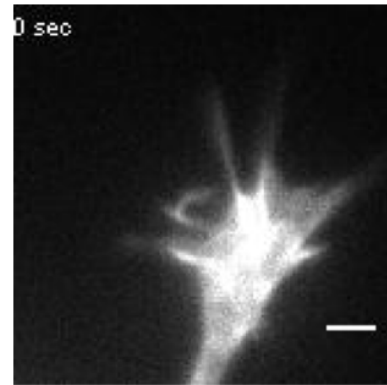
Movie 3. Movie showing a growth cone from a LifeAct-GFP-transfected non-replated neuron at DIV1. Images were acquired every 5 s for 5 min. Scale bar: 2 μm. [View online]

differentiation including early processes such as neurite formation and outgrowth or growth cone function.

Replating of cultured neurons has been reported for various neuron subtypes including primary dorsal root ganglia (DRG) neurons, primary cortical neurons or stem cell (SC)-derived neurons (Caviedes et al., 1990a,b; Koechling et al., 2011; Saijilafu et al., 2013; Frey et al., 2015; Biswas and Kalil, 2018; Calabrese et al., 2019; Lee et al., 2020a). Neuron replating has been implemented to reduce neuron complexity and cell membrane surface area, thereby improving accessibility for electrophysiological recordings, because passive membrane properties such as membrane capacitance or resistance were altered (Caviedes et al., 1990a,b). Further, it has been implemented to transfer SC-derived neurons from normal cell culture dishes onto 384 wells before experiments (Calabrese et al., 2019), and it has been exploited as a paradigm of axon regeneration (Saijilafu et al., 2013; Frey et al., 2015; Lee et al., 2020a). These studies differed in the procedure applied, and some of them only included a

brief and rather superficial description of the method. Moreover, these studies either did not focus on early aspects of neuron differentiation, did not systematically compare non-replated and replated neurons or did not combine replating with genetic manipulation. Hence, it remained unknown whether differentiation of replated neurons differed from non-replated neurons and whether a combination of genetic manipulation before initial seeding and replating allowed to study early aspects of neuron differentiation.

We compared cultured mouse hippocampal neurons that have been replated at DIV2 with non-replated neurons, focusing on early aspects of neuron differentiation up to 2 DAR. Our comparison included a categorization of neurons according to their differentiation stage as well as a thorough morphometric analysis. Neuron categorization did not reveal any differences between non-replated and replated neurons, thereby demonstrating that differentiation was largely preserved in replated neurons. Likewise, gross morphology was normal in replated neurons. However, they displayed some changes in neuron
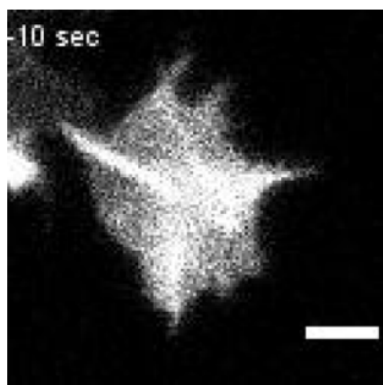
Movie 2. Movie showing GFP-actin recovery upon bleaching in the growth cone of a replated neuron at DAR1. Upon bleaching fluorescence recovery was recorded over a time course of 3 min. Scale bar: 2 μm. [View online]
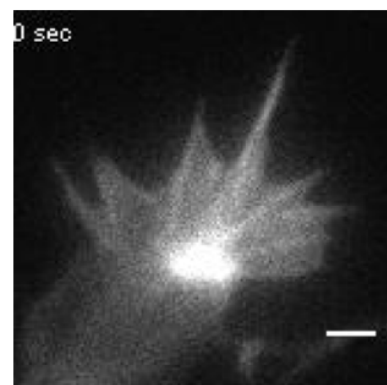
Movie 4. Movie showing a growth cone from a LifeAct-GFP-transfected replated neuron at DAR1. Images were acquired every 5 s for 5 min. Scale bar: 2 μm. [View online]
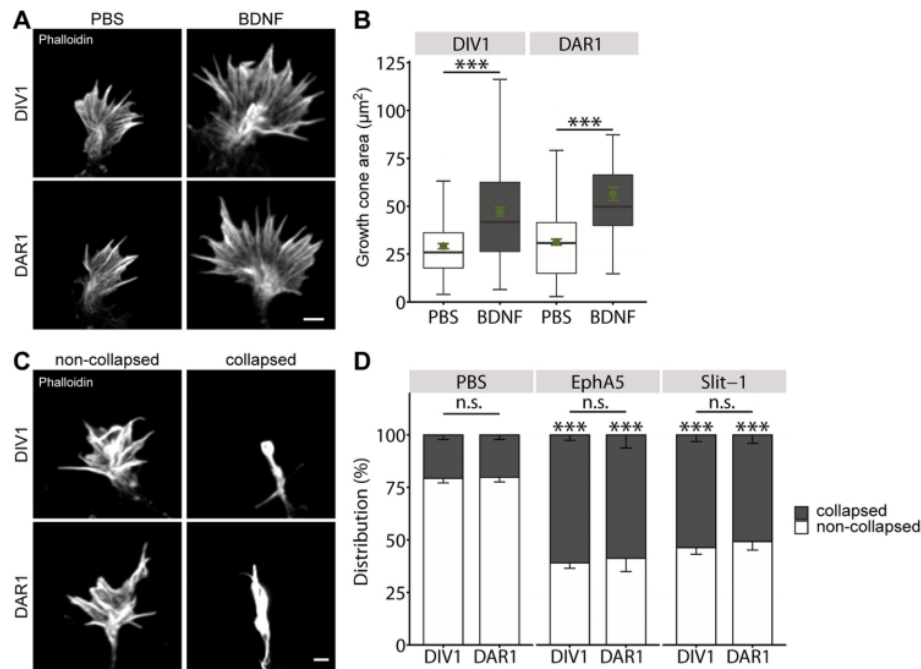
Figure 5. Normal response to guidance cues in growth cones from replated neurons. **A**, Representative micrographs of phalloidin-stained growth cones from non-replated and replated neurons treated with either PBS or BDNF. **B**, Growth cone size in non-replated and replated neurons treated with either PBS or BDNF. **C**, Representative micrographs of phalloidin-stained collapsed and non-collapsed growth cones from non-replated and replated neurons. **D**, Fractions of collapsed and non-collapsed growth cones in non-replated and replated neurons before and after treatment with EphA5 and Slit-1. Scale bars: 2 μm (**A**, **C**); ns: $p > 0.05$, ***$p < 0.001$. Green dots in **A** indicate mean values with SEM.

morphology, which are likely not biologically relevant. Our data demonstrated that our replating procedure successfully reset DIV2 primary hippocampal neurons into an undifferentiated stage and that replated neurons differentiated very similar

Figure 6. Replating allows studying the relevance of ADF/cofilin for early aspects of neuron differentiation. **A**, Representative micrographs of phalloidin-stained growth cones from non-replated and replated ADF−/−/Cfl1[flx/flx] neurons expressing either Cre or Cre-mut. **B**, Growth cone size in non-replated and replated ADF−/−/Cfl1[flx/flx] neurons expressing either Cre or Cre-mut. Scale bar: 2 μm (**A**); ns: $p > 0.05$, ***$p < 0.001$. Green dots indicate mean values with SEM.

to non-replated neurons. Hence, replated neurons faithfully reflect normal differentiation of hippocampal neurons.

Further, we combined our replating procedure with nucleofection-based transfection of hippocampal neurons before initial seeding. We expressed reporter genes such as GFP-actin or LifeAct-GFP that allowed us to determine actin turnover as well as F-actin dynamics in growth cones as functional readouts. By FRAP analysis, we found that actin turnover in growth cones was not different between replated and non-replated neurons. Similarly, retrograde F-actin flow was unchanged in replated neurons. These finding demonstrated that our replating procedure did not alter actin dynamics in growth cones and let us suggest normal growth cone functions in replated neurons. Indeed, growth cones from replated neurons did not differ to those from non-replated neurons in their response to the neurotrophin BDNF or the repellent cues EphA5 and Slit-1. Together, our analysis in hippocampal neurons did not reveal any gross defects in differentiation, morphology or growth cone function in hippocampal neurons induced by the replating procedure. In contrast to our findings, a recent study revealed functional differences between non-replated and replated DRG neurons. Specifically, this study showed that axon regeneration occurred in replated adult DRG neurons even when gene transcription was inhibited by blocking RNA Polymerase II, while axon formation and

outgrowth in non-replated adult DRG neurons required RNA Polymerase II activity (Saijilafu et al., 2013). However, it remained unknown whether such functional differences between replated and non-replated neurons is restricted to a specific cell types, i.e., adult DRG neurons, or whether these differences are present in all CNS and PNS neurons.

Apart from nucleofection of reporter genes, we exploited the Cre/loxP system to genetically remove actin-depolymerizing proteins of the ADF/cofilin family that have been previously linked to growth cone morphology (Gomez and Letourneau, 2014; Omotade et al., 2017). While growth cone size was unchanged in non-replated Cre-expressing ADF$-/-$/Cfl1$^{flx/flx}$ neurons at DIV1, it was strongly increased in replated Cre-expressing ADF$-/-$/Cfl1$^{flx/flx}$ neurons at DAR1. Differences in growth cone size between Cre-expressing ADF$-/-$/Cfl1$^{flx/flx}$ neurons at DIV1 and DAR1 can be easily explained by the fact that DAR1 neurons were 2 d longer in culture when compared with DIV1 neurons. Thus, DAR1 neurons had longer time to express Cre and to recombine the genome and, hence, to genetically remove cofilin1. In line with this, previous studies showed residual cofilin1 levels up to a few days on beginning of Cre expression in the mouse brain, but also in various cell types including isolated hippocampal neurons (Bellenchi et al., 2007; Rust et al., 2010; Flynn et al., 2012; Rehklau et al., 2012). Together, these data demonstrated that our replating protocol in combination with nucleofection-based gene inactivation allows us to study the relevance of a gene of interest for early aspects of neuron differentiation, different from nucleofected non-replated neurons. Hence, nucleofection combined with our replating protocol enables a more thorough analysis of neuron differentiation when compared with neurons that were nucleofected, but not replated.

In summary, we report a protocol to reset DIV2 primary mouse hippocampal neurons into an undifferentiated stage. This procedure is compatible with nucleofection-based genetic manipulation of primary neurons before their initial seeding. Our approach allowed us (1) to express fluorescent reporters during neuron differentiation that are needed to address specific biological processes such as actin dynamics in growth cones or (2) to inactivate a gene of interest to study its function in early aspects of neuron differentiation. This approach is highly flexible, straightforward and far less labor-intensive and expensive than previous approaches, (1) in which transgenic mice such as Lifeact-expressing strains were exploited to study actin dynamics during early differentiation in cultured hippocampal neurons (Flynn et al., 2012) or (2) which required the breeding and scarification of a large number of knock-out mice and their control littermates. Hence, our replating protocol is very helpful to reduce the number of experimental animals, and it thereby complies with the 3R principle for a more ethical use of animals in biomedical research (Russell and Burch, 1959; Lee et al., 2020b). While we here used expression of fluorescent reporters and Cre/loxP-based gene inactivation for a proof of principle, genetic manipulation can be easily expanded

to gene silencing via RNA interference or other modes of gene deletion, e.g., by exploiting the CRISPR/Cas system. Taken together, a combination of nucleofection and replating of primary mouse hippocampal neurons is a powerful and versatile approach to comprehensively study the molecular mechanisms regulating neuron differentiation.

References

Bellenchi GC, Gurniak CB, Perlas E, Middei S, Ammassari-Teule M, Witke W (2007) N-cofilin is associated with neuronal migration disorders and cell cycle control in the cerebral cortex. Genes Dev 21:2347–2357.

Biswas S, Kalil K (2018) The microtubule-associated protein tau mediates the organization of microtubules and their dynamic exploration of actin-rich lamellipodia and filopodia of cortical growth cones. J Neurosci 38:291–307.

Calabrese B, Powers RM, Slepian AJ, Halpain S (2019) Post-differentiation replating of human pluripotent stem cell-derived neurons for high-content screening of neuritogenesis and synapse maturation. J Vis Exp (150). Advance online publication. Retrieved Aug 28, 2019. doi: 10.3791/59305.

Caviedes P, Ault B, Rapoport SI (1990a) Replating improves whole cell voltage clamp recording of human fetal dorsal root ganglion neurons. J Neurosci Methods 35:57–61.

Caviedes P, Ault B, Rapoport SI (1990b) The role of altered sodium currents in action potential abnormalities of cultured dorsal root ganglion neurons from trisomy 21 (Down syndrome) human fetuses. Brain Res 510:229–236.

Chitsaz D, Morales D, Law C, Kania A (2015) An automated strategy for unbiased morphometric analyses and classifications of growth cones in vitro. PLoS One 10:e0140959.

da Silva JS, Dotti CG (2002) Breaking the neuronal sphere: regulation of the actin cytoskeleton in neuritogenesis. Nat Rev Neurosci 3:694–704.

Dos-Santos Carvalho S, Moreau MM, Hien YE, Garcia M, Aubailly N, Henderson DJ, Studer V, Sans N, Thoumine O, Montcouquiol M (2020) Vangl2 acts at the interface between actin and N-cadherin to modulate mammalian neuronal outgrowth. Elife 9:e51822.

Dotti CG, Sullivan CA, Banker GA (1988) The establishment of polarity by hippocampal neurons in culture. J Neurosci 8:1454–1468.

Dudek H, Ghosh A, Greenberg ME (2001) Calcium phosphate transfection of DNA into neurons in primary culture. Curr Protoc Neurosci Chapter 3:Unit 3.11.

Flynn KC, Hellal F, Neukirchen D, Jacob S, Tahirovic S, Dupraz S, Stern S, Garvalov BK, Gurniak C, Shaw AE, Meyn L, Wedlich-Söldner R, Bamburg JR, Small JV, Witke W, Bradke F (2012) ADF/cofilin-mediated actin retrograde flow directs neurite formation in the developing brain. Neuron 76:1091–1107.

Frey E, Valakh V, Karney-Grobe S, Shi Y, Milbrandt J, DiAntonio A (2015) An in vitro assay to study induction of the regenerative state in sensory neurons. Exp Neurol 263:350–363.

Gomez TM, Letourneau PC (2014) Actin dynamics in growth cone motility and navigation. J Neurochem 129:221–234.

Koechling T, Khalique H, Sundström E, Ávila J, Lim F (2011) A culture model for neurite regeneration of human spinal cord neurons. J Neurosci Methods 201:346–354.

Kullmann JA, Trivedi N, Howell D, Laumonnerie C, Nguyen V, Banerjee SS, Stabley DR, Shirinifard A, Rowitch DH, Solecki DJ (2020) Oxygen tension and the VHL-Hif1α pathway determine onset of neuronal polarization and cerebellar germinal zone exit. Neuron 106:607–623.

Lee J, Shin JE, Lee B, Kim H, Jeon Y, Ahn SH, Chi SW, Cho Y (2020a) The stem cell marker Prom1 promotes axon regeneration by down-regulating cholesterol synthesis via Smad signaling. Proc Natl Acad Sci USA 117:15955–15966.

Lee KH, Lee DW, Kang BC (2020b) The 'R' principles in laboratory animal experiments. Lab Anim Res 36:45.

Meier C, Anastasiadou S, Knöll B (2011) Ephrin-A5 suppresses neurotrophin evoked neuronal motility, ERK activation and gene expression. PLoS One 6:e26089.

Müller B, Stahl B, Bonhoeffer F (1990) In vitro experiments on axonal guidance and growth-cone collapse. J Exp Biol 153:29–46.

Ohki EC, Tilkins ML, Ciccarone VC, Price PJ (2001) Improving the transfection efficiency of post-mitotic neurons. J Neurosci Methods 112:95–99.

Omotade OF, Pollitt SL, Zheng JQ (2017) Actin-based growth cone motility and guidance. Mol Cell Neurosci 84:4–10.

Rehklau K, Gurniak CB, Conrad M, Friauf E, Ott M, Rust MB (2012) ADF/cofilin proteins translocate to mitochondria during apoptosis but are not generally required for cell death signaling. Cell Death Differ 19:958–967.

Riedl J, Crevenna AH, Kessenbrock K, Yu JH, Neukirchen D, Bista M, Bradke F, Jenne D, Holak TA, Werb Z, Sixt M, Wedlich-Soldner R (2008) Lifeact: a versatile marker to visualize F-actin. Nat Methods 5:605–607.

Russell WMS, Burch RL (1959) The principles of humane experimental technique. London: Methuen and Co.

Rust MB, Gurniak CB, Renner M, Vara H, Morando L, Görlich A, Sassoè-Pognetto M, Banchaabouchi MA, Giustetto M, Triller A, Choquet D, Witke W (2010) Learning, AMPA receptor mobility and synaptic plasticity depend on n-cofilin-mediated actin dynamics. EMBO J 29:1889–1902.

Saijilafu, Hur EM, Liu CM, Jiao Z, Xu WL, Zhou FQ (2013) PI3K–GSK3 signalling regulates mammalian axon regeneration by inducing the expression of Smad1. Nat Commun 4:2690.

Schindelin J, Arganda-Carreras I, Frise E, Kaynig V, Longair M, Pietzsch T, Preibisch S, Rueden C, Saalfeld S, Schmid B, Tinevez JY, White DJ, Hartenstein V, Eliceiri K, Tomancak P, Cardona A (2012) Fiji: an open-source platform for biological-image analysis. Nat Methods 9:676–682.

Sun M, Bernard LP, Dibona VL, Wu Q, Zhang H (2013) Calcium phosphate transfection of primary hippocampal neurons. J Vis Exp 81: e50808.

Viesselmann C, Ballweg J, Lumbard D, Dent EW (2011) Nucleofection and primary culture of embryonic mouse hippocampal and cortical neurons. J Vis Exp 47:2373.

Wolf M, Zimmermann AM, Görlich A, Gurniak CB, Sassoè-Pognetto M, Friauf E, Witke W, Rust MB (2015) ADF/cofilin controls synaptic actin dynamics and regulates synaptic vesicle mobilization and exocytosis. Cereb Cortex 25:2863–2875.

Ye X, Qiu Y, Gao Y, Wan D, Zhu H (2019) A subtle network mediating axon guidance: intrinsic dynamic structure of growth cone, attractive and repulsive molecular cues, and the intermediate role of signaling pathways. Neural Plast 2019:1719829.

Zeitelhofer M, Vessey JP, Thomas S, Kiebler M, Dahm R (2009) Transfection of cultured primary neurons via nucleofection. Curr Protoc Neurosci Chapter 4:Unit 4.32.

Zimmermann AM, Jene T, Wolf M, Görlich A, Gurniak CB, Sassoè-Pognetto M, Witke W, Friauf E, Rust MB (2015) Attention-deficit/hyperactivity disorder-like phenotype in a mouse model with impaired actin dynamics. Biol Psychiatry 78:95–106.

70

Article

Functional Redundancy of Cyclase-Associated Proteins CAP1 and CAP2 in Differentiating Neurons

Felix Schneider [1,2,3], Isabell Metz [1,2,3], Sharof Khudayberdiev [1,2] and Marco B. Rust [1,2,3,*]

1   Molecular Neurobiology Group, Institute of Physiological Chemistry, University of Marburg, 35032 Marburg, Germany; felix.schneider@staff.Uni-Marburg.DE (F.S.); isabell.metz@uni-marburg.de (I.M.); khudaybe@staff.uni-marburg.de (S.K.)
2   Center for Mind, Brain and Behavior (CMBB), University of Marburg, Justus-Liebig-University Giessen, Hans-Meerwein-Strasse 6, 35032 Marburg, Germany
3   DFG Research Training Group, Membrane Plasticity in Tissue Development and Remodeling, GRK 2213, University of Marburg, 35032 Marburg, Germany
*   Correspondence: rust@uni-marburg.de; Tel.: +49-6421-2865020

Abstract: Cyclase-associated proteins (CAPs) are evolutionary-conserved actin-binding proteins with crucial functions in regulating actin dynamics, the spatiotemporally controlled assembly and disassembly of actin filaments (F-actin). Mammals possess two family members (CAP1 and CAP2) with different expression patterns. Unlike most other tissues, both CAPs are expressed in the brain and present in hippocampal neurons. We recently reported crucial roles for CAP1 in growth cone function, neuron differentiation, and neuron connectivity in the mouse brain. Instead, CAP2 controls dendritic spine morphology and synaptic plasticity, and its dysregulation contributes to Alzheimer's disease pathology. These findings are in line with a model in which CAP1 controls important aspects during neuron differentiation, while CAP2 is relevant in differentiated neurons. We here report CAP2 expression during neuron differentiation and its enrichment in growth cones. We therefore hypothesized that CAP2 is relevant not only in excitatory synapses, but also in differentiating neurons. However, CAP2 inactivation neither impaired growth cone morphology and motility nor neuron differentiation. Moreover, CAP2 mutant mice did not display any obvious changes in brain anatomy. Hence, differently from CAP1, CAP2 was dispensable for neuron differentiation and brain development. Interestingly, overexpression of CAP2 rescued not only growth cone size in CAP1-deficient neurons, but also their morphology and differentiation. Our data provide evidence for functional redundancy of CAP1 and CAP2 in differentiating neurons, and they suggest compensatory mechanisms in single mutant neurons.

Keywords: cyclase-associated protein; CAP2; CAP1; SRV2; growth cone; actin dynamics; F-actin

1. Introduction

Mammalian cyclase-associated protein (CAP) and its yeast homolog suppressor of RAS2-V19 (SRV2, collectively referred to CAP in this manuscript) were both recognized, two decades ago, as actin-binding proteins (ABPs) [1,2], but their molecular functions remained largely unknown until recently. By exploiting recombinant proteins and mutant yeast strains, studies of the past few years implicated CAP in various steps of the actin treadmilling mechanism, thereby identifying it as a crucial regulator of actin dynamics [3–8]. Specifically, these studies revealed a cooperation with the actin-depolymerizing protein ADF/cofilin in the dissociation of actin subunits from filamentous actin (F-actin) and, hence, in F-actin disassembly [5,7,9]. Moreover, they revealed a role for CAP in nucleotide exchange on globular actin monomers (G-actin) relevant for G-actin recycling and F-actin assembly [4], and they reported an inhibitory function towards the F-actin assembly factor, inverted formin 2 (INF2) [6,8]. While these studies significantly advanced our knowledge of CAP's molecular activities, little is known about the cellular and physiological functions.

Unlike lower eukaryotes and most invertebrate species that possess a single CAP homolog, vertebrates express two closely related family members, CAP1 and CAP2, with different expression pattern [10,11]. In mice, CAP1 is present in most tissues except skeletal muscles, while CAP2 expression is restricted to a few tissues including skeletal muscle and the heart [10]. These findings led to the assumption that both proteins acquired cell-type-specific functions with CAP2 being the dominant family member in striated muscles [2]. Indeed, recent studies identified CAP2 as a crucial regulator of myofibril differentiation in both skeletal and cardiac muscles [12,13], and they reported a cardiomyopathy associated with dilated ventricles and impaired heart physiology as well as impaired skeletal muscle development for systemic CAP2 knockout (CAP2-KO) mice [12,14–17]. Instead, systemic CAP1-KO mice died from unknown causes during embryonic development [18]. Differently from most other tissues, CAP1 and CAP2 are both expressed in the brain [10,11], and recent studies unraveled important functions for both in hippocampal neurons. Specifically, shRNA-mediated knockdown in isolated rat hippocampal neurons revealed a role for CAP2 in the morphology and function of dendritic spines [19], F-actin-enriched dendritic protrusions forming the postsynaptic compartment of most excitatory synapses in the brain [20,21]. Moreover, CAP2 dysregulation has been implicated in synaptic defects of Alzheimer's disease [19]. Instead, hippocampal neurons from brain-specific CAP1-KO mice displayed an altered morphology and function of growth cones [9], dynamic F-actin-rich structures at the tip of neurites that sense environmental guidance cues and navigate axons through the developing brain to their target regions [22]. Consequently, neuron connectivity was compromised in CAP1-KO brains [9]. These findings are in line with a model in which CAP1 controls actin-dependent mechanisms during neuron differentiation, while CAP2 is relevant for actin regulation in differentiated neurons. However, the function of CAP2 during differentiation of hippocampal neurons has not been studied to date.

In the present study, we found CAP2 expressed during differentiation and abundant in growth cones from hippocampal neurons. We therefore hypothesized that CAP2 plays a crucial role in growth cones, similar to CAP1. Unlike CAP1-KO neurons, neuron differentiation and growth cone morphology were unchanged in neurons from CAP2-KO mice, and CAP2-KO brains did not display obvious brain developmental defects. However, overexpression of CAP2 rescued growth cone size and morphology in CAP1-KO neurons and normalized their differentiation. Our data revealed functional redundancy of CAP1 and CAP2 in neurons, and they suggest compensatory mechanisms in single KO mice.

2. Material and Methods

2.1. Transgenic Mice

CAP2$^{-/-}$ mice were generated by breeding heterozygous CAP2 mice (CAP2$^{+/-}$) obtained from the European Conditional Mouse Mutagenesis Program (EUCOMM). Generation of conditional CAP1 mice has been reported before [9]. CAP1-deficient hippocampal neurons were obtained from conditional CAP1 mice (CAP1$^{flx/flx}$) additionally expressing a Cre transgene under control of the nestin promoter [23]. Mice were housed in the animal facility of Marburg University on 12 h dark–light cycles with food and water available ad libitum. Treatment of mice was in accordance with the German law for conducting animal experiments and followed the guidelines for the care and use of laboratory animals of the U.S. National Institutes of Health. Sacrificing of mice was approved by internal animal welfare authorities at Marburg University (AK-5-2014-Rust, AK-6-2014-Rust, AK-12-2020-Rust), breeding of brain-specific CAP1 mutant mice was approved by the RP Giessen (G22-2016).

2.2. Cell Culture and Transfection

Primary hippocampal neurons from embryonic day 18 (E18) mice were prepared as previously described [24]. Briefly, hippocampi were dissociated individually to keep their genetic identity and seeded with a density of 31,000 neurons per cm^2 on 0.1 mg/mL poly-L-lysine-coated coverslips. Neurons were maintained for 5 h to 3 d in a humidified

incubator at 37 °C with 5% CO$_2$ in neurobasal medium containing 2% B27, 2 mM GlutaMax, 100 µg/mL streptomycin, and 100 U/mL penicillin (Gibco, Invitrogen, Waltham, MA, USA). For overexpression of plasmids, neurons were nucleofected prior to plating with the Amaxa nucleofector system (Lonza, Basel, Switzerland) according to the manufacturer's protocol. For each nucleofection, 3 µg plasmid was transfected into 250,000 neurons, which were then plated at a density of 66,000 neurons per cm^2. For replating, neurons were seeded in wells coated with 0.05 mg/mL poly-L-lysine and detached with TrypLE™ Express (Gibco) at DIV2. A detailed protocol of the replating procedure was provided in a recent study [25]. Thereafter, neurons were pelleted at 7000 rpm for 7 min, plated on 0.1 mg/mL poly-L-lysine-coated coverslips, and fixed 24 h later. The following constructs were used: GFP-CAP1, mCherry-CAP1, and myc-CAP1 [9], GFP-CAP2 and myc-CAP2 [19], and GFP (GeneScript, Piscataway, NJ, USA). Three different shRNAs were used to knockdown CAP2: sh2 (5′-CCTTTGAGAATGAGGATAA-3′), sh3 (5′-AGAAGTGGAGAGTGGAATA-3′), and sh4 (5′-CAGATGACAAGAAGACATA-3′). 5′-AAACCTTGTGGTCCTTAGG-3′ was used as control shRNA [26].

2.3. Immunocytochemistry

Cultured neurons were fixed for 10 min in 4% paraformaldehyde (PFA) in PBS under cytoskeleton preserving conditions. After 5 min incubation with 0.4% gelatin and 0.5% Triton-X100 in PBS (carrier solution), neurons were incubated with following primary antibodies (in carrier solution): rabbit anti-doublecortin (1:500, Abcam, Cambridge, UK), rabbit anti-GFP (1:1000, ThermoFisher Scientific, Waltham, MA, USA), mouse anti-c-Myc (1:200, ThermoFisher Scientific), chicken anti-mCherry (1:500, Abcam), and mouse anti-tubulin βIII (1:200, Sigma-Aldrich, St. Louis, MO, USA). Thereafter, neurons were washed in PBS and incubated with the following secondary antibodies (in carrier solution): anti-mouse and anti-rabbit IgG coupled to either AlexaFluor488 or AlexaFluor546 (1:500, Invitrogen, Waltham, MA, USA) and AlexaFluor555-coupled anti-chicken IgG (1:500, Invitrogen). F-actin was visualized by staining with phalloidin coupled to either AlexaFluor488 (1:100, Invitrogen) or AlexaFluor647 (1:100, Cell Signaling Technologies, Danvers, MA, USA). In each experiment, neurons were stained with the DNA dye Hoechst (1:1000, Invitrogen). Image acquisition was done with a Leica TCS SP5 II confocal microscope setup, and image analysis was performed with ImageJ [27]. Briefly, growth cones were outlined by exploiting the phalloidin signal. Area and shape indices were determined by using the according measuring tools from Fiji.

2.4. Growth Cone Morphology

Growth cone morphology was assessed by determining growth cone circularity (growth cone area divided by growth cone perimeter) and solidity (growth cone area divided by hull area), similar to previous studies [9].

2.5. Live Cell Imaging

For life cell imaging, neurons were seeded in a 22 mm glass-bottom dish coated with PLL as described above and cultured for 1 d. DIC imaging was done in a chamber maintained at 37 °C and the medium was exchanged with CO$_2$-saturated HBS solution. Images were acquired every 5 s for 10 min at a Leica DMi8 setup.

2.6. Protein Analysis

Cortices of E18.5 mice were homogenized in 500 µL RIPA buffer and cultured cells were lysed in 100µl RIPA buffer containing 50 mM Tris HCl (pH7.5), 150 mM NaCl, 0.5% NP40, 0.1% SDS, and protease inhibitor (Complete, Roche, Basel, Switzerland). After centrifugation at 14,000 rpm for 10 min at 4 °C, samples were boiled for 5 min at 95 °C in Laemmli buffer including 6% DTT. Equal protein amounts were separated by SDS PAGE and blotted onto a polyvinylidene difluoride membrane (Merck, Darmstadt, Germany) by using a wet/tank blotting system (Biorad, Hercules, CA, USA). Membranes were

blocked in Tris-buffered saline (TBS) containing 5% milk powder, 0.5% Tween-20, and 0.02% sodium acid for 1 h and afterwards incubated with primary antibodies in blocking solution overnight at 4 °C. As secondary antibodies, horseradish peroxidase (HRP)-conjugated antibodies (1:10,000, Thermo Fisher Scientific, Waltham, MA, USA) or fluorescent-conjugated antibodies (1:10,000, Li-Cor Bioscience, Lincoln, NE, USA) were used and detected by chemiluminescence with ECL Plus Western blot detection system (GE Healthcare, Chicago, IL, USA) or by fluorescence with Li-Cor Odyssey imaging system. The following primary antibodies were used: mouse anti-CAP1 (1:1000, Abnova, Taoyuan City, Taiwan), mouse anti-GAPDH (1:1000, R&D System, Minneapolis, MN, USA), rabbit anti-CAP2 (1:1000), and mouse anti-α-tubulin (1:2000, Sigma-Aldrich, St. Louis, MO, USA). Signal intensities of CAP1, CAP2, and GAPDH in immunoblots were determined by using ImageStudio Light Ver 5.2. CAP1 and CAP2 levels were normalized to GAPDH. CAP2 and tubulin levels were determined by using Western blot Fiji, CAP2 level was normalized to tubulin.

2.7. Histology and Immunohistochemistry

Nissl staining and immunohistochemical staining was performed as described previously [28,29]. Briefly, E18.5 mice were killed by decapitation and brains were fixed for 2 h in PBS containing 4% PFA. Thereafter, 25 μm transversal brain sections were generated by a Leica CM3050 S cryostat. For immunohistochemistry, brain sections were incubated for 1 h with 2% BSA, 3% goat serum, 10% donkey serum, and 0.5% NP40 in PBS and stained overnight at 4 °C with following primary antibody in 2% BSA and 0.5% NP40 in PBS: rabbit anti-neurofilament 200 (1:80, Sigma-Aldrich, St. Louis, MO, USA). As secondary antibody, AlexaFluor488 anti-rabbit IgG was used. For Nissl staining, brain sections were incubated in staining solution according to the manufacturer's instructions. Image acquisition was done with a Leica TCS SP5 II confocal microscope setup and Leica M80 equipped with a Leica DFC295 camera (Leica Microsystems, Wetzlar, Germany).

2.8. Statistical Analysis

Statistical tests were done in R or SigmaPlot. For comparing mean values between groups, Student's *t*-test was performed. Analyzing the rescue conditions and protein expression over time and in different brain areas, ANOVA with post-hoc test (pairwise *t*-test with correction for multiple testing) was used. Stage distribution was tested for differences with χ^2-test.

3. Results

3.1. CAP2 Is Expressed during Neuron Differentiation and Abundant in Growth Cones

Previous immunoblot analysis revealed broad expression of CAP2 in the postnatal mouse brain including hippocampus [19]. However, it remains unknown whether CAP2 is present during embryonic brain development. We therefore performed immunoblots with mouse cerebral cortex lysates between embryonic day (E) 14.5 and postnatal day (P) 0. This analysis revealed the presence of CAP2 at all developmental stages examined, similar to CAP1 (Figure 1A). Quantification of signal intensities and normalization to GAPDH that was used as the loading control revealed constant expression levels for CAP1 and CAP2 during embryonic cerebral cortex lysates (Figure 1A; CAP1: E14.5: 1.87 ± 1.10, E16.5: 3.19 ± 0.84, E18.5: 2.01 ± 0.15, P0: 3.21 ± 1.48, *n* = 3, *p* = 0.52; CAP2: E14.5: 0.32 ± 0.11, E16.5: 0.53 ± 0.12, E18.5: 0.28 ± 0.05, P0: 0.50 ± 0.16, *n* = 3, *p* = 0.52). Immunoblot analysis further revealed CAP2 expression in hippocampal lysates from P0 mice (Figure 1B). A comparison between brain regions revealed similar expression levels for CAP1 and CAP2 in the cerebral cortex and hippocampus (CAP1: cortex: 2.93 ± 0.39, hippocampus: 2.63 ± 0.68, *n* = 3, *p* = 1; CAP2: cortex: 2.73 ± 1.23, hippocampus: 1.47 ± 0.54, *n* = 3, *p* = 0.92). Moreover, CAP2 was present in lysates from hippocampal neurons kept for one or two days in vitro (DIV; Figure 1C), and CAP2 expression levels were equal in DIV1 and DIV2 cultures, similar to CAP1 (CAP1: DIV1: 0.39 ± 0.07, DIV2: 0.51 ± 0.05, *n* = 6, *p* = 0.21; CAP2: DIV1: 0.23 ± 0.01, DIV2: 0.26 ± 0.02, *n* = 6, *p* = 0.95). Together, CAP2 was expressed in the

embryonic and perinatal brain as well as in cultured hippocampal neurons, very similar to its close homolog CAP1 (Figure 1A–C) [9].
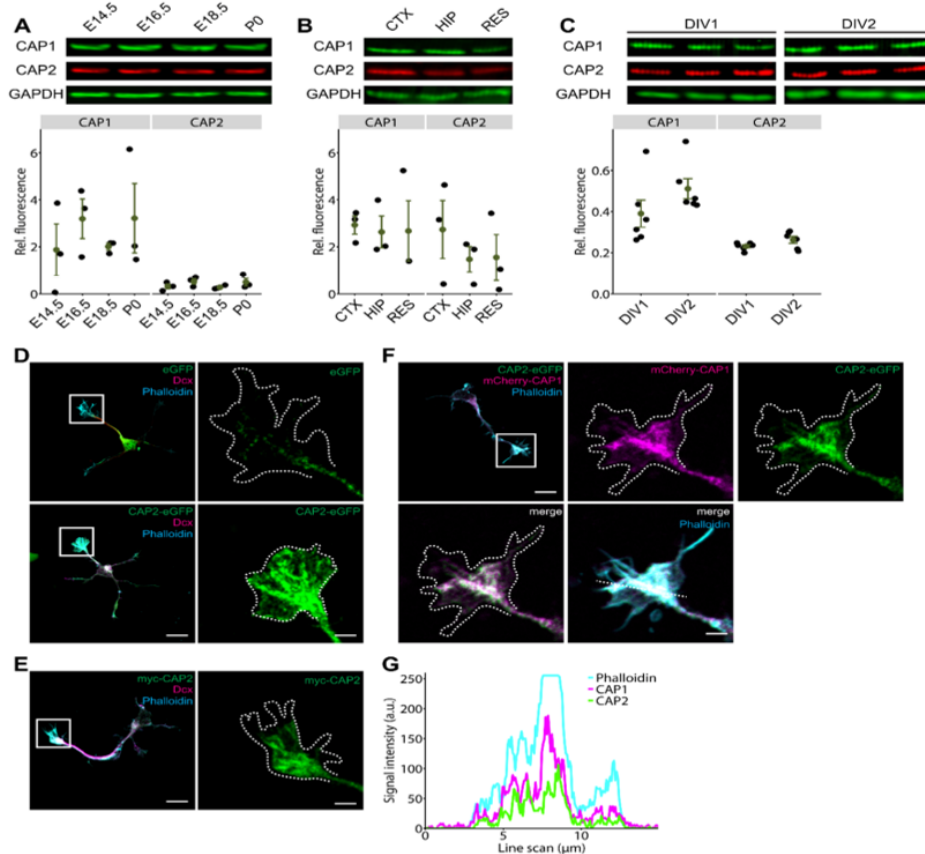
Figure 1. CAP2 is expressed in the embryonic brain and abundant in growth cones. (**A**) Immunoblots showing presence of CAP1 and CAP2 in cerebral cortex lysates during embryonic development, from embryonic day (E) 14.5 to postnatal day (P) 0. GAPDH was used as the loading control. Graph showing CAP1 and CAP2 levels normalized to the loading control, GAPDH. Black circles: normalized CAP1 and CAP2 levels in three biological replicates. Green circles and error bars: mean values (MV) and standard errors of the means (SEM). (**B**) Immunoblots showing expression levels of CAP1 and CAP2 in cerebral cortex (CTX) and hippocampus (HIP) lysates at P0. Additionally, lysate of residual brain (RES) was probed. GAPDH was used as the loading control. Graph showing CAP1 and CAP2 levels normalized to the loading control, GAPDH. Black circles: normalized CAP1 and CAP2 levels in three biological replicates. Green circles and error bars: MV and SEM. (**C**) Immunoblots showing presence of CAP1 and CAP2 in lysates from cultured cortical neurons (three biological replicates) after one and two days in vitro (DIV). GAPDH was used as the loading control. Graph showing CAP1 and CAP2 levels normalized to the loading control, GAPDH. Black circles: normalized CAP1 and CAP2 levels in six biological replicates. Green circles and error bars: MV and SEM. (**D**) Micrographs of hippocampal neurons at DIV1 expressing either GFP or GFP-CAP2 (green). Neurons were counterstained with the F-actin dye phalloidin (cyan) and the microtubule-associated protein doublecortin (Dcx, magenta). Boxes indicate areas shown at higher magnification, dashed lines outline growth cones as deduced from phalloidin staining. (**E**) Micrograph of a hippocampal neuron at DIV1 expressing myc-CAP2 visualized by myc antibody staining (green). Neuron was counterstained with phalloidin (cyan) and Dcx (magenta). Box indicates area shown at higher magnification, dashed line outlines growth cone. (**F**) Micrograph of a hippocampal neuron at DIV1 expressing GFP-CAP2 (green) and mCherry-CAP1 (magenta). Neuron was counterstained with phalloidin (cyan). Box indicates area shown at higher magnification, dashed line outlines growth cone. (**G**) Fluorescence intensity profile of GFP-CAP2, mCherry-CAP1 and phalloidin along white line shown in merge in G. Scale bars (in μm): 10 (low magnifications in (**D–F**)), 2 (high magnifications in (**D–F**)).

To determine the subcellular localization of CAP2 in differentiating neurons, we exploited hippocampal neurons isolated from E18.5 mice. Since CAP2-specific antibodies suitable for immunocytochemistry were not available, we introduced N-terminal GFP-tagged CAP2 (GFP-CAP2) into hippocampal neurons prior to plating by means of nucleofection. At DIV1, GFP-CAP2 was abundant in growth cones, which we identified by phalloidin staining of F-actin (Figure 1D). Unlike GFP-CAP2, fluorescence intensity in growth cones was much weaker in control neurons expressing GFP. In an independent experiment, we expressed CAP2 carrying a myc tag at its N-terminus (myc-CAP2). Similar to GFP-CAP2, myc-CAP2 was enriched in growth cones (Figure 1E). Moreover, we expressed GFP-CAP2 together with mCherry-tagged CAP1 in hippocampal neurons, and found both proteins enriched in growth cones (Figure 1F). Fluorescence intensity profiles of cross-sectional line scans revealed colocalization of GFP-CAP2, mCherry-CAP1, and phalloidin in growth cones (Figure 1G). Together, CAP2 was present during neuron differentiation and abundant in growth cones of differentiating neurons, very similar to CAP1. We therefore hypothesized a role for CAP2 in growth cone morphology and neuron differentiation.

3.1.1. CAP2 Is Not Relevant for Early Neuron Differentiation

To test whether CAP2 was relevant for neuron differentiation, we analyzed hippocampal neurons isolated from CAP2-KO mice [12,30]. Immunoblots confirmed efficient CAP2 inactivation and revealed unchanged CAP1 expression levels in brain lysates from CAP2-KO mice (Figure 2A; CAP1: CTR: 1.00 ± 0.40, CAP2-KO: 0.86 ± 0.29, $n = 3$, $p = 0.79$; CAP2: CTR: 1.00 ± 0.20, CAP2-KO: 0.05 ± 0.01, $n = 3$, $p < 0.05$). To test whether CAP2 was relevant for neuron differentiation, we isolated hippocampal neurons from E18.5 CAP2-KO and compared them to neurons isolated from CAP2$^{+/+}$ littermates that served as controls (CTR). First, we stained neurons at various time points after plating with an antibody against the neurite marker doublecortin (Dcx, Figure 2B). This allowed us to categorize neurons according to their differentiation stage, similar to previous studies [31]. After five hours in vitro (HIV5), we found the majority of CTR and CAP2-KO neurons in stage 1, i.e., they formed lamellipodia, but not yet neurites (Figure 2C; (%) CTR: 70.74 ± 2.93, CAP2-KO: 72.61 ± 2.46, $n > 300$ neurons from three mice). All other neurons possessed minor neurites, but not yet an axon and, hence, were assigned to stage 2 ((%) CTR: 29.26 ± 2.93, CAP2-KO: 27.39 ± 2.46). The stage distribution was not different between CTR and CAP2-KO at HIV5 ($p = 0.74$). Likewise, the stage distribution was unchanged in CAP2-KO neurons at DIV1 and DIV2 (Figure 2C; (%) DIV1: CTR: stage 1: 20.70 ± 2.71, stage 2: 76.29 ± 3.27, stage 3: 3.01 ± 1.09, CAP2-KO: stage 1: 18.91 ± 2.59, stage 2: 73.19 ± 2.66, stage 3: 7.89 ± 0.86, $n > 200/3$, $p = 0.10$; DIV2: CTR: stage 1: 3.24 ± 1.69, stage 2: 69.50 ± 2.63, stage 3: 27.26 ± 2.58, CAP2-KO: stage 1: 1.48 ± 0.98, stage 2: 75.50 ± 2.20, stage 3: 23.02 ± 1.94, $n > 130/3$, $p = 0.44$). Together, stage distribution of CAP2-KO neurons was unchanged between HIV5 and DIV2.

We further exploited Dcx-stained neurons to determine their morphology by counting the numbers of primary neurites and neurite endpoints and by calculating the ratio of neurite endpoints and primary neurites (endpoint/neurite ratio) that we used as a readout for neurite branching. None of these parameters were changed in stage 2 CAP2-KO neurons at DIV1 or DIV2 (Figure 2D–F; DIV1: neurites: CTR: 4.11 ± 0.43, CAP2-KO: 3.87 ± 0.39, $p = 0.68$; endpoints: CTR: 4.53 ± 0.49, CAP2-KO: 4.13 ± 0.40, $p = 0.54$; endpoint/neurite ratio: CTR: 1.11 ± 0.05, CAP2-KO: 1.08 ± 0.04, $p = 0.68$, $n = 15/5$; DIV2: neurites: CTR: 4.81 ± 0.21, CAP2-KO: 4.90 ± 0.22, $p = 0.75$; endpoints: CTR: 6.00 ± 0.33, CAP2-KO: 5.90 ± 0.28, $p = 0.82$; endpoint/neurite ratio: CTR: 1.24 ± 0.04, CAP2-KO: 1.22 ± 0.04, $p = 0.72$, $n > 31/3$). Moreover, we determined neurite width and total neurite length in stage 2 neurons, two parameters that we found altered in CAP1-KO neurons [9]. Instead, neither neurite width nor total neurite length was altered in CAP2-KO neurons (Figure 2G–H; width: CTR: 0.84 ± 0.06, CAP2-KO: 0.94 ± 0.13, $p = 0.49$, $n > 35/3$; total length: CTR: 188.07 ± 12.59, CAP2-KO: 177.84 ± 8.74, $p = 0.51$, $n > 30/3$). Together, the morphology of stage 2 CAP2-KO neurons was unchanged. From the normal stage distribution in CAP2-KO

cultures and from the normal morphology of CAP2-KO neurons we concluded that CAP2 was dispensable for neurite differentiation.
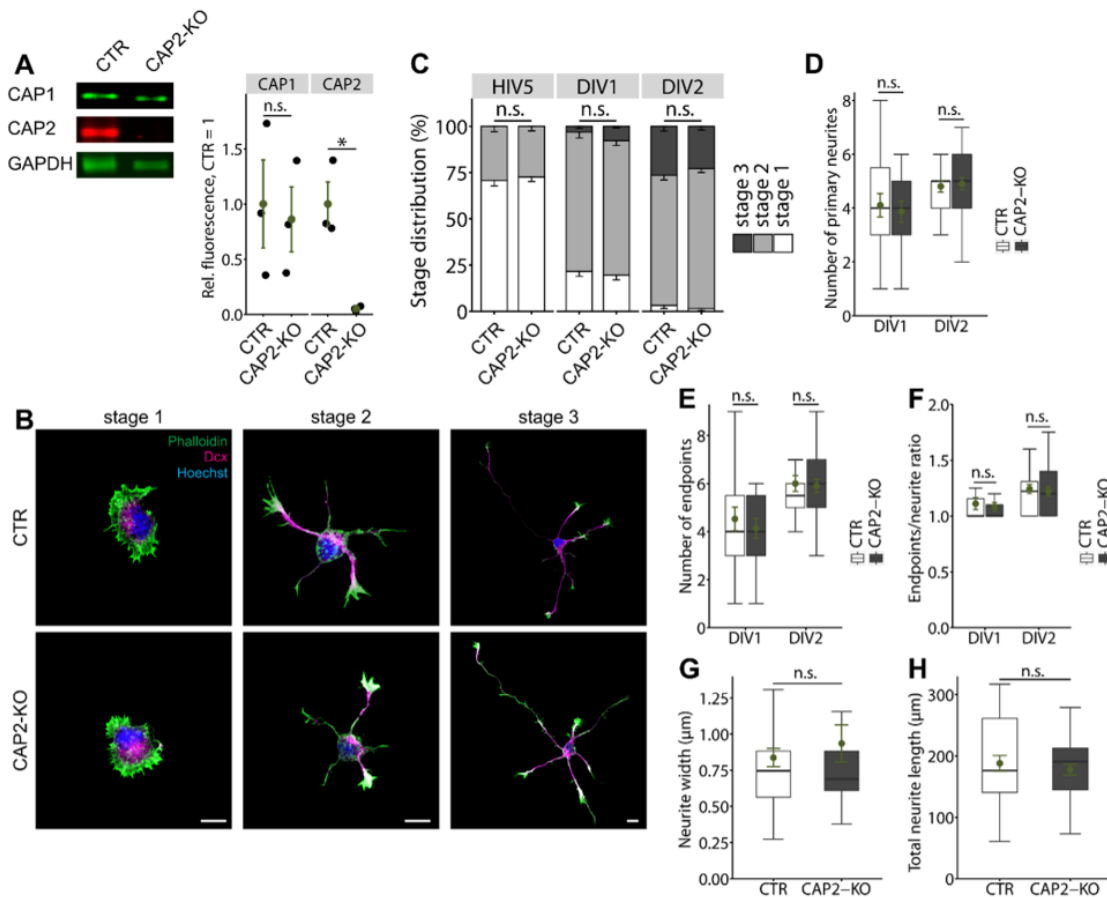
Figure 2. Normal differentiation and morphology of CAP2-KO neurons. (**A**) Immunoblots confirmed absence of CAP2 from CAP2-KO brain and unchanged expression levels of CAP1 in CAP2-KO brains. GAPDH was used as the loading control. Graph showing CAP1 and CAP2 levels normalized to the loading control, GAPDH, with CTR set to 1 in CTR and CAP2-KO brain lysates. Black circles: normalized CAP1 and CAP2 levels in three biological replicates. Green circles and error bars: MV and SEM. (**B**) Representative hippocampal neurons from CTR and CAP2-KO mice at differentiation stages 1 to 3 [31]. Neurons were stained with an antibody against doublecortin (Dcx, magenta), the DNA maker Hoechst (blue), and phalloidin (green). (**C**) Stage distribution for CTR and CAP2-KO neurons after five hours in vitro (HIV5) and at DIV1 and DIV2. Number of (**D**) primary neurites and (**E**) neurite endpoints in stage 2 CTR and CAP2-KO neurons at DIV1 and DIV2. (**F**) Endpoints/neurites ratio in stage 2 CTR and CAP2-KO neurons at DIV1 and DIV2. (**G**) Neurite width and (**H**) total neurite length in stage 2 CTR and CAP2-KO neurons. Scale bar (in µm): 10 (**B**). n.s.: $p \geq 0.05$, * $p < 0.05$. Error bars represent SEM.

3.1.2. CAP2 Is Dispensable for Growth Cone Size, Morphology, and Motility

The abundance of GFP-CAP2 in growth cones forced us to test whether CAP2 was relevant for growth cone size or morphology. To do so, we determined growth cone size in phalloidin-stained stage 2 neurons at HIV5 to DIV2. None of the investigated time points showed differences between CTR or CAP2-KO neurons (Figure 3A,B; (µm^2) HIV5: CTR: 26.96 ± 1.56, CAP2-KO: 27.36 ± 1.96, $n = 60/3$, $p = 0.87$; DIV1: CTR: 29.32 ± 3.88, CAP2-KO: 23.08 ± 3.28, $n = 30/3$, $p = 0.22$; DIV2: CTR: 23.52 ± 1.57, CAP2-KO: 23.34 ± 1.60, $n = 100/3$, $p = 0.93$). Moreover, growth cone morphology was normal in

CAP2-KO neurons as indicated by unchanged shape indices for circularity and solidity (Figure 3C; circularity: CTR: 0.27 ± 0.03, CAP2-KO: 0.26 ± 0.02, $p = 0.78$; solidity: CTR: 0.62 ± 0.03, CAP2-KO: 0.61 ± 0.03, $p = 0.84$, $n = 32/3$). Apart from CAP2-KO neurons, we tested whether acute CAP2 inactivation altered growth cone size or morphology in hippocampal neurons. To do so, we designed three different shRNAs directed against CAP2. Immunoblots confirmed efficient knockdown of CAP2 (CAP2-KD) in cerebral cortex neurons nucleofected with CAP2-sh3 and CAP2-sh4, while CAP2-sh2 only moderately decreased CAP2 levels when compared to control shRNA (CTR-shRNA)-nucleofected neurons (Figure 3D; sh2 0.69 ± 0.19, sh3: 0.32 ± 0.03, sh4: 0.31 ± 0.01, $n = 3$). To study growth cones, we nucleofected hippocampal neurons with a mixture of CAP2-sh3 and -sh4 prior to initial seeding, replated CAP2-KD neurons at DIV2 and analyzed growth cone size and morphology one day after replating (DAR1), similar to previous studies [9,25]. In DAR1 CAP2-KD neurons, growth cone size was not different from neurons nucleofected with CTR-shRNA (Figure 3E,F; (μm^2) CTR: 29.17 ± 2.06, CAP2-KD: 30.04 ± 1.96, $n = 60/3$, $p = 0.76$). Likewise, the shape index circularity was not different between neurons of both groups, while the shape index solidity was slightly increased by 9% in CAP2-KD neurons (Figure 3G; circularity: CTR: 0.19 ± 0.01, CAP2-KD: 0.22 ± 0.01, $n = 60/3$, $p = 0.12$; solidity: CTR: 0.53 ± 0.01, CAP2-KD: 0.58 ± 0.01, $n = 60/3$, $p < 0.05$). Together, neither acute nor systemic CAP2 inactivation altered growth cone size. Moreover, growth cone morphology was unchanged in CAP2-KO neurons and only slightly altered upon acute CAP2 knockdown. From these data we concluded that CAP2 was largely dispensable in growth cones. Indeed, growth cones from CAP2-KO neurons were as motile as the ones from CTR neurons (Movies S1–S2).
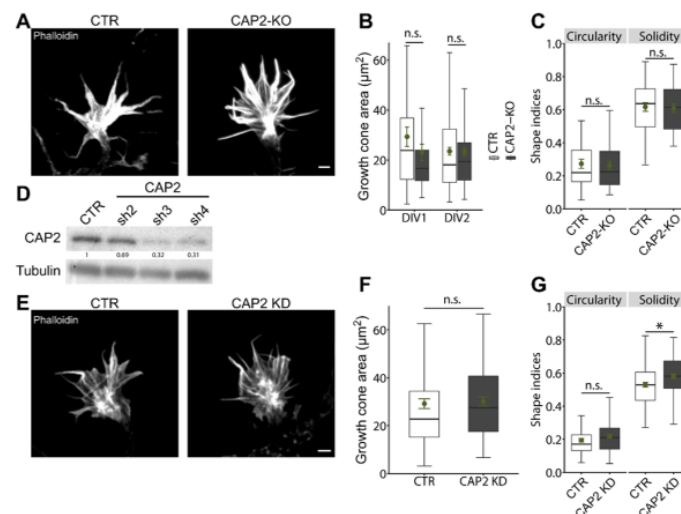
Figure 3. Normal growth cone size and morphology in CAP2-KO neurons. (**A**) Micrographs of phalloidin-stained growth cones from stage 2 CTR and CAP2-KO neurons. (**B**) Growth cone size in stage 2 CTR and CAP2-KO neurons at DIV1 and DIV2. (**C**) Growth cone shape indices for circularity and solidity for stage 2 CTR and CAP2-KO neurons. (**D**) Immunoblots with lysates from cerebral cortex neurons nucleofected with three different shRNAs directed against CAP2 (CAP2-sh2, CAP2-sh3, and CAP2-sh4) or with a control (CTR) shRNA. Tubulin was used as the loading control. Values indicate CAP2 levels in CAP2-KD neurons relative to CTR-shRNA-nucleofected controls. (**E**) Micrographs of phalloidin-stained growth cones from replated stage 2 neurons nucleofected with either CTR shRNA or a mixture of CAP2-sh3 and CAP2-sh4 (CAP2-KD). (**F**) Growth cone size and (**G**) shape indices for circularity and solidity in stage 2 neurons nucleofected with either CTR shRNA or CAP2-sh3/CAP2-sh4. Scale bars (in μm): 2 (**A**), 2 (**E**). * $p < 0.05$, n.s.: $p \geq 0.05$. Error bars represent SEM.

3.1.3. CAP2 Is Dispensable for Brain Development

The data we presented so far revealed CAP2 expression in differentiating neurons and abundance in growth cones, similar to CAP1. However, while we found CAP1 to be relevant for neuron differentiation, growth cone morphology, and growth cone motility [9], none of these processes was impaired in CAP2-KO neurons. Impaired differentiation of CAP1-KO neurons was associated with hypomorphic fiber tracks in brains from CAP1-KO mice and a somewhat altered hippocampus morphology [9]. Such changes were not present in brains from CAP2-KO mice. Specifically, Nissl-stained transversal brains sections revealed no obvious differences in cerebral cortex or hippocampus anatomy between CTR and CAP2-KO mice at E18.5 or in adult mice (Figure 4A,B). Moreover, antibody staining against the axon marker neurofilament suggested a normal appearance of fiber tracks in CAP2-KO brains (Figure 4C), different from CAP1-KO mice [9]. Together, CAP2-KO mice did not display any gross defects in brain development.
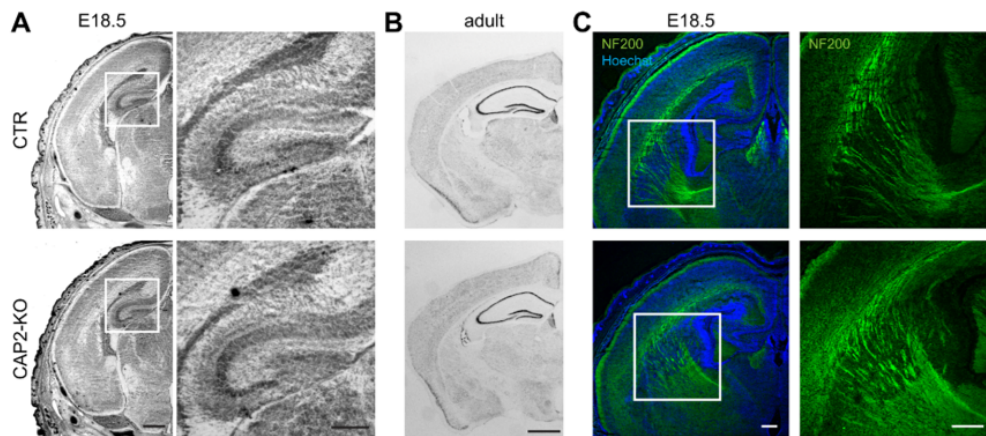
Figure 4. CAP2 inactivation does not cause obvious histological alterations in the mouse brain. (**A**) Nissl staining of transversal brain sections from CTR and CAP2-KO mice at E18.5. Boxes indicate area shown at higher magnification. (**B**) Nissl staining of transversal brain sections from adult CTR and CAP2-KO mice. (**C**) Antibody staining against the axon marker neurofilament (green) in transversal brain sections from E18.5 CTR and CAP2-KO mice. Sections were counterstained with DNA dye Hoechst (blue). Boxes indicate area shown at higher magnification. Scale bars (in μm): 500 (low magnification), 250 (high magnification) (**A**), 1000 (**B**), and 100 (**C**).

3.1.4. CAP2 Can Rescue Neuron Morphology and Differentiation in CAP1-KO Neurons

From our data and our previous analysis in CAP1-KO neurons we concluded that CAP2 is dispensable for neuron differentiation and brain development and that CAP1 is the limiting factor in differentiating neurons [9]. Absence of any defects in CAP2-KO neurons could be explained by functional redundancy of CAP1 and CAP2 during neuron differentiation. To determine whether both CAPs share redundant functions, we tested whether overexpression of CAP2 can rescue morphological changes in CAP1-deficient neurons. Hippocampal neurons deficient for CAP1 were isolated from brain-specific CAP1-KO mice that we achieved by crossing a conditional CAP1 strain and Nestin-Cre transgenic mice (CAP1$^{flx/flx,Nestin-Cre}$) [9,23]. Immunoblots confirmed absence of CAP1 from hippocampal lysates obtained from E18.5 CAP1$^{flx/flx,Nestin-Cre}$ mice (termed CAP1-KO), CAP1$^{flx/flx}$ littermates served as controls (CTR). Compared to CTR, CAP2 expression levels were unchanged in the CAP1-KO hippocampus (Figure 5A; CAP1: CTR: 1.00 ± 0.31, CAP1-KO: 0.07 ± 0.04, $n = 3$, $p = 0.09$; CAP2: CTR: 1.00 ± 0.12, CAP1-KO: 0.92 ± 0.04, $n = 3$, $p = 0.58$). Similarly to our previous study [9], differentiation was impaired in the CAP1-KO neuron. Specifically, the fraction of stage 1 neurons was increased on the expense of stage 2 and stage 3 neurons at DIV1 (Figure 5B; (%) CTR: stage 1: 10.10 ± 1.61, stage

2: 82.41 ± 2.84, stage 3: 7.49 ± 2.04; CAP1-KO: stage 1: 52.27 ± 2.59, stage 2: 47.47 ± 2.44, stage 3: 0.27 ± 0.28, $n > 300/3$, $p < 0.001$). Moreover, stage 2 CAP1-KO displayed an increased neurite width and a reduced total neurite length (Figure 5C–E; (μm) width: CTR: 0.75 ± 0.04, CAP1-KO: 2.36 ± 0.19, $p < 0.001$, $n > 80/3$; length: CTR: 53.82 ± 5.38, CAP1-KO: 34.72 ± 5.14, $p < 0.05$, $n < 40/3$). As expected, expression of *N*-terminal GFP-tagged CAP1 (GFP-CAP1) normalized stage distribution in CAP1-KO neurons (stage 1: 19.39 ± 3.19, stage 2: 76.53 ± 2.01, stage 3: 4.08XY ± 1.25, $n > 90/3$, $p < 0.001$), and it reduced neurite width and increased total neurite length ((μm) width: 0.84 ± 0.05, $p < 0.001$, $n = 85/3$; length: 57.40 ± 5.82, $p < 0.05$, $n > 40/3$). Similarly, overexpression of GFP-CAP2 normalized stage distribution in CAP1-KO neurons (Figure 5B; stage 1: 16.82 ± 2.26, stage 2: 73.83 ± 4.17, stage 3: 9.35 ± 3.40, $n > 100/3$, $p < 0.001$). Moreover, GFP-CAP2 overexpression rescued neurite width and total neurite length (Figure 5C–E; (μm) width: 0.74 ± 0.04, $p < 0.001$, $n > 90/3$; length: 55.22 ± 5.46, $p < 0.05$, $n > 35/3$). Next, by determining growth cone size we tested whether CAP2 overexpression can compensate for CAP1 loss in growth cones. As reported before [9], growth cones were enlarged by 98% in CAP1-KO neurons (Figure 5F,G; (μm^2) CTR: 25.14 ± 2.07, CAP1-KO: 49.86 ± 3.71, $n = 60/3$, $p < 0.001$). Growth cone size in CAP1-KO neurons was reduced by expression of either N-terminal myc-tagged CAP1 (myc-CAP1) or GFP-CAP1 ((μm^2): myc-CAP1: 22.08 ± 1.97, $p < 0.001$, $n = 42/3$; GFP-CAP1: 26.26 ± 2.10, $p < 0.001$, $n = 80/3$), and growth cone size in these neurons was not different from CTR neurons (myc-CAP1: $p = 0.49$; GFP-CAP1: $p = 0.74$). Similar to myc-CAP1 and GFP-CAP1, overexpression of either GFP-CAP2 or myc-CAP2 reduced growth cone size in CAP1-KO neurons ((μm^2) myc-CAP2: 32.54 ± 2.63, $p < 0.001$, $n = 37/3$; GFP-CAP2: 33.92 ± 2.44, $p < 0.001$, $n = 60/3$). When compared to CTR neurons, growth cone size was not different in myc-CAP2-overexpressing CAP1-KO neurons ($p = 0.10$), but remained enlarged in GFP-CAP2-overexpressing CAP1-KO neurons ($p < 0.05$). Together, CAP2 overexpression reduced growth cone size in CAP1-KO neurons, suggesting redundant functions of CAP1 and CAP2 in growth cones.
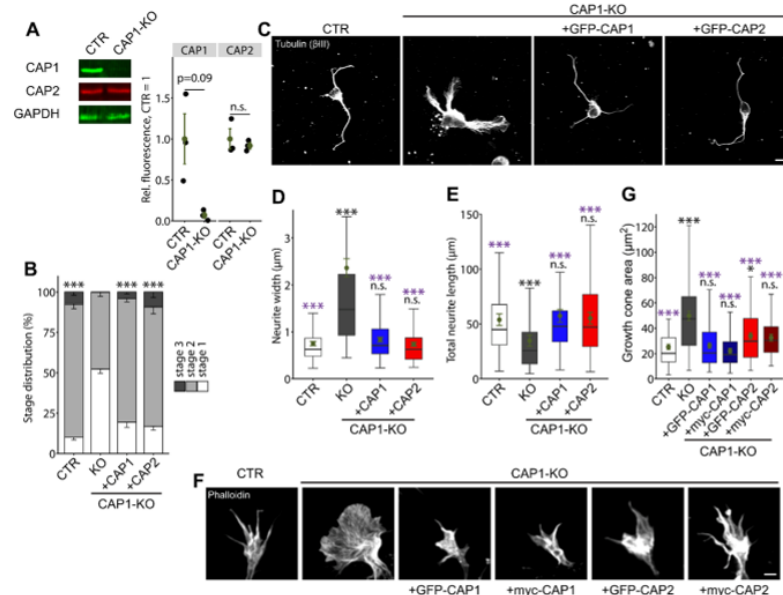
Figure 5. CAP2 overexpression partially rescues morphological changes in CAP1-KO neurons. (**A**) Immunoblots of three biological replicates showing absence of CAP1 from the CAP1-KO brain and unchanged expression of CAP2. GAPDH was used as the loading control. Graph showing CAP1 and CAP2 levels normalized to the loading control, GAPDH with CAP1 set to 1 in CAP1-KO brain lysates. Black circles: normalized CAP1 and CAP2 levels in three biological replicates. Green circles

and error bars: MV and SEM. (**B**) Stage distribution of DIV1 CTR neurons, CAP1-KO neurons, and CAP1-KO neurons expressing either GFP-CAP1 or GFP-CAP2. (**C**) βIII-tubulin-stained neurons (CTR, CAP1-KO, and CAP1-KO expressing either GFP-CAP1 or GFP-CAP2) that were used for the analysis of neurite width and total neurite length shown in (**D,E**). (**F**) Growth cones from phalloidin-stained neurons (CTR, CAP1-KO, and CAP1-KO expressing either GFP- or myc-tagged CAP1 or GFP- or myc-tagged CAP2) that were used for the analysis of growth cones size shown in (**G**). Scale bars (in μm): 10 (**C**), 2 (**F**). n.s.: $p \geq 0.05$, * $p < 0.05$, *** $p < 0.001$. Error bars represent SEM. Black asterisks and n.s. indicate comparison to CTR neurons and purple asterisks and n.s. indicate comparison to CAP1-KO neurons.

4. Discussion

The present study aimed at deciphering the role for CAP2 in early neuron differentiation, which we found expressed in the embryonic and perinatal brain and abundant in growth cones from hippocampal neurons, similar to its close homolog CAP1 [9,11,32,33]. While we recently reported important CAP1 functions in neuron differentiation, growth cone morphology, and neuron connectivity in the mouse brain [9], neuron differentiation and growth cone morphology was normal in CAP2-KO neurons, and CAP2-KO mice did not display obvious defects in brain development or neuron connectivity. Interestingly, CAP2 overexpression rescued morphological changes in isolated hippocampal neurons from CAP1-KO mice, suggesting that CAP1 and CAP2 share redundant functions in differentiating neurons.

Normal stage distribution and morphology of isolated hippocampal CAP2-KO neurons together with normal growth cone size and morphology and absence of any obvious histological changes in CAP2-KO brains revealed that CAP2 was dispensable for neuron differentiation and brain development. Instead, a previous study unraveled important functions for CAP2 in differentiated neurons [19]. Specifically, this study implicated CAP2 in regulating the morphology of dendritic spines, the F-actin-enriched postsynaptic compartments of most excitatory synapses in the brain. Moreover, it revealed an interaction of CAP2 with the actin-depolymerizing protein cofilin1, a key regulator of synaptic actin dynamics, spine morphology, synaptic plasticity, brain function, and behavior [21,34–40]. Further, this study implicated the interaction of CAP2 with cofilin1 in structural plasticity of excitatory synapses, and it provided evidence that CAP2-cofilin1 interaction is compromised in Alzheimer's disease patients, which may contribute to the underlying disease mechanism [19]. Spine morphological changes upon CAP2 inactivation were also reported in a second study, which unfortunately did not provide detailed mechanistic insights [41]. Together, these studies and our findings in CAP2-KO neurons and brains suggest that CAP2 acquires important functions in differentiated neurons, but is dispensable during neuron differentiation.

Unlike most other cell types, hippocampal neurons express both CAP family members, and our group recently demonstrated important functions for CAP1 in regulating the actin cytoskeleton during neuron differentiation [9]. Specifically, we showed that CAP1 controls organization and dynamics of F-actin in growth cones. F-actin defects impaired growth cone function in CAP1-KO neurons and retarded their differentiation, which likely caused compromised neuron connectivity in CAP1-KO mouse brains [9]. Interestingly, we found a cooperation of CAP1 and cofilin1 during neuron differentiation, and our data suggested functional interdependency for both actin regulators in growth cones. Hence, CAP1 was relevant for cofilin1-dependent actin dynamics in growth cones of differentiating neurons, while CAP2 controls cofilin1 in dendritic spines from differentiated neurons.

Absence of any defects in differentiating CAP2-KO neurons led us suggest that CAP1 is the dominant family member during neuron differentiation and brain development. However, CAP2 overexpression rescued neuron differentiation as well as neurite width and total neurite length in CAP1-KO neurons, and it partially rescued growth cone size. These data revealed that CAP2 can compensate CAP1 inactivation in isolated neurons during differentiation, suggesting that CAP1 and CAP2 share overlapping and redundant

functions during neuron differentiation. Moreover, this finding led us to speculate compensatory mechanisms in single KO neurons, which could explain normal differentiation and growth cone morphology in CAP2-KO neurons. Differently from the brain, CAP1 is absent from skeletal muscles and only weakly expressed in the heart [10,11]. Hence, CAP1 cannot compensate CAP2 inactivation in striated muscles, thereby explaining why systemic CAP2-KO mice displayed defects in heart physiology and myofibril differentiation, but not in neuron differentiation or brain development [12,14,15]. Functional redundancy of mouse CAP1 and CAP2 has been postulated earlier [15], and is in good agreement with the roughly 60% identity and 75% similarity both proteins share in their primary sequences [1,11]. Moreover, the overlapping functions in the brain is supported by recent findings (i) demonstrating that CAP1 and CAP2 both interact with cofilin1 to control neuronal actin dynamics [9,19] and (ii) identifying both CAP1 and CAP2 as components of a protein complex isolated from the mouse brain that was able to inhibit the F-actin assembly factor INF2 [6,8]. Apart from this, most studies that investigated the molecular functions of mammalian CAPs primarily focused on CAP1 (for review: [2]), and it therefore remains to be tested whether (i) CAP1 and CAP2 acquired specific functions in actin regulation, (ii) they possess specific interaction partners, (iii) they are controlled by specific regulatory mechanisms, (iv) they are addressed by specific signaling cascades, and (v) they share redundant functions in vivo. It will be exciting to decipher, in future studies, common and specific upstream and downstream mechanisms of CAP1 and CAP2 in neurons.

References

1. Ono, S. The role of cyclase-associated protein in regulating actin filament dynamics—More than a monomer-sequestration factor. *J. Cell Sci.* **2013**, *126*, 3249–3258. [CrossRef] [PubMed]
2. Rust, M.B.; Khudayberdiev, S.; Pelucchi, S.; Marcello, E. CAPt'n of Actin Dynamics: Recent Advances in the Molecular, Developmental and Physiological Functions of Cyclase-Associated Protein (CAP). *Front. Cell Dev. Biol.* **2020**, *8*, 586631. [CrossRef] [PubMed]

3. Johnston, A.B.; Collins, A.; Goode, B.L. High-speed depolymerization at actin filament ends jointly catalysed by Twinfilin and Srv2/CAP. *Nat. Cell Biol.* **2015**, *17*, 1504–1511. [CrossRef] [PubMed]

4. Kotila, T.; Kogan, K.; Enkavi, G.; Guo, S.; Vattulainen, I.; Goode, B.L.; Lappalainen, P. Structural basis of actin monomer re-charging by cyclase-associated protein. *Nat. Commun.* **2018**, *9*, 1892. [CrossRef] [PubMed]

5. Kotila, T.; Wioland, H.; Enkavi, G.; Kogan, K.; Vattulainen, I.; Jegou, A.; Romet-Lemonne, G.; Lappalainen, P. Mechanism of synergistic actin filament pointed end depolymerization by cyclase-associated protein and cofilin. *Nat. Commun.* **2019**, *10*, 5320. [CrossRef] [PubMed]

6. Mu, A.; Fung, T.S.; Kettenbach, A.N.; Chakrabarti, R.; Higgs, H.N. A complex containing lysine-acetylated actin inhibits the formin INF2. *Nat. Cell Biol.* **2019**, *21*, 592–602.

7. Shekhar, S.; Chung, J.; Kondev, J.; Gelles, J.; Goode, B.L. Synergy between Cyclase-associated protein and Cofilin accelerates actin filament depolymerization by two orders of magnitude. *Nat. Commun.* **2019**, *10*, 5319. [CrossRef] [PubMed]

8. Mu, A.; Fung, T.S.; Francomacaro, L.M.; Huynh, T.; Kotila, T.; Svindrych, Z.; Higgs, H.N. Regulation of INF2-mediated actin polymerization through site-specific lysine acetylation of actin itself. *Proc. Natl. Acad. Sci. USA* **2020**, *117*, 439–447.

9. Schneider, F.; Duong, T.A.; Metz, I.; Winkelmeier, J.; Hübner, C.A.; Endesfelder, U.; Rust, M.B. Mutual functional dependence of cyclase-associated protein 1 (CAP1) and cofilin1 in neuronal actin dynamics and growth cone function. *Prog. Neurobiol.* **2021**, *202*, 102050. [CrossRef] [PubMed]

10. Bertling, E.; Hotulainen, P.; Mattila, P.K.; Matilainen, T.; Salminen, M.; Lappalainen, P. Cyclase-associated protein 1 (CAP1) promotes cofilin-induced actin dynamics in mammalian nonmuscle cells. *Mol. Biol. Cell* **2004**, *15*, 2324–2334. [CrossRef]

11. Peche, V.; Shekar, S.; Leichter, M.; Korte, H.; Schroder, R.; Schleicher, M.; Holak, T.A.; Clemen, C.S.; Ramanath, Y.B.; Pfitzer, G.; et al. CAP2, cyclase-associated protein 2, is a dual compartment protein. *Cell Mol. Life Sci.* **2007**, *64*, 2702–2715. [CrossRef]

12. Kepser, L.J.; Damar, F.; De Cicco, T.; Chaponnier, C.; Proszynski, T.J.; Pagenstecher, A.; Rust, M.B. CAP2 deficiency delays myofibril actin cytoskeleton differentiation and disturbs skeletal muscle architecture and function. *Proc. Natl. Acad. Sci. USA* **2019**, *116*, 8397–8402. [CrossRef]

13. Colpan, M.; Iwanski, J.; Gregorio, C.C. CAP2 is a regulator of actin pointed end dynamics and myofibrillogenesis in cardiac muscle. *Commun. Biol.* **2021**, *4*, 365. [CrossRef]

14. Peche, V.S.; Holak, T.A.; Burgute, B.D.; Kosmas, K.; Kale, S.P.; Wunderlich, F.T.; Elhamine, F.; Stehle, R.; Pfitzer, G.; Nohroudi, K.; et al. Ablation of cyclase-associated protein 2 (CAP2) leads to cardiomyopathy. *Cell Mol. Life Sci.* **2013**, *70*, 527–543. [CrossRef]

15. Field, J.; Ye, D.Z.; Shinde, M.; Liu, F.; Schillinger, K.J.; Lu, M.; Wang, T.; Skettini, M.; Xiong, Y.; Brice, A.K.; et al. CAP2 in cardiac conduction, sudden cardiac death and eye development. *Sci. Rep.* **2015**, *5*, 17256. [CrossRef]

16. Stockigt, F.; Peche, V.S.; Linhart, M.; Nickenig, G.; Noegel, A.A.; Schrickel, J.W. Deficiency of cyclase-associated protein 2 promotes arrhythmias associated with connexin43 maldistribution and fibrosis. *Arch. Med. Sci.* **2016**, *12*, 188–198. [CrossRef]

17. Xiong, Y.; Bedi, K.; Berritt, S.; Attipoe, B.K.; Brooks, T.G.; Wang, K.; Margulies, K.B.; Field, J. Targeting MRTF/SRF in CAP2-dependent dilated cardiomyopathy delays disease onset. *JCI Insight* **2019**, *4*, e124629. [CrossRef]

18. Jang, H.D.; Lee, S.E.; Yang, J.; Lee, H.C.; Shin, D.; Lee, H.; Lee, J.; Jin, S.; Kim, S.; Lee, S.J.; et al. Cyclase-associated protein 1 is a binding partner of proprotein convertase subtilisin/kexin type-9 and is required for the degradation of low-density lipoprotein receptors by proprotein convertase subtilisin/kexin type-9. *Eur. Heart J.* **2019**, *41*, 239–252. [CrossRef]

19. Pelucchi, S.; Vandermeulen, L.; Pizzamiglio, L.; Aksan, B.; Yan, J.; Konietzny, A.; Bonomi, E.; Borroni, B.; Padovani, A.; Rust, M.B.; et al. Cyclase-associated protein 2 dimerization regulates cofilin in synaptic plasticity and Alzheimer's disease. *Brain Commun.* **2020**, *2*, fcaa086. [CrossRef]

20. Bosch, M.; Hayashi, Y. Structural plasticity of dendritic spines. *Curr. Opin. Neurobiol.* **2012**, *22*, 383–388. [CrossRef]

21. Rust, M.B. ADF/cofilin: A crucial regulator of synapse physiology and behavior. *Cell Mol. Life Sci.* **2015**, *72*, 3521–3529. [CrossRef] [PubMed]

22. Dent, E.W.; Gupton, S.L.; Gertler, F.B. The growth cone cytoskeleton in axon outgrowth and guidance. *Cold Spring Harb. Perspect. Biol.* **2011**, *3*, a001800. [CrossRef] [PubMed]

23. Tronche, F.; Kellendonk, C.; Kretz, O.; Gass, P.; Anlag, K.; Orban, P.C.; Bock, R.; Klein, R.; Schutz, G. Disruption of the glucocorticoid receptor gene in the nervous system results in reduced anxiety. *Nat. Genet.* **1999**, *23*, 99–103. [CrossRef] [PubMed]

24. Antoniou, A.; Khudayberdiev, S.; Idziak, A.; Bicker, S.; Jacob, R.; Schratt, G. The dynamic recruitment of TRBP to neuronal membranes mediates dendritogenesis during development. *EMBO Rep.* **2018**, *19*, e44853. [CrossRef]

25. Schneider, F.; Duong, T.A.; Rust, M.B. Neuron replating—A powerful and versatile approach to study early aspects of neuron differentiation. *eNeuro* **2021**, *8*. [CrossRef]

26. Bicker, S.; Khudayberdiev, S.; Weiß, K.; Zocher, K.; Baumeister, S.; Schratt, G. The DEAH-box helicase DHX36 mediates dendritic localization of the neuronal precursor-microRNA-134. *Genes Dev.* **2013**, *27*, 991–996. [CrossRef]

27. Schindelin, J.; Arganda-Carreras, I.; Frise, E.; Kaynig, V.; Longair, M.; Pietzsch, T.; Preibisch, S.; Rueden, C.; Saalfeld, S.; Schmid, B.; et al. Fiji: An open-source platform for biological-image analysis. *Nat. Methods* **2012**, *9*, 676–682. [CrossRef]

28. Kullmann, J.A.; Neumeyer, A.; Gurniak, C.B.; Friauf, E.; Witke, W.; Rust, M.B. Profilin1 is required for glial cell adhesion and radial migration of cerebellar granule neurons. *EMBO Rep.* **2012**, *13*, 75–82. [CrossRef]

29. Kullmann, J.A.; Meyer, S.; Pipicelli, F.; Kyrousi, C.; Schneider, F.; Bartels, N.; Cappello, S.; Rust, M.B. Profilin1-Dependent F-Actin Assembly Controls Division of Apical Radial Glia and Neocortex Development. *Cereb. Cortex* **2019**, *30*, 3467–3482. [CrossRef]

30. Kepser, L.J.; Khudayberdiev, S.; Hinojosa, L.S.; Macchi, C.; Ruscica, M.; Marcello, E.; Culmsee, C.; Grosse, R.; Rust, M.B. Cyclase-associated protein 2 (CAP2) controls MRTF-A localization and SRF activity in mouse embryonic fibroblasts. *Sci. Rep.* **2021**, *11*, 4789. [CrossRef]

31. Dotti, C.G.; Sullivan, C.A.; Banker, G.A. The establishment of polarity by hippocampal neurons in culture. *J. Neurosci.* **1988**, *8*, 1454–1468. [CrossRef]

32. Nozumi, M.; Togano, T.; Takahashi-Niki, K.; Lu, J.; Honda, A.; Taoka, M.; Shinkawa, T.; Koga, H.; Takeuchi, K.; Isobe, T.; et al. Identification of functional marker proteins in the mammalian growth cone. *Proc. Natl. Acad. Sci. USA* **2009**, *106*, 17211–17216. [CrossRef]

33. Lu, J.; Nozumi, M.; Takeuchi, K.; Abe, H.; Igarashi, M. Expression and function of neuronal growth-associated proteins (nGAPs) in PC12 cells. *Neurosci. Res.* **2011**, *70*, 85–90. [CrossRef]

34. Hotulainen, P.; Llano, O.; Smirnov, S.; Tanhuanpaa, K.; Faix, J.; Rivera, C.; Lappalainen, P. Defining mechanisms of actin polymerization and depolymerization during dendritic spine morphogenesis. *J. Cell Biol.* **2009**, *185*, 323–339. [CrossRef]

35. Rust, M.B.; Gurniak, C.B.; Renner, M.; Vara, H.; Morando, L.; Gorlich, A.; Sassoe-Pognetto, M.; Banchaabouchi, M.A.; Giustetto, M.; Triller, A.; et al. Learning, AMPA receptor mobility and synaptic plasticity depend on n-cofilin-mediated actin dynamics. *EMBO J.* **2010**, *29*, 1889–1902. [CrossRef]

36. Gu, J.; Lee, C.W.; Fan, Y.; Komlos, D.; Tang, X.; Sun, C.; Yu, K.; Hartzell, H.C.; Chen, G.; Bamburg, J.R.; et al. ADF/cofilin-mediated actin dynamics regulate AMPA receptor trafficking during synaptic plasticity. *Nat. Neurosci.* **2010**, *13*, 1208–1215. [CrossRef]

37. Bosch, M.; Castro, J.; Saneyoshi, T.; Matsuno, H.; Sur, M.; Hayashi, Y. Structural and molecular remodeling of dendritic spine substructures during long-term potentiation. *Neuron* **2014**, *82*, 444–459. [CrossRef]

38. Wolf, M.; Zimmermann, A.M.; Gorlich, A.; Gurniak, C.B.; Sassoe-Pognetto, M.; Friauf, E.; Witke, W.; Rust, M.B. ADF/Cofilin Controls Synaptic Actin Dynamics and Regulates Synaptic Vesicle Mobilization and Exocytosis. *Cereb. Cortex* **2015**, *25*, 2863–2875. [CrossRef]

39. Zimmermann, A.M.; Jene, T.; Wolf, M.; Gorlich, A.; Gurniak, C.B.; Sassoe-Pognetto, M.; Witke, W.; Friauf, E.; Rust, M.B. Attention-Deficit/Hyperactivity Disorder-like Phenotype in a Mouse Model with Impaired Actin Dynamics. *Biol. Psychiatry* **2015**, *78*, 95–106. [CrossRef]

40. Duffney, L.J.; Zhong, P.; Wei, J.; Matas, E.; Cheng, J.; Qin, L.; Ma, K.; Dietz, D.M.; Kajiwara, Y.; Buxbaum, J.D.; et al. Autism-like Deficits in Shank3-Deficient Mice Are Rescued by Targeting Actin Regulators. *Cell Rep.* **2015**, *11*, 1400–1413. [CrossRef]

41. Kumar, A.; Paeger, L.; Kosmas, K.; Kloppenburg, P.; Noegel, A.A.; Peche, V.S. Neuronal Actin Dynamics, Spine Density and Neuronal Dendritic Complexity Are Regulated by CAP2. *Front. Cell Neurosci.* **2016**, *10*, 180. [CrossRef] [PubMed]

List of academic teachers

My academic teachers were:

at the University of Stuttgart	at the Philipps-University
Groß	Bartsch
Gudat	Buchholz
Hartenbach	Elsässer
Hauber	Hänze
Heyer	Jacob
Hörning	Lill
Jeltsch	Rust
Kästner	Schmeck
Kleinow	Schmidt
Kontermann	Timmesfeld
Lemloh	
Nußberger	
Peters	
Pleiss	
Radde	
Rauhut	
Rudolph	
Schweikert	
Sprenger	
Takors	
Tovar	
Voß	
Wege	
Weiß	

Acknowledgements